

POLITECNICO DI MILANO

Facoltà di Ingegneria Industriale

Corso di Laurea Magistrale in INGEGNERIA MECCANICA



Scale Model Design of 5MW Offshore Wind Turbine

Relatore:

Prof. Alberto ZASSO

Correlatori:

Ing. Ilmas Andrea BAYATI

Ing. Matteo Maria CACCIALANZA

Tesi di Laurea di:

Ehsan DERUCHI

Matricola: 783811

ANNO ACCADEMICO 2014-2015

ACKNOWLEDGEMENTS

The researcher acknowledges extreme gratitude and appreciation to those who have given their respective assistance in this research. Without their inspiring, challenging and encouraging support, this Thesis would not have materialized. To them, the researcher gives his sincerest thanks.

I would like to sincerely thank my research advisor, Prof. Alberto Zasso and also Ilmas Andrea Bayati and Matteo Maria Caccialanza for being a patient mentor over the course of my degree completion. Their guidance and constant support helped me to stay motivated. I learned a great deal from them about scientific writing and problem solving in the area of mechanical engineering, control systems and aerodynamics.

Last but not least I wish to avail this opportunity and express a sense of gratitude and love to my parents in Iran for their moral support and my friends in Italy for their strength and help. The love given by them all has been a real source of strength and comfort throughout my work.

EHSAN DERUCHI

TABLE OF CONTENTS

ACKNOWLEDGEMENTS.....	I
TABLE OF CONTENTS.....	III
LIST OF FIGURES.....	VII
LIST OF TABLES.....	XI
ABSTRACT.....	XIII
SOMMARIO.....	XV
INTRODUCTION.....	1
CHAPTER 1. REFERENCE MODEL.....	5
1.1. General Machine Properties.....	5
1.2. Blade Structural Properties.....	6
1.3. Blade Aerodynamic Properties.....	7
1.4. Nacelle and Hub Properties.....	8
1.5. Drivetrain Properties.....	8
1.6. Tower Properties.....	9
1.7. Control System Properties.....	10
CHAPTER 2. SCALING METHODOLOGIES.....	13
2.1. Scaling Bonds.....	13
2.2. Parameter Optimization.....	15
2.3. Scaling Laws Formulation.....	16
2.4. Scaled Model Properties.....	19
2.5. Natural Frequencies.....	21
CHAPTER 3. COMPONENT SELECTION.....	23
3.1. Pitch Motor Selection.....	23
3.1.1. Trajectory Planning.....	23
3.1.2. Motor Selection Method Formulation.....	30

3.1.3. Blade Inertia and Aerodynamic Loads.....	33
3.1.4. Motor and Gearbox Selection.....	36
3.1.5. IPC Motor Check.....	44
3.2. Main Motor Selection.....	46
3.2.1. Wind Turbine Inertia and Torque.....	47
3.2.2. Motor, Gearbox and Encoder Selection.....	48
3.3. Bearing Selection.....	51
3.4. Slip ring Selection	53
CHAPTER 4. WIND TURBINE LAYOUT.....	55
4.1. Blade and Hub Layout.....	55
4.1.1. Blade Loads.....	56
4.1.2. Aerodynamic Load on the Blade	56
4.1.3. Blade Weight.....	58
4.2. Blade First Layout Configuration.....	59
4.2.1. Blade Fixing Components.....	60
4.2.2. Blade Bending Moment Absorber.....	61
4.2.3. FEM Analysis.....	63
4.2.4. Blade Layout with the B.M.A.....	65
4.2.5. Blade Components.....	66
4.3. Hub Layout for the first blade configuration.....	67
4.4. Blade Second Layout Configuration.....	69
4.4.1 Blade second Layout Fixing Components.....	70
4.4.2 Blade Second Configuration Hub Layout.....	71
4.4.3. Blade Second Configuration Components.....	73
4.5. Nacelle and Drivetrain Layout.....	73
4.5.1. First Configuration.....	75
4.5.2. Second Configuration.....	78
CHAPTER 5. WIND TURBINE CONTROL SYSTEM.....	81

5.1. Generator Power Control.....	81
5.1.1. Generator Power Control Formulation.....	83
5.2. Pitch Control.....	85
5.2.1. Pitch Control Formulation.....	86
5.2.2. Blade Pitch Sensitivity.....	89
5.3. Feedforward Control System Design.....	95
5.3.1. Simulation Results (Full Scale).....	97
5.3.2. DC Motor Simulink Scheme.....	100
5.3.3. Simulation Results (Scaled Model).....	102
5.4. Feedback Control System Design.....	106
5.4.1. Simulation Results (Full Scale).....	106
5.4.2. Simulation Results (Scaled Model).....	110
CONCLUSIONS	115
APPENDIX A.....	117
APPENDIX B.....	119
APPENDIX C.....	133
NOMECLATURE.....	139
ABBREVIATIONS AND ACRONYMS.....	141
REFERENCES.....	143

LIST OF FIGURES

Figure 1. Polimi wind tunnel.....	2
Figure 2. Left picture: low speed section. Right picture: high speed section of the Polimi wind tunnel.	3
Figure 1.1. Control system flowchart[9].	11
Figure 2.1. this figure shows the difference of choosing 2 different optimization coefficient on other scaling factors under study.....	16
Figure 2.2. Bode plot of generator speed low pass filter frequency response.	22
Figure 3.1. Displacement, Velocity and Acceleration of the Triangular Velocity Profile. Units are respectively [rad], [rad/s] and [rad/s ²].	25
Figure 3.2. Displacement, Velocity and Acceleration of Cyclical trajectory profile. Units are respectively [rad], [rad/s] and [rad/s ²].	26
Figure 3.3. Displacement, Velocity and Acceleration of the S-Curve trajectory profile. Units are respectively [rad], [rad/s] and [rad/s ²].	27
Figure 3.4. Comparison of the velocity behavior of 3 different trajectory profiles.....	28
Figure 3.5. Comparison of acceleration behavior of 3 different trajectory profiles.	28
Figure 3.6. Blade section.....	35
Figure 3.7. 3D corrected coefficients of the DU40 airfoil	36
Figure 3.8. Alfa, Beta diagram of the triangular velocity profile for different motors.....	39
Figure 3.9. Alfa, Beta diagram of the cyclical profile trajectory for different motors.	39
Figure 3.10. Alfa, Beta diagram of the s-curve trajectory for different motors.....	40
Figure 3.11. Reduction ratio limitation of the triangular velocity profile for each motor.	41
Figure 3.12. Reduction ratio limitation of the cyclical profile for each motor.....	41
Figure 3.13. Reduction ratio limitation of the triangular S-curve profile for each motor.	42
Figure 3.14. 3D view of the motor of the blade pitch control.	43
Figure 3.15. Motor of the blade pitch control.	44
Figure 3.16. In this figure is reported the limitation of the pitch motor due to each rotation of the rotor.....	45
Figure 3.17. Blade pitch angles due to wind speed variation of the DTU 10 MW wind turbine.	46
Figure 3.18. Brake units of a commercial wind turbine.	48
Figure 3.19. Velocity profile defined as the usual behavior of the rotor of the scaled model.	49
Figure 3.20. Technical information of the bearings used to connect the drivetrain to the nacelle.	52
Figure 3.21. Technical information of the bearing used in the blade (First Blade Layout).....	52
Figure 3.22. Thrust bearing used in the blade, hub connection (Second Blade Layout)	53
Figure 4.1. Blade Layout.....	599
Figure 4.2. Pitch Motor Fixing Component	60
Figure 4.3. Blade Fixing Component	60
Figure 4.4. Blade bending moment absorber layout.....	61
Figure 4.5. In this figure is reported the B.M.A connected to the bearing that will be connected to the secondary shaft.....	62

Figure 4.6. Gearbox, B.M.A, Secondary shaft, Hub connection.....	62
Figure 4.7. FEM analysis of the B.M.A.....	63
Figure 4.8. Blade layout with the B.M.A.....	65
Figure 4.9. Blade Components.....	66
Figure 4.10. Hub of the scaled model.	67
Figure 4.11.a Hub layout using the blade with the B.M.A.....	68
Figure 4.11.b Hub layout using the blade with the B.M.A.	68
Figure 4.11.c. Hub layout using the blade with the B.M.A.....	69
Figure 4.12. Blade layout using the thrust bearing.....	69
Figure 4.13. Motor fixing component for the second blade layout	70
Figure 4.14. second fixing component for the second blade layout	71
Figure 4.15. Second blade configuration Hub.....	71
Figure 4.16. Second blade configuration rotor design	72
Figure 4.17. Second blade configuration rotor design	72
Figure 4.18. Second blade configuration components	73
Figure 4.19. Perpendicular gearbox configuration.	74
Figure 4.20. Scaled model using the motor in the tower and transferring the motion to the drivetrain trough a perpendicular gearbox [14].....	75
Figure 4.21. view of the scaled model wind turbine layout (First configuration).	76
Figure 4.22. view of the bearing position of the scaled model wind turbine (First configuration)	76
Figure 4.23. view of the scaled model wind turbine layout (First configuration)	77
Figure 4.24. Components of the scaled wind turbine drivetrain (First layout).....	77
Figure 4.25. Wind turbine scaled model layout (second configuration)	78
Figure 4.26. Wind turbine Nacelle view (second configuration).	79
Figure 4.27. Wind turbine components (second layout).	80
Figure 4.28. Wind turbine Nacelle and drivetrain connection view.....	80
Figure 5.1. Generator torque in different rotational speed (Scaled model).	82
Figure 5.2. Generator torque in different rotational speed (Full scale model) [9].....	83
Figure 5.3. Generator power control Simulink scheme.....	84
Figure 5.4. Generator Power in different rotational speed (scaled model).....	85
Figure 5.5. Pitch sensitivity variation with respect of the blade pitch angle. Red line is the interpolation of the linearization results (blue points).....	92
Figure 5.6. Integral and proportional gains of the scaled model	92
Figure 5.7. integral and proportional gains of the full scale model [9].	95
Figure 5.8. Blade pitch angle variation with respect to the wind speed for the scaled model (Stationary condition). The Red line is the second order interpolation of the FAST linearization results (Blue points) using the first column and third column of Table 5.2.	96
Figure 5.9. Feedforward pitch control Simulink scheme	97
Figure 5.10. Wind speed variation in 25 seconds from.	98
Figure 5.11. Pitch angles in stationary condition due to wind speed variation.	98
Figure 5.12. Integral gain variation in time.	99
Figure 5.13. Proportional gain variation of the control system.	99
Figure 5.14. Pitch sensitivity variation in time.	100

Figure 5.15. DC Motor Simulink Scheme.....	101
Figure 5.16. DC motor transition behavior with the gains used for the position control of the motor. Yellow: requirement of the control system. Red response of the motor.	101
Figure 5.17. Simulink scheme of the Feedforward control, for the scaled model with the DC Motor model for the pitch control.	102
Figure 5.18. Wind speed in the scaled model.....	102
Figure 5.19 Blade Pitch angles due to the input wind speed.	103
Figure 5.20. Integral Gains.....	104
Figure 5.21. Proportional Gains.	104
Figure 5.22. Blade pitch sensitivity.....	105
Figure 5.23. Rotor rotational velocity.	105
Figure 5.24. Impulse imposed to the rotational velocity of the rotor.	106
Figure 5.25. Integral Gain.	107
Figure 5.26. Proportional gain.	107
Figure 5.27. Pitch angle variation.	108
Figure 5.28. Aerodynamic torque of the blade.....	109
Figure 5.29. Generator torque due to power generator control.	109
Figure 5.30. Full scale controlled system rotor rotational velocity.	110
Figure 5.31. Impulse imposed on the rotational velocity of the rotor (rad/s).	111
Figure 5.32. Rotor rotational velocity of the controlled system at 393 rpm.	111
Figure A.1 Aerodynamic coefficients of DU40 airfoil	117
Figure A.2 Distributed tower property of the NREL 5MW wind turbine	117

LIST OF TABLES

Table 1.1. Gross properties of the NREL 5 MW Baseline wind turbine [9].	6
Table 1.2. Undistributed blade structural properties of the blade [9].	7
Table 1.3. Undistributed blade aerodynamic properties[9].	7
Table 1.4. Nacelle and hub properties[9].	8
Table 1.5. Drivetrain properties[9].	9
Table 1.6. Undistributed tower properties [9].	10
Table 1.7. Variable speed generator torque and blade pitch control properties of the NREL 5 MW wind turbine[9].	10
Table 2.1. scaling formulation used to obtain the scaled model and the effective scaling ratio.	19
Table 2.2. Scaled model properties and comparison with the full scale model.	20
Table 2.3. Full scale model natural frequencies[9].	21
Table 2.4. Scaled model natural frequencies.	21
Table 3.1. Geometrical properties of the NREL 5 MW blade.	34
Table 3.2. Characteristics of the motors studied for choosing the optimal pitch motor.	37
Table 3.3. Technical data of the slipring.	54
Table 4.1. Blade Characteristics used to calculate the load on the blade.	56
Table 5.1. Pitch sensibility table of the wind turbine in different wind speed and rated rotational velocity of the blade (Full scale model) [9].	90
Table 5.2. Pitch sensibility table of the wind turbine in different wind speed and rated rotational velocity of the blade model (Scaled model).	90

ABSTRACT

Wind energy is one of the fastest growing renewable energies in the world. The generation of power from wind turbines is non-polluting, it doesn't produce any by-products. This thesis presents the development of a 1/58th model of a multi megawatt wind turbine. The model is based on a 5 MW wind turbine designed by the National Renewable Energy Laboratory (NREL) commonly utilized in numerical modeling efforts. The developed model in this thesis is going to be realized in the Mechanical Department of the Politecnico di Milano in Milan, Italy. The ultimate goal of the model is to do different tests and studies on the realized model in the wind tunnel of the Politecnico di Milano. This thesis will present information on the scaling methodology used for the development of the scaled model and it will introduce the physical characteristics of the obtained model. The discussion of scaling methodology will include a presentation of scaling optimization used to have the best solution between different objectives of the model. Particular attention is paid to adequate Reynolds number, frequency scaling factor and optimal velocity scaling factor to use the maximum available range of wind velocity of the wind tunnel. This thesis will also present a detailed information on different components for the construction of the model as the main motor that will be used for power generation, the pitch motor that will regulate the pitch angles of each blade to maintain the rotational velocity of the rotor constant and equal to the rated value. The other components that have been used are discussed in the next chapters. Furthermore the thesis will propose different layouts for the construction of the model, each of them with their benefits and weakness. The last part of this thesis is dedicated to design the generator power control and in more detail the pitch control of the scaled wind turbine. With simulations for the full scale and scaled model and a comparison between the results of the pitch control for the full scale and scaled model.

Keywords: *Scaled Wind Turbine, Pitch Control, Multi Megawatt Wind Turbines, PID Control, Wind Turbine Layout, Simulink.*

SOMMARIO

Fra le varie forme di fonti di energia rinnovabile nel mondo, quello dell'eolico è uno dei settori in più rapido sviluppo. La generazione di energia dal vento è non inquinante e non produce alcuna emissione. Questa tesi presenta lo sviluppo di un modello in scala 1:58 di una turbina eolica multi-MW. Il modello si basa su una turbina eolica da 5 MW progettata dal National Renewable Energy Laboratory (NREL), comunemente utilizzata nei lavori di modellazione numerica. Il modello sviluppato in questa tesi sta per essere realizzato nel Dipartimento di Meccanica del Politecnico di Milano in Italia. L'obiettivo finale del modello è quello di permettere l'esecuzione di diversi studi e test presso la Galleria del Vento del Politecnico di Milano. Questa tesi presenta informazioni sulla metodologia usata per lo sviluppo del modello in scala, specificando le caratteristiche fisiche del modello ottenuto. La discussione del metodo di scalatura include un processo di ottimizzazione utilizzato per ottenere la migliore soluzione tra i diversi obiettivi che ci si è preposti durante la costruzione del modello. Particolare attenzione è rivolta a mantenere un adeguato rapporto fra modello al vero e modello scalato in termini di numero di Reynolds e di fattore di scala della frequenza e di utilizzare la massima disponibile gamma di velocità del vento compatibilmente con i limiti della Galleria del Vento. Questa tesi presenta anche informazioni dettagliate sui diversi componenti per la costruzione del modello come il motore principale che verrà utilizzato per la generazione di energia, il motore per il controllo del pitch che regola l'angolo di ciascuna pala per mantenere la velocità di rotazione del rotore costante e pari al valore nominale. Inoltre la tesi propone diversi layout della disposizione degli organi meccanici per la costruzione del modello, ciascuno con i loro vantaggi e svantaggi. L'ultima parte di questa tesi è dedicata alla progettazione del controllo della potenza elaborata dal generatore e più in dettaglio il controllo del pitch per la turbina eolica in scala, con simulazioni effettuate a partire delle caratteristiche sia del modello di riferimento (NREL 5MW) che del modello in scala e proponendo infine un confronto fra i risultati ottenuti.

Parole Chiave: *Modello in scala delle turbine eoliche, Controllo pitch, Turbine Eoliche Multi Megawatt, Controllo PID, Layout Delle Turbine Eoliche, Simulink.*

INTRODUCTION

Wind power was recognized as a valuable resource thousands of years before internal combustion engines and modern power plants were developed. Long ago, for example, people built windmills for milling grain and installed sails on their boats in order to reduce human labor demands [1]. In recent decades, wind has experienced a resurgence in popularity by helping to meet the increasing energy consumption of a growing world population through the use of a renewable, non-polluting energy source [2].

To be competitive in the electricity market, wind turbines must produce electricity at a cost comparable to that of fossil fuel technology. Since the fuel (wind) is free, the major cost of wind energy comes from the initial capital outlay for the machine itself (roughly \$1000 per kW of installed capacity) [3] and the supporting infrastructure. Relatively small costs are associated with operating and maintaining the turbine throughout its lifetime. Therefore, technology advances that reduce the initial cost of the turbine or allow it to capture more energy during operation, result in a cost of energy (COE) decrease. Current wind technology is rapidly becoming cost competitive with fossil fuel energy [4].

The current trend in wind energy is to place the wind turbine in offshore locations. This has many advantages such as availability of higher wind speeds and less turbulence at offshore locations. Size of rotors can be increased without the need to worry about lack of space and affecting agricultural and living spaces [5].

Until now huge efforts have been made by companies operating in wind sector and by national governments in terms of financial support to the research, whose contribution to innovation has allowed the development of even more efficient and high-tech wind turbines [6]. Furthermore, it is also quite clear as research and innovation should

focus on lowering the cost of wind energy, which has to become competitive when compared to the price of energy produced by traditional sources, like fossil fuels. However, this latter has not been reached yet and constant research and development is therefore needed [7],[8].

Politecnico di Milano as one of the important research poles of Italy and Europe is investing on research and innovation in this field of technology. This is possible because of the important labs and infrastructures available in politecnico di Milano that permits the studies in this field. One of the important facilities is the wind tunnel available in the university that permits studies in the aerodynamic field. The details of the POLIMI wind tunnel has been reported below: The GVPM is a close circuit wind tunnel. Two test section are available, a low turbulence level test section, suitable for aerospace engineering applications, and a boundary layer large dimensions test section, built in the return tube, for civil engineering applications.



Figure 1. Polimi wind tunnel.

The civil (boundary layer) test section where it is possible to achieve a maximum velocity of 14 [m/s], is situated on the second floor of the building, in the return tube, and has an overall dimension of 3.84 x 13.84 x 36 [m] respectively the height, width and length that permits to perform tests on very large models with low blockage effects and to reproduce atmospheric boundary conditions. The aeronautical test section and has a section area of 4 x 3.84 m, it is located almost at

ground height and it lies between the contraction cone and the diffuser; the maximum flow velocity is 55 [m/s].

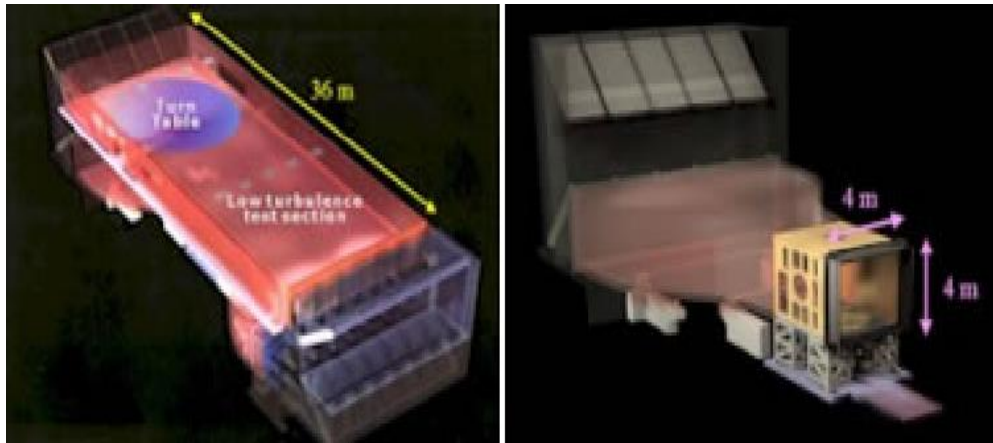


Figure 2. Left picture: low speed section. Right picture: high speed section of the Polimi wind tunnel.

In this thesis we will base the design of our scaled model of the 5MW wind turbine on being compatible with the introduced wind tunnel as this model is going to be realized in Politecnico di Milano and tested in the GVPM.

This thesis provides the following research contributions to the scientific community:

1. Defining scaling methods and modeling techniques needed to perform accurate rigid scaling model of multi megawatt floating wind turbines.
2. Disclosing design details and characterization results of a 1/58th scale model of the NREL 5 MW wind turbine for others to use for future model tests.
3. Providing method that could be employed to correct undesired effects of scaling on frequency scaling factor Reynolds scaling factor and wind velocity scaling factor.

4. Providing the methodologies for choosing different components of the scaled wind turbine as well as the pitch motor, the power generator, slip ring, ball bearing and, etc.

5. Proposing different layouts for the scaled wind turbine considering all of the details on the dimension and the limitations due to the scaled model dimensions discussing the benefits and limitations of each layout.

6. Defining the control design of the blade pitch angle and the design of the power generation control that are two main control systems of the modern wind turbines.

CHAPTER 1

FULL SCALE REFERENCE MODEL

We have used the NREL offshore 5MW baseline wind turbine [9] as our reference model. This is because this reference has been already used in other papers [10] and the information about our model is complete and accessible. This wind turbine is a conventional three bladed upwind variable speed variable blade pitch wind turbine. The NREL offshore 5MW baseline wind turbine has been used to establish the reference specifications for a number of research projects supported by the U.S. DOE's Wind & Hydropower program. In addition, the integrated European Union Upwind research program and the International Energy Agency (IEA) and other research groups have adopted the NREL offshore 5MW baseline wind turbine as their reference model. The model has been, and will likely continue to be used as a reference by research teams throughout the world to standardize baseline offshore wind turbine specifications and to quantify the benefits of advanced land and sea based wind energy technologies. The specifics of the NREL 5-MW baseline including the aerodynamic, structural and control system properties and the rationale behind its development has been reported below.

1.1 General Machine Properties:

As shown in Table 1.1 the rotor radius is 63 m and the blade length is about 61.5 m. The hub height for the baseline wind turbine is 90 m, this gives a 15 m air gap between the blade tips at their lowest point when the wind turbine is undeflected. The (x,y,z) coordinates of the overall center of mass (CM) location of the wind turbine are indicated in a tower base coordinate system, which originates along the tower centerline at ground or mean sea level (MSL). The x-axis of this coordinate system is directed nominally downwind, the y-axis is directed

transverse to the nominal wind direction, and the z-axis is directed vertically from the tower base to the yaw bearing.

Table 1.1. Gross properties of the NREL 5 MW Baseline wind turbine [9].

Rating	5 MW
Rotor Orientation, Configuration	Upwind, 3 Blades
Control	Variable Speed, Collective Pitch
Drivetrain	High Speed, Multiple-Stage Gearbox
Rotor, Hub Diameter	126 m, 3 m
Hub Height	90 m
Cut-In, Rated, Cut-Out Wind Speed	3 m/s, 11.4 m/s, 25 m/s
Cut-In, Rated Rotor Speed	6.9 rpm, 12.1 rpm
Rated Tip Speed	80 m/s
Overhang, Shaft Tilt, Precone	5 m, 5°, 2.5°
Rotor Mass	110,000 kg
Nacelle Mass	240,000 kg
Tower Mass	347,460 kg
Coordinate Location of Overall CM	(-0.2 m, 0.0 m, 64.0 m)

In addition it's useful to indicate the values of wind speed & rotor speed:

Cut-In, Rated , Cut-Out Wind Speed 3 m/s ,11.4 m/s ,25 m/s

Cut, In, Rated Rotor Speed 6.9 rpm ,12.1 rpm

This information is important for the design of the control system that has to maintain the rotational velocity constant and the power production equal to the rated power production.

1.2 Blade Structural Properties:

The NREL offshore 5MW baseline wind turbine has three blades each of them has the properties indicated in the Table 1.2. The distributed blade structural properties of each blade is based on the structural properties of the 62.6-m-long LM Glassfiber blade used in the DOWEC study [11]. Because the blades in the DOWEC study were 1.1 m longer than the 61.5-m-long LM Glassfiber blades [12] used on the actual REpower 5M machine, the reference truncated the 62.6m blades at 61.5m span to obtain the structural properties of the NREL 5MW baseline blades.

Table 1.2. Undistributed blade structural properties of the blade [9].

Length (w.r.t. Root Along Preconed Axis)	61.5 m
Mass Scaling Factor	4.536 %
Overall (Integrated) Mass	17.740 kg
Second Mass Moment of Inertia (w.r.t. Root)	11,776,047 kg-m ²
First Mass Moment of Inertia (w.r.t. Root)	363,231 kg-m
c.g. Location (w.r.t. Root Along Preconed Axis)	20.475 m
Structural Damping Ratio (All Modes)	0.477465 %

1.3 Blade Aerodynamic Properties:

Similar to the blade structural properties, the blade aerodynamic properties of the NREL 5MW baseline wind turbine is based on the DOWEC blades. It has been used 17 different sections with different aerodynamic properties to design the blade. The first 3 sections the section is cylindrical. In the next sections, (DU) refers to Delft University and (NACA) refers to the National Advisory Committee for Aeronautics that have been used as reference for the airfoils in the design of the NREL 5 MW. In the Table 1.3 blade node locations, labeled as (RNodes) are directed along the blade pitch axis from the rotor center to the blade cross sections. The element lengths, (DRNodes) sum to the total blade length of 61.5. The aerodynamic twist is reported in the (AeroTwst) column.

Table 1.3. Undistributed blade aerodynamic properties [9].

Node (-)	RNodes (m)	AeroTwst (deg)	DRNodes (m)	Chord (m)	Airfoil Table (-)
1	2.8667	13.308	2.7333	3.542	Cylinder1.dat
2	5.6000	13.308	2.7333	3.854	Cylinder1.dat
3	8.3333	13.308	2.7333	4.167	Cylinder2.dat
4	11.7500	13.308	4.1000	4.557	DU40_A17.dat
5	15.8500	11.480	4.1000	4.652	DU35_A17.dat
6	19.9500	10.162	4.1000	4.458	DU35_A17.dat
7	24.0500	9.011	4.1000	4.249	DU30_A17.dat
8	28.1500	7.795	4.1000	4.007	DU25_A17.dat
9	32.2500	6.544	4.1000	3.748	DU25_A17.dat
10	36.3500	5.361	4.1000	3.502	DU21_A17.dat
11	40.4500	4.188	4.1000	3.256	DU21_A17.dat
12	44.5500	3.125	4.1000	3.010	NA64_A17.dat
13	48.6500	2.319	4.1000	2.764	NA64_A17.dat
14	52.7500	1.526	4.1000	2.518	NA64_A17.dat
15	56.1667	0.863	2.7333	2.313	NA64_A17.dat
16	58.9000	0.370	2.7333	2.086	NA64_A17.dat
17	61.6333	0.106	2.7333	1.419	NA64_A17.dat

In Appendix A it has been reported the drag, lift and pitching moment coefficients of the DU40.

1.4 Nacelle and Hub Properties:

As indicated before, the hub of the NREL 5MW baseline wind turbine has been located 5 m upwind of the tower centerline at an elevation of 90 m above the ground when the system is undeflected. The vertical distance from the tower top to the hub height has been considered equal to, 2.4 m. Consequently, the elevation of the yaw bearing above ground or MSL is 87.6 m, with a shaft tilt of 5°. This makes the distance directed along the shaft from the hub center to the yaw axis 5.01910 m and the vertical distance along the yaw axis from the tower top to the shaft 1.96256 m. The distance directed along the shaft from the hub center to the main bearing is 1.912 m. Further information about the Nacelle and Hub has been reported in the Table 1.4.

Table 1.4 Nacelle and hub properties [9].

Elevation of Yaw Bearing Above MSL	87.6 m
Vertical Distance Along Yaw Axis from Yaw Bearing to Shaft	1.96256 m
Distance Along Shaft from Hub Center to Yaw Axis	5.01910 m
Distance Along Shaft from Hub Center to Main Bearing	1.912 m
Hub Mass	56,780 kg
Hub Inertia About Shaft Axis	115,926 kg-m ²
Nacelle Mass	240,000 kg
Nacelle Inertia About Yaw Axis	2,607,890 kg-m ²
Nacelle c.g. Location Downwind of Yaw Axis	1.9 m
Nacelle c.g. Location Above of Yaw Bearing	1.75 m
Equivalent Nacelle Yaw Linear Spring Constant	9,028,320,000 N-m/rad
Equivalent Nacelle Yaw Linear Damping Constant	19,160,000 N-m/rad/s

1.5 Drivetrain Properties:

The NREL 5MW baseline wind turbine has a rated speed of the low speed shaft equal to 12.1 rpm and a gearbox ratio of 97 and a high speed shaft rotational velocity of 1173.7 rpm. In the scaled model the low speed shaft velocity should be scaled accurately because all of the system dynamics is related to the low speed shaft. The high speed shaft rotational velocity can't be scaled properly because of

the limitations of the motor selection and it depends on the gearbox ratio of the motor that is going to be chosen. Other information about the Drivetrain Properties is reported in Table 1.5.

Table 1.5. Drivetrain properties [9].

Rated Rotor Speed	12.1 rpm
Rated Generator Speed	1173.7 rpm
Gearbox Ratio	97 :1
Electrical Generator Efficiency	94.4 %
Generator Inertia About High-Speed Shaft	534.116 kg-m ²
Equivalent Drive Shaft Torsional Spring Constant	867,637,000 N-m/rad
Equivalent Drive Shaft Torsional Damping Constant	6,215,000 N-m/rad/s
Fully-Deployed High-Speed Shaft Brake Torque	28,116.2 N-m
High-Speed Shaft Brake Time Constant	0.6 sec

1.6 Tower Properties:

The properties of the tower for the NREL offshore 5MW baseline wind turbine will depend on the support structure used to carry the rotor-nacelle assembly. The type of support structure will depend on the installation site, whose properties vary significantly through differences in water depth, soil type, and wind. Offshore support-structure types include fixed bottom monopiles, gravity bases and space frames such as tripods, quad pods, and lattice frames (jackets) and floating structures. This section documents the tower properties for the equivalent land based version of the NREL 5MW baseline wind turbine. These properties provide a basis with which to design towers for site specific offshore support structures.

The distributed properties of the land based tower for the NREL 5 MW baseline wind Turbine is based on the base diameter (6 m) and thickness (0.027 m), top diameter (3.87 m) and thickness (0.019 m), and effective mechanical steel properties of the tower that is reported in the DOWEC study [11]. The radius and thickness of the tower are assumed to be linearly tapered from the tower base to tower top. The distributed tower property of the wind turbine has been reported in Appendix A. The undistributed Tower properties of the tower has been reported in Table 1.6.

Table 1.6 Undistributed tower properties [9].

Height Above MSL	87.6 m
Overall (Integrated) Mass	347,460 kg
c.g. Location (w.r.t. MSL Along Tower Centerline)	38.234 m
Structural Damping Ratio (All Modes)	1 %

1.7 Control System Properties

The control system specifications and the natural frequencies of the system will be presented in the next chapters. Below is reported the summary of the control system and the rated working condition specifications.

Table 1.7. Variable speed generator torque and blade pitch control properties of the NREL 5 MW wind turbine [9].

Corner Frequency of Generator Speed Low Pass Filter	0.25 Hz
Peak Power Coefficient	0.482
Tip Speed Ratio at Peak Power Coefficient	7.55
Rotor Collective Blade Pitch Angle at Peak Power Coefficient	0.0 °
Generator Torque Constant in Region 2	0.0255764 N-m/rpm ²
Rated Mechanical Power	5.296610 MW
Rated Generator Torque	43,093.55 N-m
Transitional Generator Speed Between Regions 1 and 1 1/2	670 rpm
Transitional Generator Speed Between Regions 1 1/2 and 2	871 rpm
Transitional Generator Speed Between Regions 2 1/2 and 3	1,161.963 rpm
Generator Slip Percentage in Region 2 1/2	10 %
Minimum Pitch For Ensuring Region 3 Torque	1 °
Maximum Generator Torque	47,402.91 N-m
Maximum Generator Torque Rate	15,000 N-m/s
Proportional Gain at Minimum Pitch Setting	0.01882681 sec
Integral Gain at Minimum Pitch Setting	0.008068634
Pitch Angle at Which Rotor Power Has Doubled	6.302336 °
Minimum Pitch Setting	0 °
Maximum Pitch Setting	90 °
Maximum Absolute Pitch Rate	8 °/sec
Equivalent Blade Pitch Linear Spring Constant	1,069,020,000 N-m/rad
Equivalent Blade Pitch Linear Damping Constant	230,000 N-m/rad/s

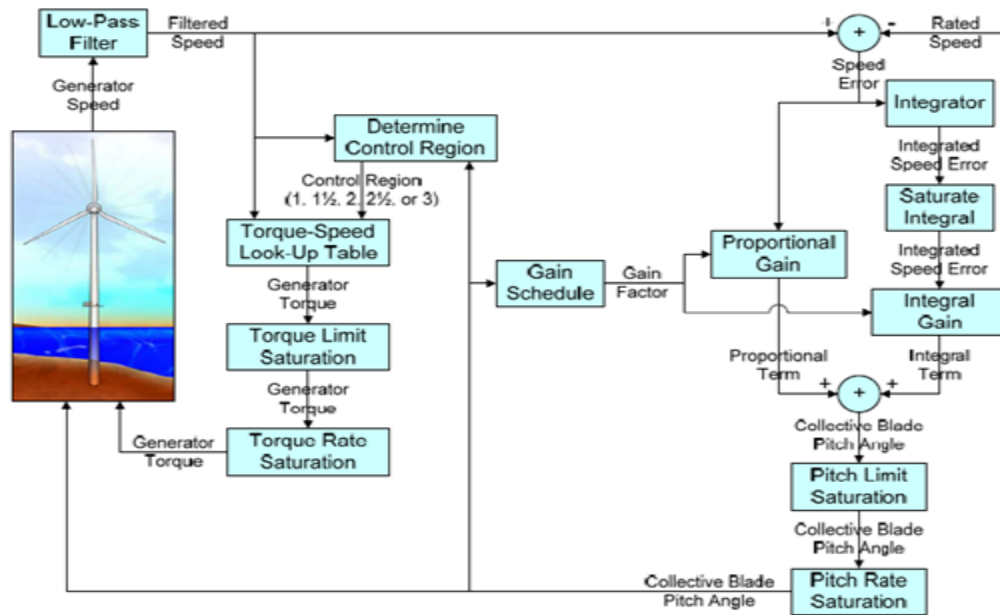


Figure 1.1 Control system flowchart [9].

CHAPTER 2

SCALING METODOLOGY

Proper scaling of a model and environmental conditions for scale model testing is essential to complete a valid and reliable test. For floating wind turbine testing, proper scaling and modeling techniques have yet to be established. This chapter will present and discuss the scaling relationships, scale factors, and modeling techniques used to design the scaled model of the wind turbine presented in the previous chapter. In addition, target design values derived from scaling methodology for the scale model wind turbine is also presented.

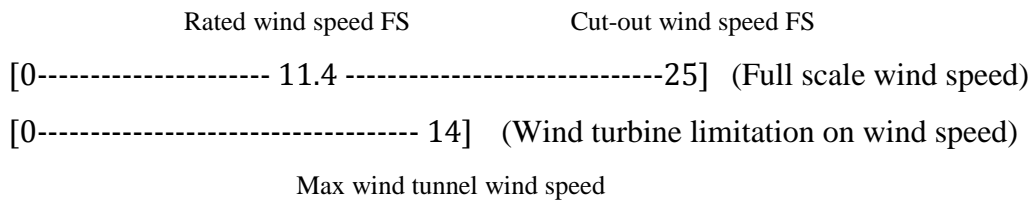
2.1 Scaling Bonds

For the scaling purpose, first we have to fix our primary bonds, knowing the objective of the model that we want to obtain. The first parameter that we are going to bond is the λ_L that is the geometrical scaling factor. In our case we obtained that the optimal value for our wind tunnel dimensions is $1/58^{th}$.

$$\lambda_L = \frac{1}{58} \quad (2.1)$$

The second parameter that we have bonded is the velocity scaling factor λ_V . To obtain our limits on this parameter we have studied the limits of wind velocity in our wind tunnel and compared with the full scale wind condition with reference to NREL 5MW working condition. As discussed before the Cut-In, Rated, and the cut-out wind speed in the full scale wind turbine are respectively 3 m/s, 11.4 m/s and 25 m/s and the maximum velocity of our wind tunnel is 14 m/s [13].

So it is important to choose a velocity scaling factor that prevents information loss because of huge reduction that can be problematic because of the fact that the phenomenon in the scaled model will be compressed in a smaller range of wind velocity. Obviously to avoid this problem the best velocity scaling factor is $1/1^{\text{th}}$, but there are also other problems that will be discussed later that avoid choosing this value. The first problem is due to the limitation of the wind tunnel maximum velocity.



If we choose a small λ_v (near to 1) we can't work on the whole range of the wind turbine working condition because of the limited velocity of the wind tunnel. To avoid this problem we have two options. The first option is to use the turbine just for a limited range of wind velocity. The second option is to use the high velocity wind tunnel to achieve higher velocities that permits the possibility of using the model in the whole range of wind velocity with the $1/1^{\text{th}}$ wind velocity scaling factor. As we want to use the low speed wind tunnel and our objective is to use our scaled model to study the behavior of the wind turbine in the whole range of the wind velocity we are not going to use λ_v near to 1.

From the other side if we choose a high λ_v it's possible to lose some information because of the fact that the full scale phenomenon are compressed in a smaller range of velocity(frequency) and it may be difficult to distinguish different phenomenon in different frequencies.

Considering the limitation of our wind tunnel we have:

$$\lambda_v = \frac{\text{max wind speed of full scale model}}{\text{max wind speed of the wind tunnel}} = \frac{1}{1,7857} \quad (2.2)$$

This value is the minimum value that we can obtain in case that we use the low speed wind tunnel and we want to study the whole range of the wind turbine.

2.2 Parameter Optimization

There are still few considerations that have to be done to optimize our choice. The first fact is that we want to minimize the value of λ_f for the further controls that can be implemented on our model (modern control techniques). The second fact is that we want to limit the value of λ_{Re} , to have a difference between the Reynolds number of the scaled model and full scale model to be minimum[14]. For this aim we define the following equation that should be minimized.

$$\min\left(\frac{1}{\lambda_{Re}} + \lambda_f\right) \quad \text{Varying } \lambda_V \quad (2.3)$$

That is equal to:

$$\min\left(\frac{1}{k^2\lambda_V\lambda_L} + \frac{\lambda_V}{\lambda_L}\right) \quad \text{Varying } \lambda_V \quad (2.4)$$

In this equation the first term is to optimize the value of λ_{Re} and the second term is to optimize λ_f . We have used a coefficient to give different weight to the optimization of each of the parameters. This coefficient is arbitrary and has to be chosen in such a way that both the Reynolds and frequency scaling factors are more or less near to the value that is adequate for our scaled model. In this case if we use a value of k equal to 2 the value of frequency and Reynolds are more compatible with objectives of our work. Deriving the equation we find that to have the minimum value of the equation we have $k = \frac{1}{\lambda_V}$.

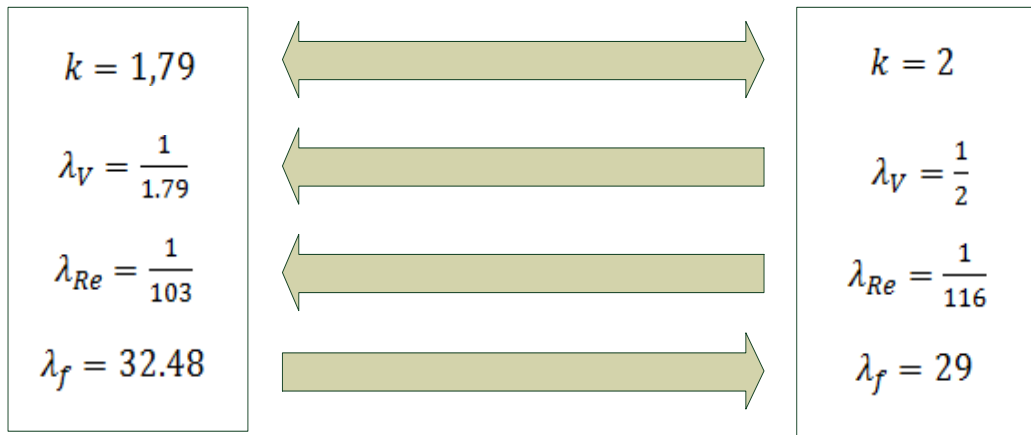


Figure 2.1. This figure shows the difference of choosing 2 different optimization coefficient on other scaling factors under study.

As we can see from the Figure 2.1 using $k=1.79$, we are using in the optimal way the range of velocity of the wind tunnel, also the value of Reynolds number is higher than using $k=2$. As a result we are going to obtain a more rigid model, but from the other side having higher value of k (near to 2) we will have benefits on the frequency scaling factor. As one of the objectives of creating the wind turbine model is to test the Modern control laws in the wind tunnel to study the benefits of different control laws on the wind turbine, lower frequency scaling factors are required. The other important point is that using higher value of k we can reduce the dimensions of the motors and consequently gearbox encoder and etc. Because of the fact that using higher values of k the rotational velocity for the scaled model reduces. This can be useful because in the scaled model we have limitations on the dimensions and weight of the model.

In this case we decided to choose the $k=1.79$, this is because of the fact that as shown in the Figure 2.1 the value of frequency scaling factor is not too high with respect to the case using $k=2$, but to avoid dimensional problems, after choosing the motors we have to verify whether the motors can generate the required movements for the scaled model or not and if there is any problem due to the dimensions and the weight of the motors.

2.3 Scaling laws formulation

Now we can proceed with the calculation of other scaling parameters using the two parameters defined before [15].

Mass Scaling Factor: To obtain the mass scaling factor, it is important to notice that we have done a hypothesis that the full scale model and the scaled model are both constructed with the same material so the blade as indicated before is made of glassfiber with the same density of the full scale model.

$$\lambda_m = \frac{\text{scale model mass}}{\text{full scale mass}} = \frac{\rho_{\text{model}} L_{\text{model}}^3}{\rho_{\text{Real}} L_{\text{Real}}^3} = \lambda_L^3 \quad (2.5)$$

Acceleration Scaling Factor:

$$\lambda_a = \frac{L_{\text{model}} t_{\text{Real}}^2}{L_{\text{Real}} t_{\text{model}}^2} = \frac{\lambda_L}{\lambda_t^2} \quad (2.6)$$

Time Scaling Factor:

$$\lambda_t = \frac{\lambda_L}{\lambda_v} \quad (2.7)$$

Frequency Scaling Factor:

$$\lambda_f = \frac{1}{\lambda_t} \quad (2.8)$$

Force Scaling Factor:

$$\lambda_F = \frac{M_{\text{model}} L_{\text{model}} t_{\text{Real}}^2}{M_{\text{Real}} L_{\text{Real}} t_{\text{model}}^2} = \frac{\lambda_m \lambda_L}{\lambda_t^2} \quad (2.9)$$

Area Scaling Factor:

$$\lambda_A = \lambda_L^2 \quad (2.10)$$

Rotor speed Scaling Factor: the tip speed ratio remains constant between the scaled model and the full scale wind turbine [16] so as a result:

$$TSR_{\text{model}} = TSR_{\text{Real}} \rightarrow \frac{\omega_{\text{Real}} R_{\text{Real}}}{V_{\text{Real}}} = \frac{\omega_{\text{model}} R_{\text{model}}}{V_{\text{model}}} \quad (2.11)$$

$$\frac{\omega_{model}}{\omega_{Real}} = \frac{R_{Real}V_{model}}{R_{model}V_{Real}} \quad (2.12)$$

$$\lambda_{\omega} = \frac{\lambda_V}{\lambda_L} \quad (2.13)$$

Torque Scaling Factor:

$$1 Nm = \frac{1Kg \ 1m}{s^2} \ 1m = \frac{Kg \ m^2}{s^2} \quad (2.14)$$

$$\lambda_T = \frac{\lambda_m \lambda_L^2}{\lambda_t^2} \quad (2.15)$$

Power Scaling Factor:

$$1W = \frac{1J}{1s} = \frac{1N \ m}{s} = \frac{1 \ Kg \ m}{s^2} \frac{m}{s} = \frac{Kg \ m^2}{s^3} \quad (2.16)$$

$$\lambda_W = \frac{\lambda_m \lambda_L^2}{\lambda_t^3} \quad (2.17)$$

Second Mass Moment Of Inertia:

$$\lambda_I = \lambda_m \lambda_L^2 \quad (2.18)$$

Reynolds Scaling Factor:

$$\lambda_{Re} = \lambda_V \lambda_L \quad (2.19)$$

Mach Scaling Factor:

$$\lambda_{Ma} = \lambda_V \quad (2.20)$$

The obtained results has been summarized in Table 2.1.

Table 2.1. Scaling formulation used to obtain the scaled model and the effective scaling ratio.

	<i>Scaling formula</i>	<i>Scaling ratio</i>
<i>Length (m)</i>	λ_L	1:58
<i>Velocity ($\frac{m}{s}$)</i>	λ_V	1: 1.78
<i>Mass(kg)</i>	$\lambda_m = \lambda_L^3$	1: 195110
<i>Acceleration ($\frac{m}{s^2}$)</i>	$\lambda_a = \frac{\lambda_L}{\lambda_t^2}$	18.19: 1
<i>Time (s)</i>	$\lambda_t = \frac{\lambda_L}{\lambda_V}$	1: 32.48
<i>Frequency (HZ)</i>	$\lambda_f = \frac{1}{\lambda_t}$	32.48: 1
<i>Force (N)</i>	$\lambda_F = \frac{\lambda_m \lambda_L}{\lambda_t^2}$	1:10727
<i>Area (m²)</i>	$\lambda_A = \lambda_L^2$	1: 3364
<i>Rotor speed ($\frac{rad}{s}$)</i>	$\lambda_\omega = \frac{\lambda_V}{\lambda_L}$	32.48: 1
<i>Torque (Nm)</i>	$\lambda_T = \frac{\lambda_m \lambda_L^2}{\lambda_t^2}$	1:622170
<i>Power (W)</i>	$\lambda_W = \frac{\lambda_m \lambda_L^2}{\lambda_t^3}$	1: 19155
<i>Second Mass Moment(kgm²)</i>	$\lambda_I = \lambda_m \lambda_L^2$	1:656360000
<i>Reynolds</i>	$\lambda_{Re} = \lambda_V \lambda_L$	1: 103.57
<i>Mach</i>	$\lambda_{Ma} = \lambda_V$	1: 1.78

2.4 Scaled Model Properties

Using the scaling laws defined in this chapter we can design our scaled wind turbine. The characteristics of our wind turbine are compared with the full scale model in the following Table.

Table 2.2. Scaled model properties and comparison with the full scale model.

	<i>Full Scale</i>	<i>Unit</i>	<i>Scaled Model</i>	<i>Unit</i>
<i>Rating</i>	5	<i>MW</i>	261.03	<i>W</i>
<i>Rotor Configuration</i>	3 Blade	-	3 Blade	-
<i>Rotor Diameter</i>	126	<i>m</i>	2.17	<i>m</i>
<i>Hub Diameter</i>	3	<i>m</i>	0.052	<i>m</i>
<i>Hub Height</i>	90	<i>m</i>	1.55	<i>m</i>
<i>Cut In Wind Speed</i>	3	$\frac{m}{s}$	1.68	$\frac{m}{s}$
<i>Rated Wind Speed</i>	11.4	$\frac{m}{s}$	6.38	$\frac{m}{s}$
<i>Cut Out Wind Speed</i>	25	$\frac{m}{s}$	14	$\frac{m}{s}$
<i>Cut In Rotor Speed</i>	6.9	<i>rpm</i>	224.11	<i>rpm</i>
<i>Rated Rotor Speed</i>	12.1	<i>rpm</i>	393.01	<i>rpm</i>
<i>Rated Tip Speed</i>	80	$\frac{m}{s}$	44.7	$\frac{m}{s}$
<i>Tip Speed Ratio</i>	7	-	7	-
<i>Overhang</i>	5	<i>m</i>	0.09	<i>m</i>
<i>Rotor Mass</i>	110000	<i>kg</i>	0.56	<i>kg</i>
<i>Nacelle Mass</i>	240000	<i>kg</i>	1.23	<i>kg</i>
<i>Tower Mass</i>	347460	<i>kg</i>	1.78	<i>kg</i>
<i>Blade Length</i>	61.5	<i>m</i>	1.06	<i>m</i>
<i>Blade Overall Mass</i>	17740	<i>kg</i>	0.09	<i>kg</i>
<i>Blade Second Moment Of Inertia</i>	11776047	<i>kgm²</i>	0.02	<i>kgm²</i>

2.5 Natural Frequencies

As indicated in [9], the input for the generator torque control and the pitch control is the generator speed measurement as the sole feedback input. To mitigate the high frequency excitation of the control system we filtered the generator speed measurement for both the torque and pitch controllers using a recursive, single pole low pass filter with exponential smoothing [17]. In the full scale model the corner frequency of the low pass filter is designed to be roughly one quarter of the blade's first edgewise natural frequency or 0.25 Hz. The natural frequency of the full scale model is reported below, calculated with two different programs (ADAMS [18] & FAST)

Table 2.3. Full scale model natural frequencies [9].

Mode	Description	FAST	ADAMS
1	1 st Tower Fore-Aft	0.324	0.319
2	1 st Tower Side-to-Side	0.312	0.316
3	1 st Drivetrain Torsion	0.620	0.609
4	1 st Blade Asymmetric Flapwise Yaw	0.666	0.630
5	1 st Blade Asymmetric Flapwise Pitch	0.667	0.669
6	1 st Blade Collective Flap	0.699	0.702
7	1 st Blade Asymmetric Edgewise Pitch	1.079	1.074
8	1 st Blade Asymmetric Edgewise Yaw	1.090	1.088
9	2 nd Blade Asymmetric Flapwise Pitch	1.934	1.651
10	2 nd Blade Asymmetric Flapwise Pitch	1.992	1.856
11	2 nd Blade collective Flap	2.020	1.960
12	2 nd Tower Fore-Aft	2.900	2.859
13	2 nd Tower Side-to-Side	2.939	2.941

In the following table we have reported the natural frequency of the scaled model using the scaling law defined before.

Table 2.4 Scaled model natural frequencies.

Mode	Description	FAST	ADAMS
1	1 st Tower Fore-Aft	10,523	10,377
2	1 st Tower Side-to-Side	10,134	10,276

3	1 st Drivetrain Torsion	20,153	19,793
4	1 st Blade Asymmetric Flapwise Yaw	21,644	20,449
5	1 st Blade Asymmetric Flapwise Pitch	21,680	21,716
6	1 st Blade Collective Flap	22,713	22,797
7	1 st Blade Asymmetric Edgewise Pitch	35,055	34,883
8	1 st Blade Asymmetric Edgewise Yaw	35,397	35,328
9	2 nd Blade Asymmetric Flapwise Pitch	62,806	53,614
10	2 nd Blade Asymmetric Flapwise Pitch	62,436	60,276
11	2 nd Blade collective Flap	65,625	63,664
12	2 nd Tower Fore-Aft	94,202	92,860
13	2 nd Tower Side-to-Side	95,364	95,517

In the scaled model the corner frequency of the low pass filter to be roughly one-quarter of the blade's first edgewise natural frequency is 8.12 Hz.

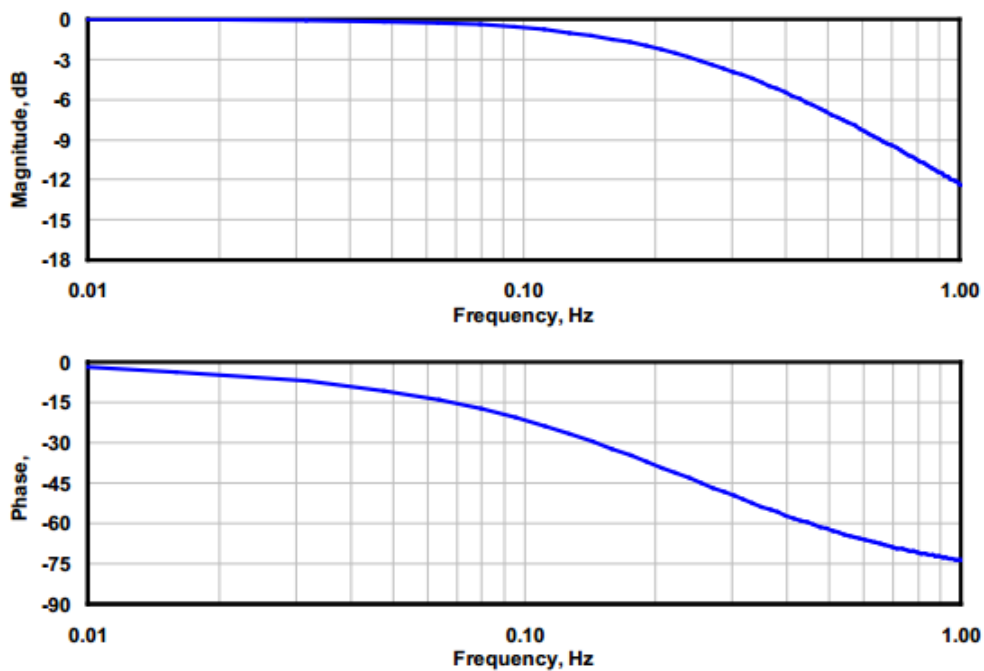


Figure 2.2 Bode plot of generator speed low pass filter frequency response.

Having all the information of our scaled model now we can pass to details of different components that are necessary for the design of the wind turbine. In the next chapter it is reported the details due to the selection of different components necessary for the wind turbine.

CHAPTER 3

COMPONENT SELECTION

In this chapter we will select different components necessary for creating the scale model of the wind turbine. For each component we will use the specific methodology to obtain the optimal choice. The first component is the pitch motor and gearbox that will be used for the blade pitch control. After that we will select motor for the power generation and the encoder to measure the rotational velocity and rotation of the blade. Then the ball bearings that are going to be used for the blade and drivetrain are going to be selected. The last component that is going to be selected in this chapter is the slip ring. The remaining components will be designed in the next chapter.

3.1 Pitch Motor Selection

3.1.1 Trajectory Planning

The first step to find the optimal motor is the trajectory planning [19], there are a lot of different trajectory models with different displacement, velocity and acceleration profiles, each of them have their benefits and weakness. We will use few of these profiles to see their influence on the velocity and acceleration, and the time that each one of them takes to arrive to the final position.

The use of motor in our case is just to rotate the blade from zero till a maximum value of 90 degrees. We know that in the normal working condition of the wind turbine the blade will rotate few degrees but we consider the worst case that there is a huge variation on wind speed and the blade has to rotate 90 degrees knowing that in real case it is recommended to don't have pitch angles higher than 25 degrees [20]. This overestimation is because of the fact that we will use the

Hypothesis of the collective pitch control for choosing the motor but we are interested also to use the independent pitch control IPC for our scaled wind turbine.

To define the trajectory that the blade has to follow, there are a lot of different standard trajectory profiles. We have chosen 3 of them and we will study one by one the influence of the chosen trajectory profile on the acceleration and velocity of the system.

As mentioned before the first parameter that we have fixed is the displacement of the blade that we decided to rotate 90 degrees. The second parameter that we are going to fix is the maximum rotational velocity of the blade. We know that the reference full scale NREL 5MW has a maximum pitch speed of $8^\circ/\text{second}$ [21]. Scaling this parameter with the scaling laws defined in the previous chapter we have:

$$\lambda_{pitch\ speed} = \lambda_\omega = \frac{\lambda_V}{\lambda_L} \quad (3.1)$$

The max pitch speed in the scaled model is $259.84^\circ/\text{second}=4.53\ \text{rad}/\text{second}$.

It is important to notice that the limitation of maximum pitch velocity is for the case of the NREL 5MW and this reference has used a collective pitch regulation. As in our case we are also interested on IPC (independent pitch control). We have to do further verification if the motor can guarantee the required movement due to the IPC control.

We will design the trajectory profiles in such a way that the maximum velocity of each profile under study arrives to the maximum value defined before ($4.53\ \text{rad}/\text{second}$). As each trajectory profile has its own velocity profile and consequently its own mean speed, each trajectory profile will achieve the final point in different unit of time. So the one that has a higher mean velocity arrives to final position faster than the one that has a lower mean velocity. And also the one that has lower arrival time to the final position will have a higher acceleration.

The first trajectory profile that we will study is the trapezoidal trajectory.

Trapezoidal trajectory is an approach for planning a trajectory computing linear segments joined with parabolic blends. In the linear tract, the velocity is constant while, in the parabolic blends, it is a linear function of time. In trapezoidal trajectories, the duration is divided into three parts:

- In the first part, a constant acceleration is applied, then the velocity is linear and the position a parabolic function of time.
- In the second, the acceleration is null, the velocity is constant and the position is linear in time.
- In the last part a (negative) acceleration is applied, then the velocity is a negative ramp and the position a parabolic function.

Usually, the acceleration and the deceleration phases have the same duration ($t_a=t_d$) Therefore, symmetric profiles, with respect to a central instant $(t_f-t_i)/2$, are obtained. In our case we have eliminated the second part to have the maximum acceleration variation in the middle part of the trajectory so the profile is less smooth possible (as we are using the trajectory profile just for verification). The equations to find the trajectory are shown below. This particular condition of the trapezoidal profile is called Triangular Velocity Profile.

$$y(t) = \begin{cases} y_i + \frac{\dot{y}_v}{2t_a} t^2 & 0 \leq t < t_a \\ y_f - \frac{\dot{y}_v}{t_a} \frac{(t_f - t)^2}{2} & t_f - t_a \leq t < t_f \end{cases} \quad (3.2)$$

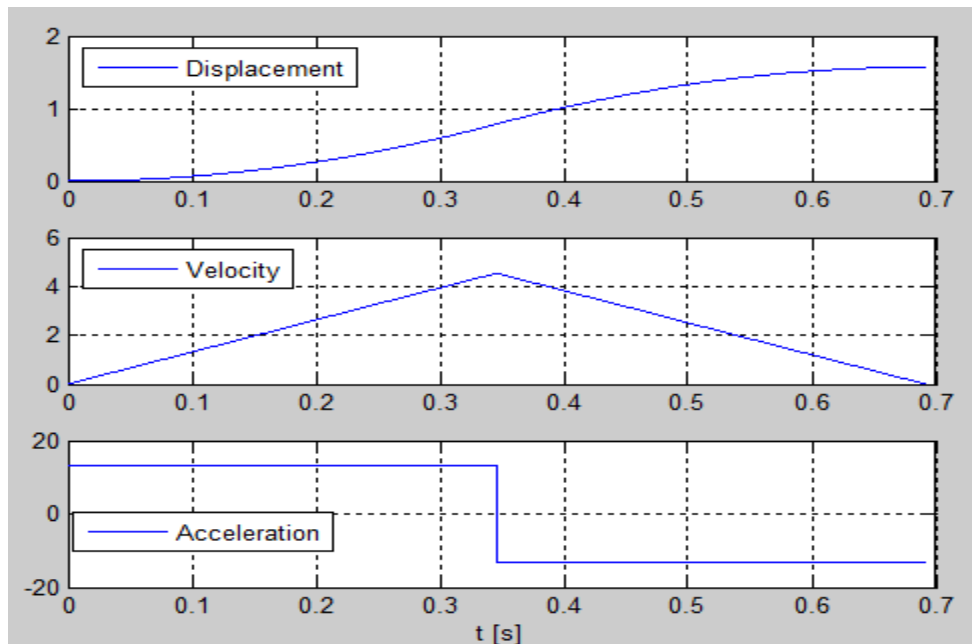


Figure 3.1. Displacement, Velocity and Acceleration of the Triangular Velocity Profile. Units are respectively [rad], [rad/s] and [rad/s²].

The second trajectory profile that we will study is the cyclical trajectory. This trajectory profile does not have any discontinuity in the velocity and acceleration profile to avoid any huge instantaneous variation on the inertia and velocity of the system. The cyclical trajectory is used in many industrial applications so we have decided to use it as one of our reference profiles for verification of the motor. In this trajectory profile the coefficient of velocity and the coefficient of acceleration are respectively 2 and 2π . The analytical expression is reported below.

$$\begin{cases} \dot{y} = c_a \frac{h}{t_a^2} \sin\left(\frac{2\pi t}{t_a}\right) \\ \dot{y} = \frac{h}{t_a} \left[1 - \cos\left(\frac{2\pi t}{t_a}\right)\right] \\ y = h \left[\frac{t}{t_a} - \frac{1}{2\pi} \sin\left(\frac{2\pi t}{t_a}\right)\right] \end{cases} \quad (3.3)$$

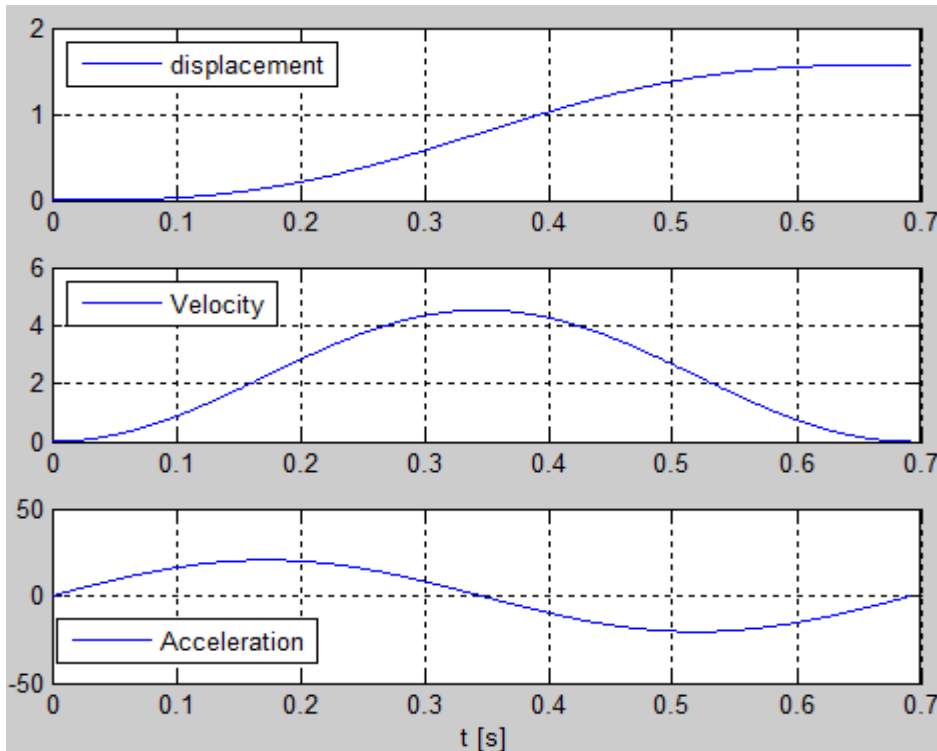


Figure 3.2. Displacement, Velocity and Acceleration of Cyclical trajectory profile. Units are respectively [rad], [rad/s] and [rad/s²].

S-Curve profile is basically a trapezoidal trajectory but it has been modified to achieve a smoother profile. We have used also this profile to verify our motor as its one of the mostly used profiles in robotics.

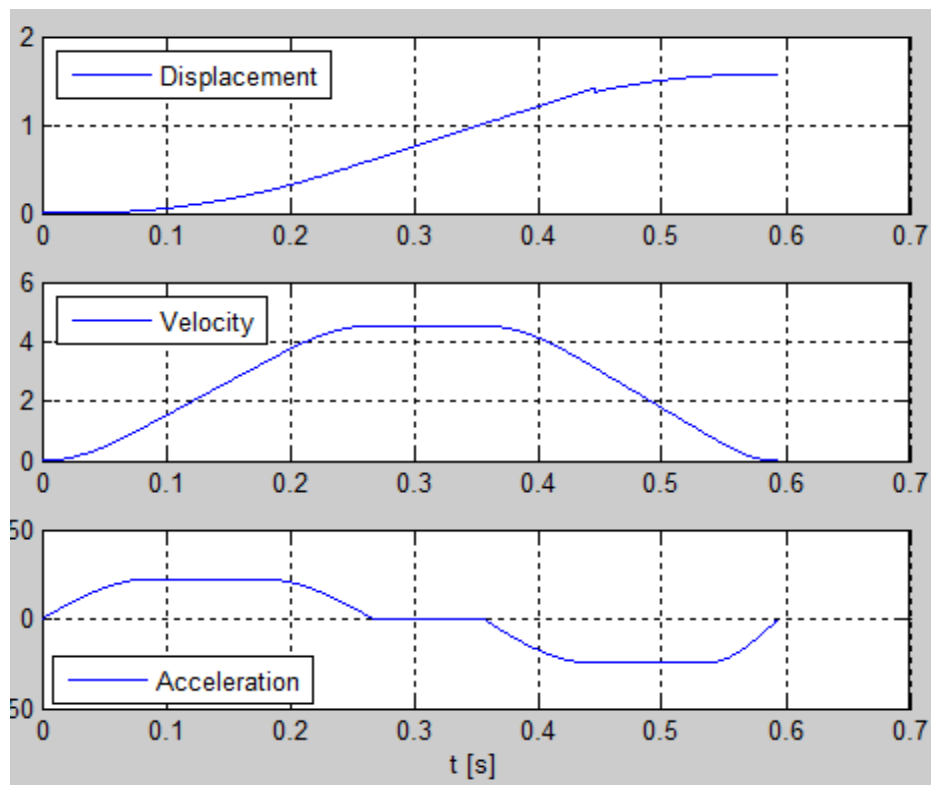


Figure 3.3. Displacement, Velocity and Acceleration of the S-Curve trajectory profile. Units are respectively [rad], [rad/s] and [rad/s²].

Now putting the profiles together we can see the difference in the velocity and acceleration behavior. An important point is that as shown in the plot and mentioned before the time that each profile takes to arrive to the final point is different.

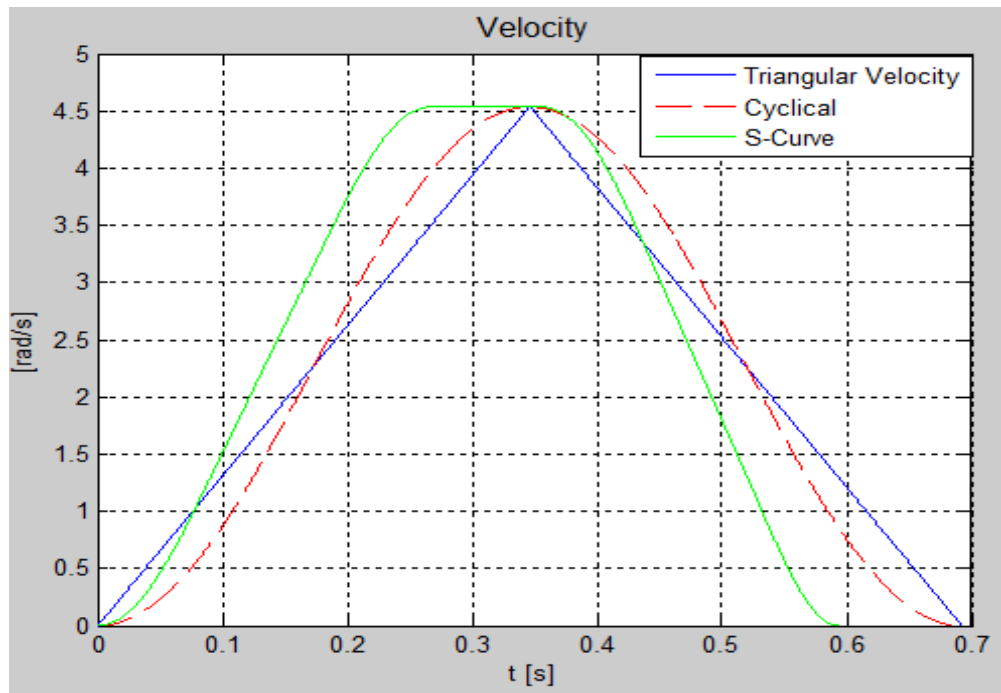


Figure 3.4. Comparison of the velocity behavior of 3 different trajectory profiles.

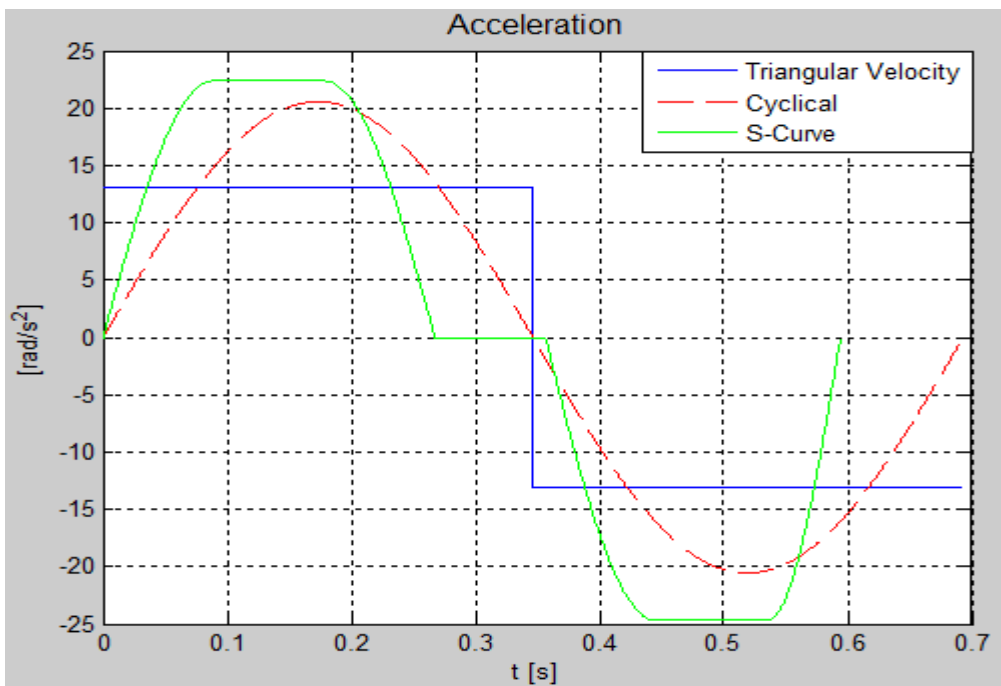


Figure 3.5. Comparison of acceleration behavior of 3 different trajectory profiles.

To find the time that each trajectory profile takes to arrive to the final position, we use the so called normalized mean velocity (non dimensional). To calculate this expression we use the following formula:

$$V_{mean_normalized} = \frac{\int V dt}{T V_{max}} \quad (3.4)$$

This value for each of the trajectory profiles is:

Triangular velocity profile=0.5005

Cyclical profile=0.5

S-Curve profile=0.5829

From the other side we can calculate the minimum time that a trajectory profile can achieve the final position. This is the case that we have a profile that proceeds the trajectory with a constant velocity equal to the maximum pitch speed equal to $259.84^{\circ}/second$. The value that we obtain is equal to:

$$T_{min} = 0.3464 S$$

Dividing the minimum time to the normalized mean velocity we obtain the effective time each profile takes to go from initial point to the final point.

$$T_{effective} = \frac{T_{min}}{V_{mean_normalized}} \quad (3.5)$$

Doing the calculations we find that the time that each one takes to arrive to the final point is:

$$T_{Triangular\ velocity} = 0.692 S$$

$$T_{Cycloidal} = 0.6927 S$$

$$T_{S-Curve} = 0.5942$$

These are the minimum values that can be achieved with each of the trajectory profiles. We can see that the S-Curve trajectory takes less time to arrive to the final point.

One of the important parameters that we will extract from the trajectory profiles to use for the selection of the motor is the mean quadratic value of the acceleration. This value is reported below for each of the trajectory profiles.

$$\ddot{y}_q = \sqrt{\frac{\int \dot{y}^2 dt}{T}} \quad (3.6)$$

$$\ddot{y}_{q_triangular\ Velocity} = 13.12 \frac{rad}{s^2}$$

$$\ddot{y}_{q_cycloidal} = 14.54 \frac{rad}{s^2}$$

$$\ddot{y}_{q_s-curve} = 17.83 \frac{rad}{s^2}$$

3.1.2 Motor Selection Method Formulation

These are the parameters that are going to be used by a method that finds the optimal motor [22]. This method puts together all of the limitations of choosing an optimal motor using two parameters (α, β), then it gives indications to find the optimal motor using the RMS value of acceleration. Below will find the equations that are used in this method.

In a motor we have:

$$\omega_r = \tau \omega_m \quad (3.7)$$

$$\dot{\omega}_r = \tau \dot{\omega}_m \quad (3.8)$$

Where τ is the transmission ratio between the motor and the system.

The equation to obtain the movement equilibrium on the system side is:

$$\frac{C_m}{\tau} - C_r = \left(\frac{J_m}{\tau^2} + J_r \right) \dot{\omega}_r \quad (3.9)$$

For choosing the transmission ratio τ and the actuator itself we will proceed as reported below:

$$C_m = \tau C_r^* + J_m \frac{\dot{\omega}_r}{\tau} \quad (3.10)$$

We know that:

$$C_{m,q}^2 = \int \frac{C_m^2}{t_a} dt = \int \left(\tau C_r^* + J_m \frac{\dot{\omega}_r}{\tau} \right)^2 \frac{dt}{t_a} = \int \left(\tau^2 C_r^{*2} + J_m^2 \frac{\dot{\omega}_r^2}{\tau^2} + 2J_m C_r^* \dot{\omega}_r \right) \frac{dt}{t_a} \quad (3.11)$$

So we obtain:

$$C_{m,q}^2 = \tau^2 C_{r,q}^{*2} + J_m^2 \frac{\dot{\omega}_{r,q}^2}{\tau^2} + 2J_m (\dot{\omega}_r C_r^*)_{mean} \quad (3.12)$$

For the thermal limitation of the motor C_n has to be:

$$C_n^2 \geq C_{m,q}^2 = \tau^2 C_{r,q}^{*2} + J_m^2 \frac{\dot{\omega}_{r,q}^2}{\tau^2} + 2J_m (\dot{\omega}_r C_r^*)_{mean} \quad (3.13)$$

In other words:

$$\begin{aligned} \frac{C_n^2}{J_m} &\geq \tau^2 \frac{C_{r,q}^{*2}}{J_m} + J_m \frac{\dot{\omega}_{r,q}^2}{\tau^2} + 2J_m (\dot{\omega}_r C_r^*)_{mean} = \\ \tau^2 \frac{C_{r,q}^{*2}}{J_m} + J_m \frac{\dot{\omega}_{r,q}^2}{\tau^2} + 2J_m (\dot{\omega}_r C_r^*)_{mean} - 2C_{r,q}^* \dot{\omega}_{r,q} + 2C_{r,q}^* \dot{\omega}_{r,q} &= \\ \left(\frac{\tau}{\sqrt{J_m}} C_{r,q}^* - \frac{\sqrt{J_m}}{\tau} \dot{\omega}_{r,q} \right)^2 + 2(\dot{\omega}_r C_r^*)_{mean} + 2C_{r,q}^* \dot{\omega}_{r,q} & \end{aligned} \quad (3.14)$$

The final expression is:

$$\frac{C_n^2}{J_m} \geq \left(\frac{\tau}{\sqrt{J_m}} C_{r,q}^* - \left(\frac{\sqrt{J_m}}{\tau} \dot{\omega}_{r,q} \right) \right)^2 + 2[(\dot{\omega}_r C_r^*)_{mean} + C_{r,q}^* \dot{\omega}_{r,q}] \quad (3.15)$$

We introduce a new parameter α named accelerator coefficient:

$$\alpha = \frac{C_n^2}{J_m} \quad (3.16)$$

And β as resistance coefficient:

$$\beta = 2[\dot{\omega}_{r,q} C_{r,q}^* + (\dot{\omega}_r C_r^*)_{mean}] \quad (3.17)$$

The β coefficient represents the resistance requirement from the actuator. Both of the coefficients have the same unit (W/s).

Now we introduce α & β in the equation [8] and we obtain:

$$\alpha > \beta + \left[C_{r,q}^* \left(\frac{\tau}{\sqrt{J_m}} \right) - \omega_{r,q}^* \left(\frac{\sqrt{J_m}}{\tau} \right) \right]^2 \quad (3.18)$$

The value of τ that minimizes the accelerator factor is the so called optimal transmission ratio:

$$\tau_{opt}^2 = J_m \frac{\dot{\omega}_{r,q}}{C_{r,q}^*} \quad (3.19)$$

According to this method the optimal choice for the motor is the one with nearest higher α value to β . So having the α value of all of the motors under

study and knowing the β of the system we can find the optimal choice for our system.

In the case that $\alpha = \beta$ the only transmission value that we can use is the optimal one defined in equation (3.19).

In case that $\alpha > \beta$ we can use the transmission value between τ_{min} and τ_{max} where:

$$\tau_{min}, \tau_{max} = \sqrt{J_m} \frac{\sqrt{\alpha - \beta + 4\dot{\omega}_{r,q} C_{r,q}^*} \pm \sqrt{\alpha - \beta}}{2C_{r,q}^*} \quad (3.20)$$

There is a limitation on τ from which we can't have lower values because the motor can't generate the required velocity.

$$\tau > \tau_p = \frac{\omega_{r,max}}{\omega_{m,max}} \quad (3.21)$$

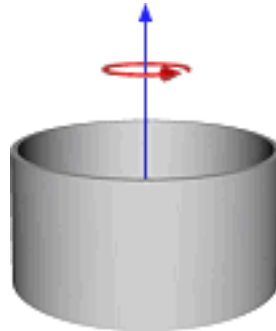
- If $\tau_p > \tau_{max}$ we have to choose a motor with higher τ_{max} .
- If $\tau_{min} < \tau_p < \tau_{max}$ we have to use a gearbox with $\tau_p < \tau < \tau_{max}$.
- If $\tau_p < \tau_{min}$ we can choose a gearbox with $\tau_{min} < \tau < \tau_{max}$.

At the end we can verify the result with the following inequality.

$$C_{m,max} > (\tau C_r^* + \frac{J_m}{\tau} \dot{\omega}_r)_{max} \quad (3.22)$$

3.1.3 Blade Inertia and Aerodynamic Loads

We have calculated the inertia of the blade considering that the blade is a thin cylinder with diameter equal to the maximum chord of the blade and having the same mass of the blade.



In this case the inertia of the blade [23] is equal to:

$$J = MR^2 \quad (3.23)$$

M=17740 kg, R=2,326 m.

The resulting inertia is 95978, 3 kgm^2 this value has to be scaled by the scaling factor λ_r .

The aerodynamic pitch torque that in our equations is the C_r , has been calculated dividing the total length of the blade in different sections. The sections are slightly bigger than the real one to ensure that in the case that the blades have any small modification in the dimension still our model is good enough. We have used 17 sections for the model using the length and chord reported in Table 3.1. The information of the blade in detail has been taken from the Q-Blade software [24] that has all of the information of the blades used for the NREL 5 MW wind turbine.

Table 3.1. Geometrical properties of the NREL 5 MW blade.

<i>Section</i>	<i>Sec 1</i>	<i>Sec 2</i>	<i>Sec 3</i>	<i>Sec 4</i>	<i>Sec 5</i>	<i>Sec 6</i>	<i>Sec 7</i>	<i>Sec 8</i>	<i>Sec 9</i>
<i>Length</i>	2.87	2.73	2.73	3.42	4.1	4.1	4.1	4.1	4.1
<i>Chord</i>	3.54	3.85	4.17	4.56	4.65	4.46	4.25	4.01	3,75
<i>Section</i>	<i>Sec10</i>	<i>Sec11</i>	<i>Sec 12</i>	<i>Sec 13</i>	<i>Sec 14</i>	<i>Sec 15</i>	<i>Sec 16</i>	<i>Sec 17</i>	
<i>Length</i>	4.1	4.1	4.1	4.1	4.1	3.42	2.73	2.73	
<i>Chord</i>	3.5	3.256	3.01	2.76	2.52	2.31	2.09	1.42	

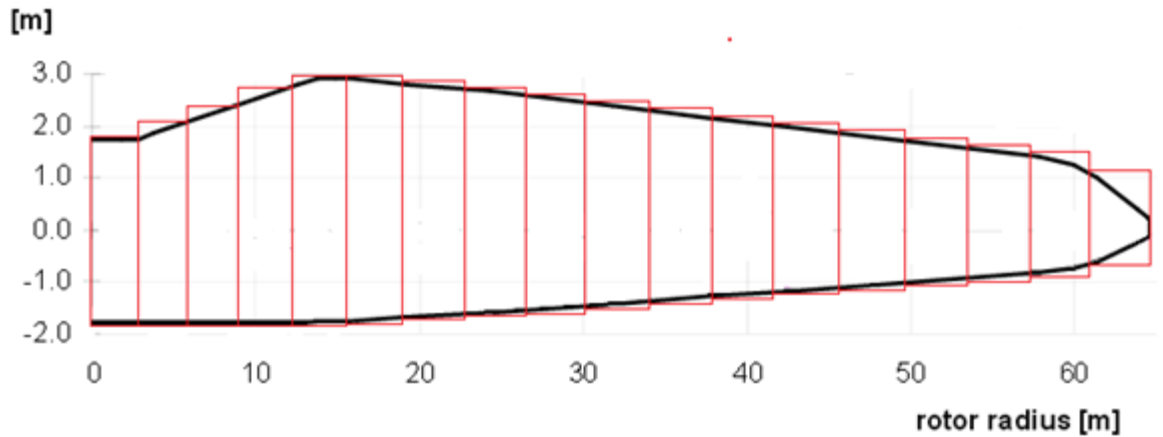


Figure 3.6. Blade section.

Now having the sections we can calculate the aerodynamic pitch moment that will be used for choosing the motor. For the aerodynamic force we have:[25]

$$T = \frac{1}{2} \rho C_M A b V_{rel}^2 \quad (3.24)$$

Where:

ρ =Density of Air

C_M =Aerodinamic Pitch Coefficient

A = Section

b = Chord

$$V_{rel}^2 = \sqrt{V_{wind}^2 + U_{rotor}^2} \quad (3.25)$$

The density of air is equal to $1,225 \frac{kg}{m^3}$ the chord of each section has been reported in Table 3.1. We have considered the drag coefficient in all of the sections equal to 0.5 that is rounded value of 0.487. This value is the maximum value of the drag coefficient of all of the sections [26]. Using this value we are over estimating the aerodynamic force. Below it has been reported the aerodynamic coefficients of the DU 40 Airfoil.

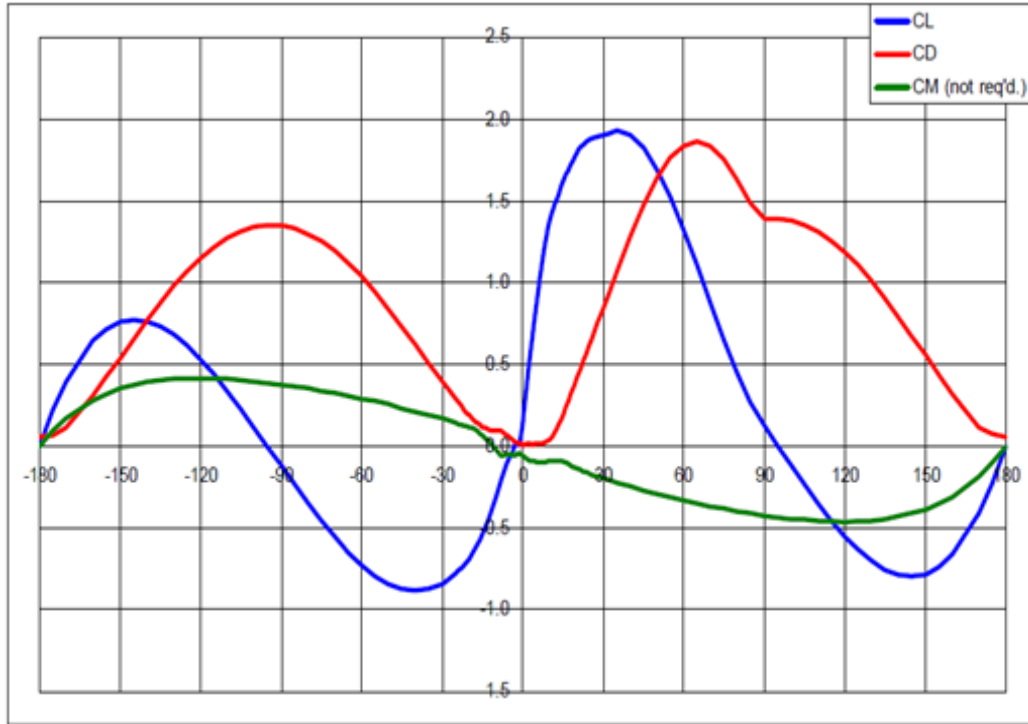


Figure 3.7. 3D corrected coefficients of the DU40 airfoil [9].

Calculating the aerodynamic force as explained before we have the total pitch moment equal to 564804 Nm this value has to be scaled with the following scaling factor that has been introduced in chapter 2.

$$\lambda_T = \frac{\lambda_m \lambda_L^2}{\lambda_t^2} \quad (3.26)$$

Scaling the aerodynamic moment we have $C_r = 0.9078$ Nm.

3.1.4 Motor, Gearbox and Encoder Selection

As seen before the method has two main parameters α and β . The procedure for choosing the motor has two steps the first step is to choose the motor that

has nearest higher α value to β . The second step consists on choosing a transmission ratio that is in the range of interest knowing that the best choice for the transmission ratio is the optimal one that equalizes the value of α and β .

In our case we have used as reference the DC-Micrometers of FAULHABER Company. The data are available on the www.faulhaber.com website [27].

We have verified 40 different motors and among them we have arrived to the optimal motor for our scaled wind turbine. One of our important limits is the limitation on dimension of the motor, as the diameter of the cylindrical part of our blade is less than 5 cm. We have to choose a motor that is compatible with the dimension of the blade, for this reason the biggest actuator that we have used in this analysis has diameter equal to 3.8 cm that is 1 cm less than the blade diameter.

The motors that we have used in our analysis have been reported below. The first column is the list of the motors that we have used, the second column is the maximum speed of the rotor of the motor. The third column is the inertia of the motor and the fourth column is the rated torque of each motor. The last two columns are for verifying which motors have the requirement from the point of view of (α, β) diagram and the transmission ratio limitation to generate the required speed.

Table 3.2. Characteristics of the motors studied for choosing the optimal pitch motor.

	<i>MOTORS</i>	$n_{MAX}(RPM)$	$J_M(gcm^2)$	$T_{Rated}(mNm)$	(α, β)	τ
1	0615N4,5S	24000	0.01	0.15	No	No
2	0816K0012SR	16000	0.049	0.61	Ok	No
3	1016N012G	22000	0.05	0.5	Ok	No
4	1024N012S	17000	0.12	1.3	Ok	No
5	1219N015G	19000	0.11	0.62	Ok	No
6	1224N012SR	16000	0.18	1.7	Ok	No
7	1319T012SR	17000	0.4	1.4	Ok	No
8	1331T012SR	12000	0.67	3.8	Ok	No
9	1336U012CXR	10000	0.57	3.6	Ok	No
10	1516T018SR	15000	0.4	0.93	No	No
11	1524T018SR	13000	0.66	2.8	Ok	No
12	1624T024S	17000	0.78	1.9	Ok	No
13	1717T024SR	16000	0.59	2.2	Ok	No
14	1724T018SR	10000	1	4.5	Ok	No

15	172700C	9000	1.3	5.1	Ok	No
16	1741006CRX	9000	1.8	8.8	Ok	Ok
17	2224U003SR	9000	2.4	2.2	No	No
18	2224U018SR	9000	2.8	6.8	Ok	Ok
19	2230T015S	11000	2.7	4.7	Ok	Ok
20	2230T003S	11000	3.7	2	No	No
21	2232U006SR	8000	4.8	10	Ok	Ok
22	2233T4.5S	10000	2.6	3.4	Ok	No
23	2233T012S	10000	2.2	5.9	Ok	Ok
24	2237S006CXR	8000	3.1	11	Ok	Ok
25	2342S006CR	11000	5.6	14	Ok	Ok
26	2342S036CR	11000	6.5	19	Ok	Ok
27	2642012CXR	7000	12	25	Ok	Ok
28	2642W024CR	7000	11	32	Ok	Ok
29	2657012CXR	7000	17	39	Ok	Ok
30	2657W012CR	7000	16	45	Ok	Ok
31	2657W024CR	7000	17	51	Ok	Ok
32	3242G024CR	6000	26	41	Ok	Ok
33	3257G024CR	7000	41	71	Ok	Ok
34	3272G012CR	6000	67	75	Ok	Ok
35	3272G024CR	6000	63	119	Ok	Ok
36	3863H012CR	7000	120	69	Ok	Ok
37	3863h024CR	7000	120	129	Ok	Ok
38	3890H018CR	6000	164	139	Ok	Ok
39	3890H024CR	6000	164	182	Ok	Ok
40	3890H036CR	6000	171	222	Ok	Ok

In the following figures we can see the α value of the motor that shows a function of the rated torque and the inertia of the rotor and β that is acceleration and torque imposed by the blade to the actuator. This plot has been reported for all the three trajectory profiles defined previously.

Now we are going to filter all of the actuators that have:

$$\beta > \alpha \quad (3.27)$$

Using the constant acceleration and cycloidal trajectories we see that we have to filter the actuator number 1,10, 17 and 20 in the list. The results of this verification is reported in the 5th column of the Table 3.2.

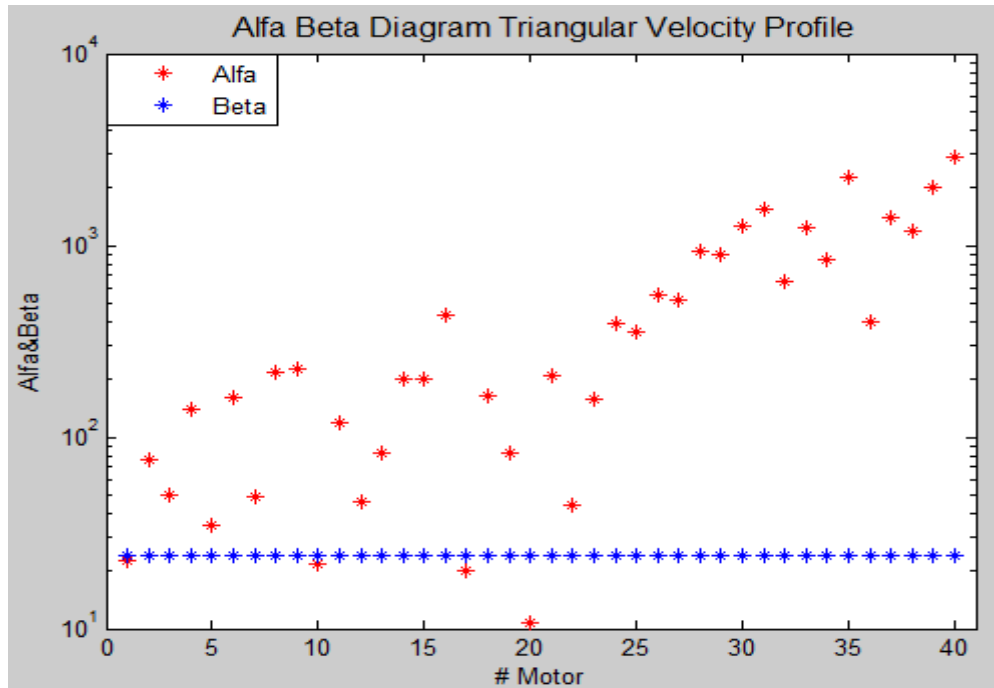


Figure 3.8. Alfa, Beta diagram of the triangular velocity profile for different motors.

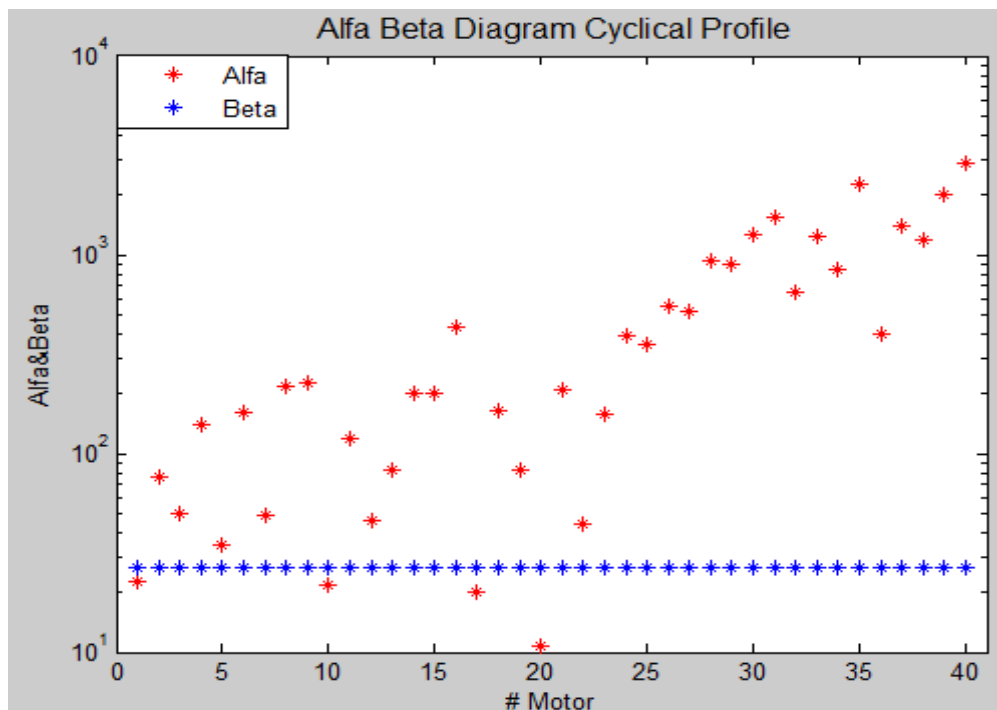


Figure 3.9. Alfa, Beta diagram of the cyclical profile trajectory for different motors.

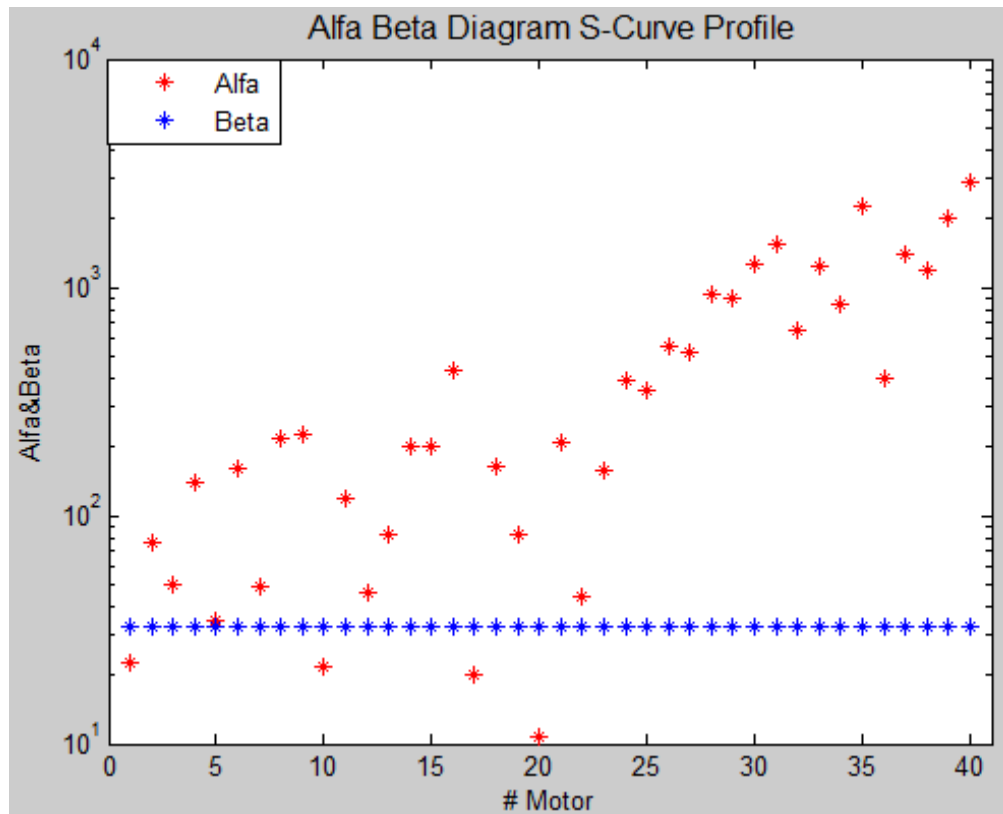


Figure 3.10 Alfa, Beta diagram of the s-curve trajectory for different motors.

The next step is to filter all of the actuators that can't generate the velocity required of the trajectory profiles. To verify this condition the τ_{max} should be higher than τ_p . If this condition is verified the actuator theoretically can generate the required velocity, Also if it is still dependent on the fact that the actuator is or isn't compatible with any gearhead in the available range. We are going to filter all of the actuators that do not satisfy this condition.

$$\tau_{max} < \tau_p \quad (3.28)$$

As reported in the Table 3.2 all of the actuators that don't verify this condition have been filtered. Furthermore the actuators that give a very small range of possibility for choosing τ have been filtered because of the fact that it is very difficult to find a gearhead that enters in the range of interest.

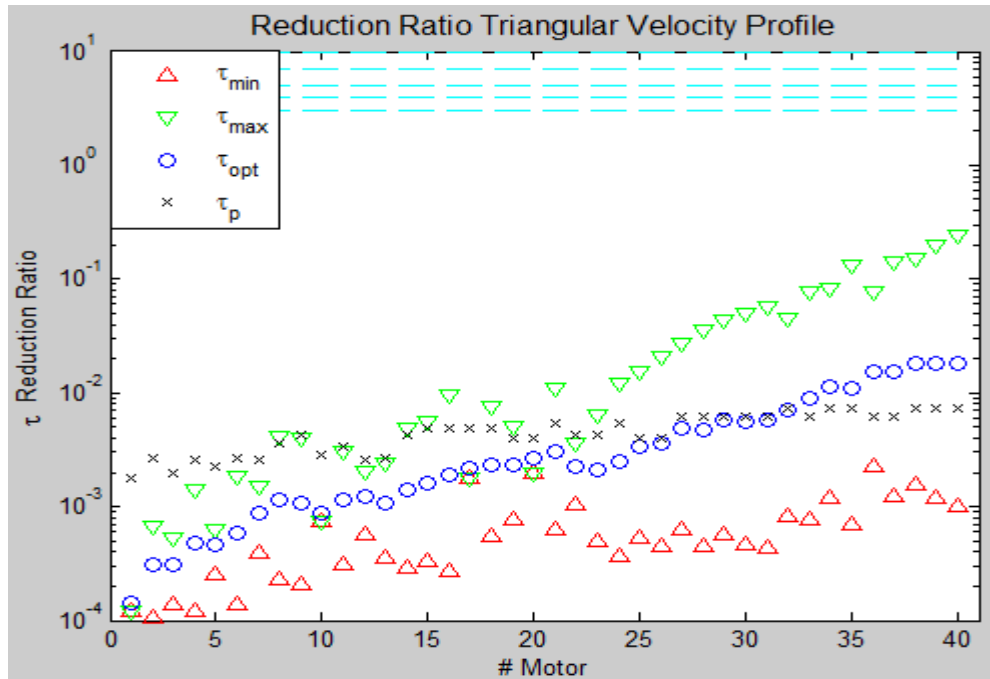


Figure 3.11. Reduction ratio limitation of the triangular velocity profile for each motor.

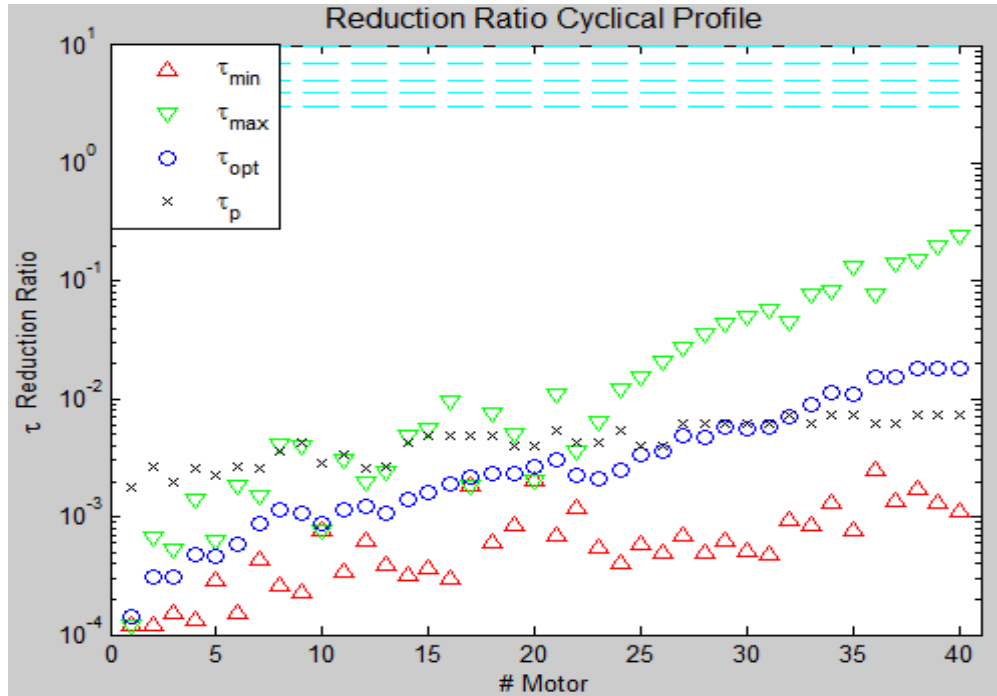


Figure 3.12. Reduction ratio limitation of the cyclical profile for each motor.

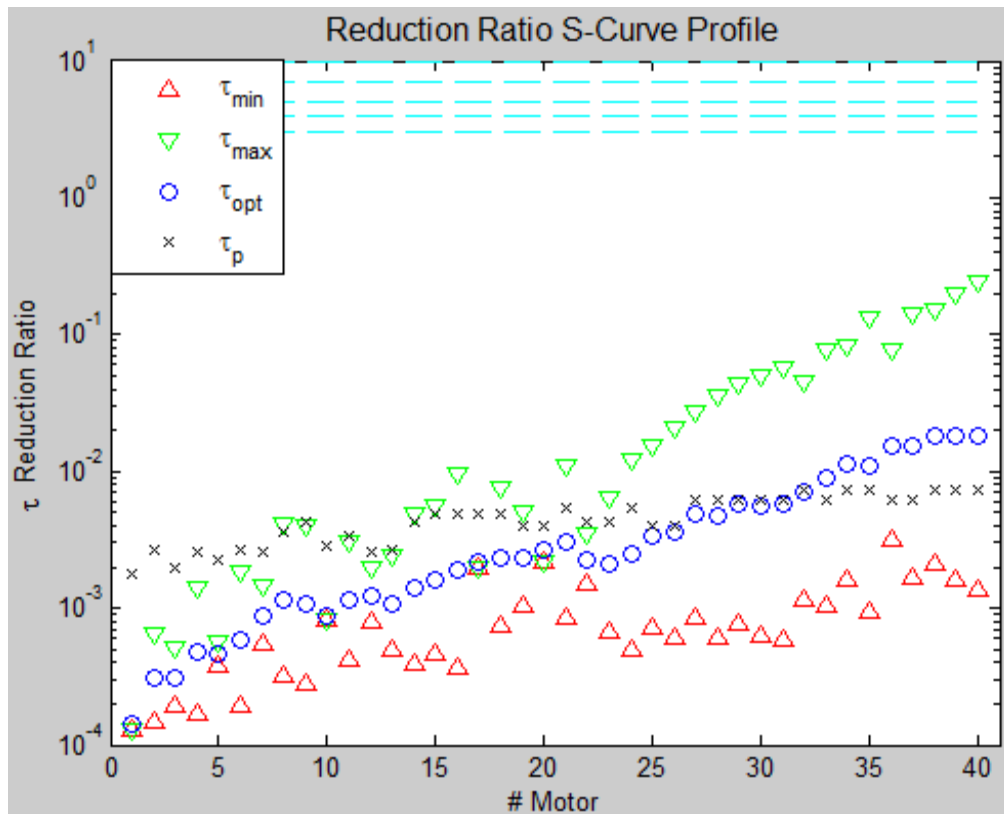


Figure 3.13. Reduction ratio limitation of the triangular S-curve profile for each motor.

Now theoretically the motor that is the best choice for our system among the remaining motors is the one that has α as near as possible to β . The only possible problem is if the gearhead compatible with the motor is not in our range of interest. Among the remaining motors, the motor number 18, 19 and 16 have the requirements to be our optimal choice, but as the range of τ is still small we choose the motor number 23 (2233T012S) that is a bit higher than our limits and gives a huge range of possibilities for the gearhead. Now we have to choose a gearhead that has the following characteristics.

$$\tau_p < \tau < \tau_{max} \tag{3.29}$$

Where $\tau_p = 0.00433$ and $\tau_{max} = 0.006463$

This motor is compatible with the following gearheads. 20/1, 22E, 22EKV, 22/7, 23/1, 22/2, 22/5.

We have selected a gearhead that has a $\tau = \frac{1}{190} = 0.0053$ this gearhead is a planetary gearhead from the 22/7 series with 4 stages and compatible with the motor that we have selected.

$$C_{m,max} > \tau C_r + \left(\frac{J_m}{\tau} + J_r \tau \right) \dot{\omega}_{r,max} \quad (3.30)$$

Note that $C_{m,max} = 0.0173 \text{ Nm}$ for the motor.

The value of the right side of the equation (3.32) using the $\tau = \frac{1}{190}$ gearhead and with the S-Curve trajectory profile is:

$$C_{m,max} = 0.0173 \text{ Nm} > 0.0058 \text{ Nm}$$

This is the optimal motor and gearhead that we could have chosen among the 40 motors under study.

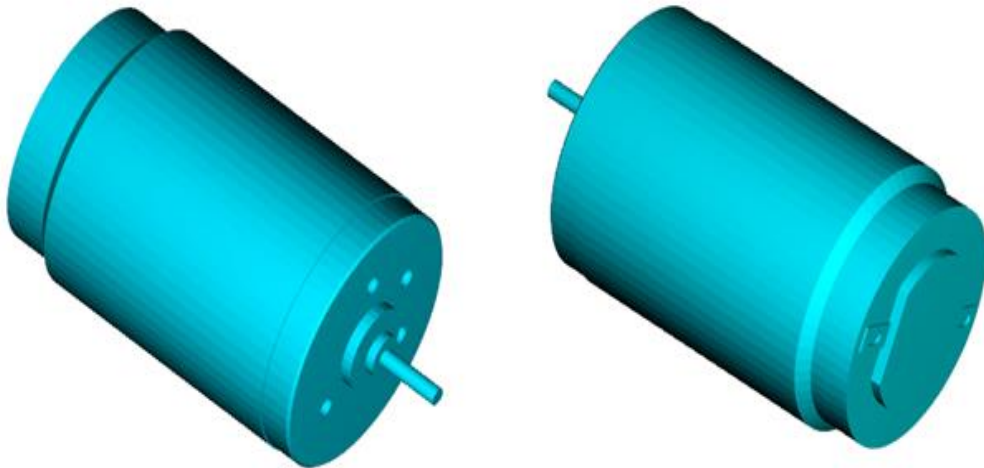


Figure 3.14. 3D view of the motor of the blade pitch control.



Figure 3.15. Motor of the blade pitch control.

The datasheet of the gearhead and the actuator have been reported in the Appendix B.

We have chosen the HEDS 5500 that is an optical encoder with 500 lines per revolution and 2 channels with digital output. The information of the encoder is reported in the Appendix B.

3.1.5 IPC Motor Check

We know from the previous section that the blade pitch motor can generate a maximum velocity equal to 10000 RPM and it has a gearhead with reduction ratio equal to $\frac{1}{190}$, so the maximum rotational velocity of the blade that the actuator can generate is 52.63 RPM. And the maximum frequency of the pitch motor is 0.877 Hz.

$$\text{Max frequency of pitch motor} = \frac{10000}{190 \times 60} = 0.877 \text{ Hz}$$

Now from the other side its note that the rotor rotational speed using $k=1.79$ is 393 RPM. The frequency of the rotor is equal to 6.55 Hz. If we want that the control system acts twice in each rotation of the rotor (as Usual IPC systems), the control system should act 13.1 times each second. So the frequency of control system is 13.1 Hz.

Knowing the maximum frequency of the motor it is easy to calculate that the pitch motor can generate 315.72 degrees /s.

So each time that the control system acts on the system, the motor can generate 24.1 degrees (24.1 degrees in 0.0764 second). This means that the maximum rotation of the blade for each rotation of the rotor is 44.2 degrees.

The resistance torque due to the aerodynamic forces has been considered constant and equal to $C_{r,max} = C_{r,n} = 0.0058 Nm$ in this working condition the nominal rotational velocity of the motor (referring to the motor curve) and the limitation of the gearhead is 4000 rpm. As a result the maximum rotation of the blade in the case that the turbine is working in the full load condition is 26.52 degrees for each rotation of the rotor. The summary has been reported in the Figure 3.16 .

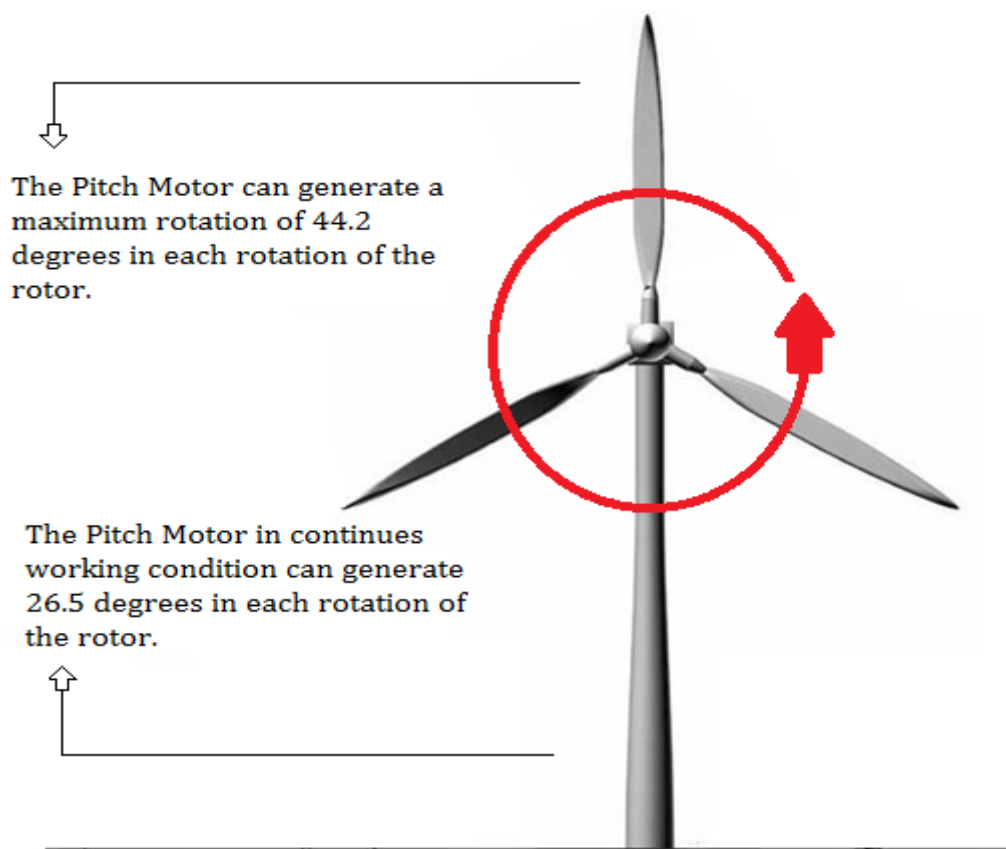


Figure 3.16. In this figure is reported the limitation of the pitch motor due to each rotation of the rotor.

Now we will investigate the problem from the other side, below we have reported one of the simulations of the pitch control on the DTU 10 MW wind turbine [28], [29]. The maximum variation of the blade pitch due to the pitch control is lower than 25 degrees and as shown in the figure this occurs in 600 second for the full scale. Scaling the time with our scaling laws and using the same blade coefficients we have that the same behavior will occur in 18.47 seconds. So the motor that we have chosen can generate movements with orders higher than the movement required from the control system.

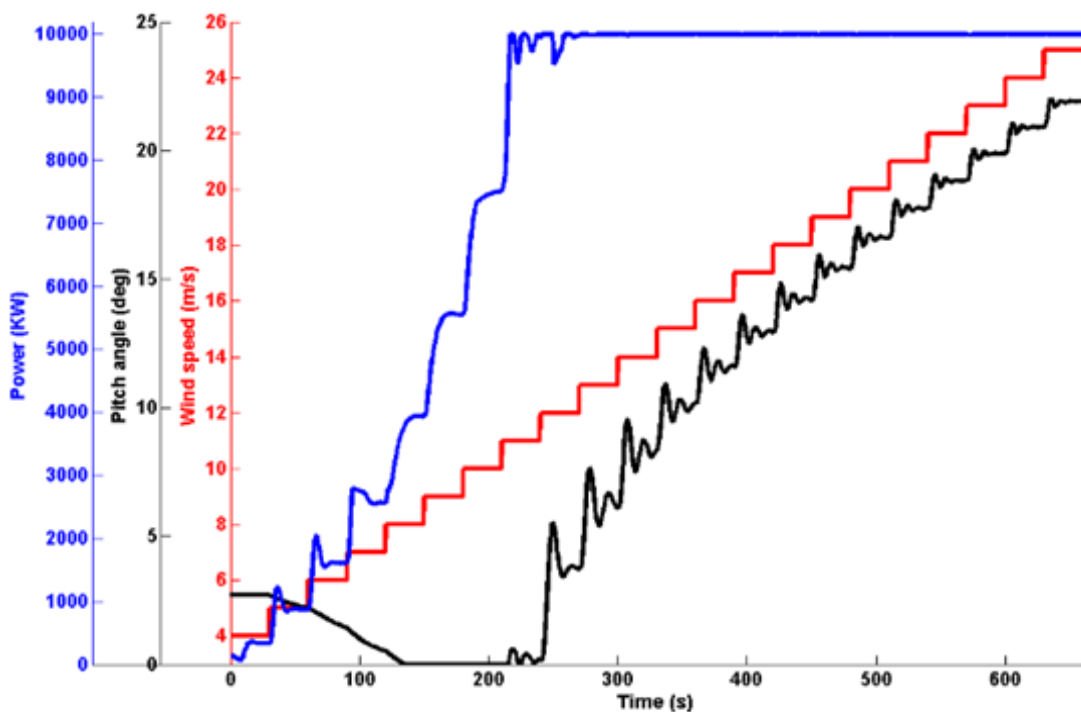


Figure 3.17. Blade pitch angles due to wind speed variation of the DTU 10 MW wind turbine [29].

3.2 Main Motor Selection

The aim of the main motor is to bring the rotor to the rated working condition and also by adding the necessary electronic equipment it can be used as

generator to simulate the real model. Because of this reason we will use a brushless DC motor that offers a higher control on the system behavior. A primary indication on the power of the motor that we have to choose is obtained by scaling with our scaling laws, the rated power of the full scale reference wind turbine.

$$\lambda_w = \frac{\lambda_m \lambda_L^2}{\lambda_t^3} \quad (3.31)$$

Using the power scaling law we obtain that the motor should have 277 W of rated power. Now we will do the calculations in detail and find the optimal motor that we can use for this objective.

3.2.1 Wind Turbine Inertia and Torque

The first step is to calculate the value of inertia of the blade, drivetrain and generator and the torque due to the aerodynamic forces on the blade. For the full scale model we have [11]

$$J_{Drivetrain} = J_{slow} + J_{gearbox} + (J_{break} + J_{HSS} + J_{generator})i^2 \quad (3.32)$$

This value is equal to $5.025 \cdot 10^6 \text{ Kgm}^2$ for the full scale wind turbine.

The inertia of the rotor as indicated in the reference is 36340000 Kgm^2 [11] and the inertia of the Hub is equal to 115926 Kgm^2 .

The total inertia is equal to 41481426 Kgm^2 .

$$J_{TOT} = J_{Drivetrain} + J_{Rotor} + J_{Hub} \quad (3.33)$$

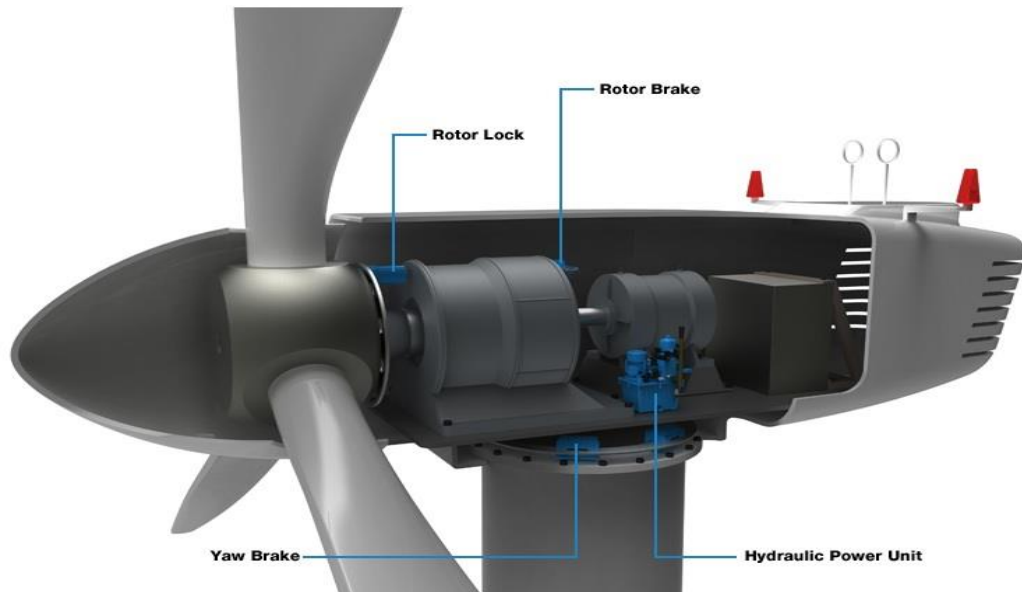


Figure 3.18. Brake units of a commercial wind turbine.

The aerodynamic torque in the rated power condition is equal to 3946000 Nm. Calculated as

$$C_r = i * \eta_{gear} * C_{Gen} \quad (3.34)$$

C_{Gen} =Generator Torque

The rated generator torque is equal to 43093 Nm and the gearbox ratio i is 97 with an efficiency η_{gear} of 94.4% [30].

For the scaled model we have:

$$C_r = 6,34 \text{ Nm and } J_{TOT} = 0.0632 \text{ Kgm}^2$$

3.2.2 Gearbox and Motor Selection

To choose the motor we have verified different producers of motors (Faulhaber, Maxon, Crouzet, Portescap, Canon, Delta, Belect, Teleco motion, Parker) the only ones that have motors in the range of power required for

our application are Parker [31] and portescap [32]. Also maxon has motors till 480 W but they are for application in oil and are not useful for our application. Furthermore the portescap provides possibility to have double shaft motor if required by the customer that can be useful for our application. In the following part we will do the calculation for choosing the motor [33].

The first step is to define the speed diagram for our motor. According to the reference [34], the acceleration time for the rotational speed of the rotor in the simulations is between 100 and 200 seconds in case of full scale wind turbine. Scaling this value we will obtain that the minimum acceleration time is 3 seconds. For the constant velocity section we know that this part should be long because it's the part in which the pitch control and power production are required. We decided to use 10 seconds for the second part because if we use higher values, we reduce the influence of the acceleration part. We don't consider the deceleration part (switch off) because we saw that in our case it is not too relevant.

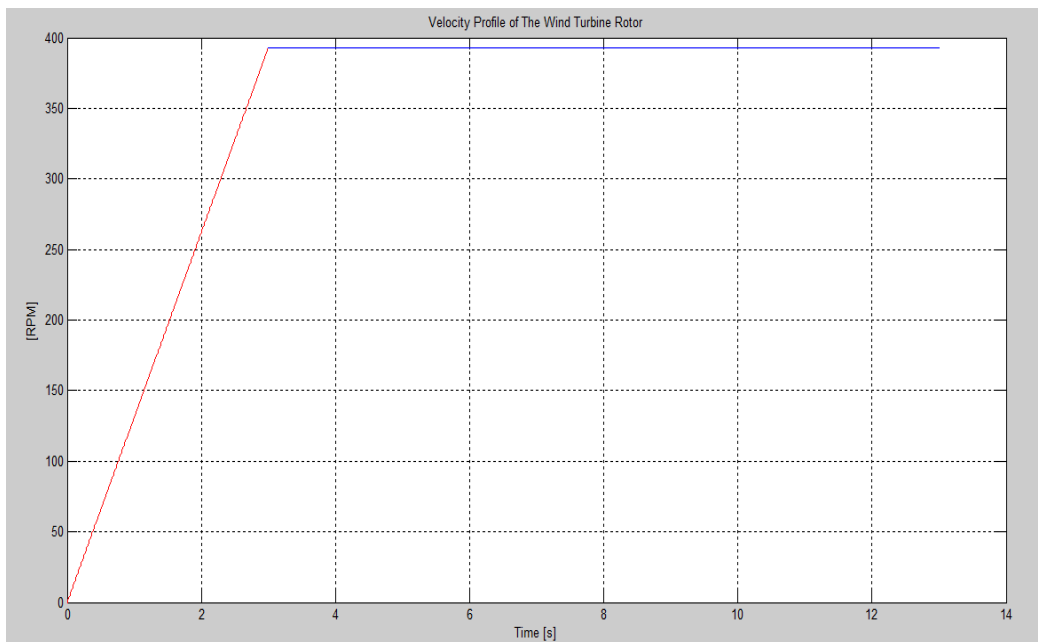


Figure 3.19. Velocity profile defined as the usual behavior of the rotor of the scaled model.

The torque required for acceleration is calculated as follows.

$$C_r = J_{TOT} \frac{\pi \Delta n}{30 \Delta t} = 0.0632 * \frac{\pi}{30} * \frac{393}{3} = 0.867 Nm \quad (3.35)$$

For different parts of motion we have

1) Acceleration phase: Duration 3 S 7.2 Nm

2) Constant speed: Duration 10 S 6.34 Nm

The peak torque occurs during acceleration phase. The RMS torque of the entire work cycle is:

$$C_{RMS} = \sqrt{\frac{1}{t_{tot}} (t_1 C_1^2 + t_2 C_2^2)} = 6.55 Nm \quad (3.36)$$

The maximum speed occurs at the end of the acceleration phase at maximum torque, thus the peak mechanical power is:

$$P_{max} = C_{max} n_{max} \frac{\pi}{30} = 296.7 W \quad (3.37)$$

$$C_{max} = 7.2 Nm$$

A gear box is required with a maximum continuous torque of at least $M_{RMS} = 6.55 Nm$ and an intermittent torque of at least equal to $C_{max} = 7.2 Nm$. a compatible gearhead with the requirements indicated before is NE34 of Parker Company with high efficiency and low weight. The recommended input of 4000 rpm allows a maximum reduction of:

$$i_{max} = \frac{n_{max,G}}{n_B} = 10.18 \quad (3.38)$$

The selection falls on gearhead with reduction ratio equal to 10:1. The efficiency of the selected gearhead is 98 % (from the catalog).

Once the gearhead is selected we proceed with the following steps to find the motor.

The speed and torque on the motor shaft are calculated as follows:

$$n_{motor} = i * n_B = 10 * 393 = 3930 \text{ rpm} \quad (3.39)$$

$$C_{mot,rms} = \frac{C_{rms}}{i * \eta} = 0.669 \text{ Nm} \quad (3.40)$$

$$C_{mot,max} = \frac{C_{max}}{i * \eta} = 0.736 \text{ Nm} \quad (3.41)$$

The selection falls on the BE232F, the only problem is the weight of the motor, because we have limitation on the weight of the Nacelle so we have 2 options, the first option is to use an efficient cooling system that permits the use of BE231D that has a $C_{mot,rms}$ slightly lower than required one, the other choice is to use the portescap B1515 series. This company provides also possibility to have a dual axis motor if required by the customer that can be useful for our application.

3.3 Bearing Selection

We have used 2 ball bearings for the connection of the drivetrain and nacelle to minimize the friction of the rotor and to ensure the structural strength of the model. We have used the SKF company [35] products as reference for our ball bearing selection. We don't have limitation on external diameter of the ball bearing. The internal diameter is 20mm (equal to the external diameter of the drivetrain shaft). As reported below, the rotational speed limit and the load limitation of the ball bearing is very higher than the requirements for our case. The selection in this case falls on the 61904 bearing that is a single row deep groove ball bearing. The internal diameter is 20 mm the external diameter is 37mm and the width of the ball bearing is 9mm, the rotational speed limit is 43000rpm that it higher than the rotational speed of the shaft.



Deep groove ball bearings, single row

Principal dimensions			Basic load ratings		Speed ratings	Limiting speed	Designation
d	D	B	dynamic C	static C0	Reference speed		
mm			kN		r/min		* SKF Explorer bearing
20	37	9	6,37	3,65	43000	26000	61904

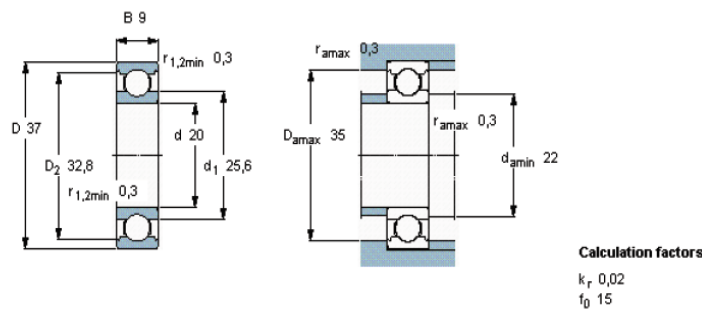


Figure 3.20. Technical information of the bearings used to connect the drivetrain to the nacelle.

It has been used 2 ball bearings, for the proposed layouts in chapter 4. The first bearing is a deep groove single row ball bearing that is going to be used in the first blade layout configuration. The second bearing is a thrust ball bearing that is used in the second blade layout configuration. The details of both of the bearings has been reported below.



Deep groove ball bearings, single row

Principal dimensions			Basic load ratings		Speed ratings	Limiting speed	Designation
d	D	B	dynamic C	static C0	Reference speed		
mm			kN		r/min		* SKF Explorer bearing
15	24	5	1,56	0,8	60000	30000	61802-2Z

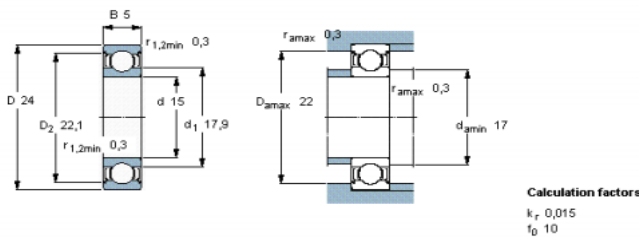


Figure 3.21 Technical information of the bearing used in the blade (First Blade Layout).



Thrust ball bearings

Principal dimensions				Basic load ratings		Speed ratings		Designations	
d	D	H	H1	dynamic C	static C0	Reference speed	Limiting speed	Bearing	Seat washer
mm				kN		r/min		-	
30	60	21	-	35,8	65,5	3800	5300	51306	-

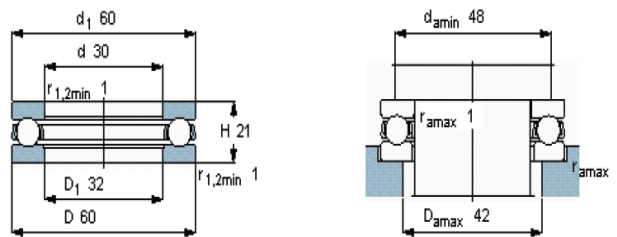


Figure 3.22. Thrust bearing used in the blade, hub connection (Second Blade Layout)

3.4 SLIP RING SELECTION

As we are interested in controlling all of our motors (main motor & 3 blade pitch motors) we have to transfer data from the rotating shaft to the off board electronic equipment, transferring data of the encoders, measurement systems, control signals and, etc. This problem can be solved by using a slip ring. As we don't know exactly the number of the signals that have to be transferred, we decided to use a slip ring with number of channels higher than the usual slip rings used in scaled wind turbines. As usually the size of the slip ring depends on the number of channels that the slip ring can transfer, in case that later on it is decided to use a smaller slip ring, we will not have to change the dimensions of the Nacelle. The second reason that we have used a 56 channel slip ring is due to the fact that we are interested in the IPC. So each motor has to be controlled independently and the control needs more channels for the control signals. Below it has been reported the table of the technical information and the details of the slip ring that we have used for our model.

Table 3.3. Technical data of the slipring.

Technical Data			
Circuits No	2~56(Pls refer to below table)	Current	standard 10A per circuit,2A(signal) per circuit, optional 20A per circuit
Voltage	440 VDC/VAC	Max speed	600RPM
Through hole size	25.4mm(or <=25.4mm)	OD	86mm
Housing material	AL alloy	Torque	0.1N.m;+0.03N.m/6 circuits
Working life	> 80millions revolutions(depends on working speed,environment)	Contact material	Precious metal:gold-gold
Electrical Noise	< 10mΩ @6VDC,50mA,5RPM	Contact Resistance	<20mΩ(AWG16#,300mm)
Dielectric Strength	800VDC@50Hz,10s	Lead wire Spec	UL Teflon@Awg22,Awg16
Insulation Resistance	1000MΩ@600VDC,10s	Lead wire length	300mm
Work Temperature	-40°C to 85°C	IP grade	IP51
Mechanical vibration	MIL-SID-810E	Work Humidity	10% to 85% RH
Material	RoHS compliant	CE certificate	YES

This slip ring is a through pass slip ring .The bore size of the slip ring is equal to the external diameter of our shaft but still if we have any variation on the size of the shaft the bore of the slip ring can be smaller using the equipment that is already in the market that can regulate the size of the slip ring bore. The limitation on the maximum rotational velocity of the slip ring is 600 RPM that is higher than the 393 RPM of our maximum rotational speed.

CHAPTER 4

WIND TURBINE LAYOUT

We have used Autodesk Inventor [36] to design the blade, tower, drivetrain, and all of the components of our scaled wind turbine. In the following figures the layout of the blade in our scaled model has been reported. The blade overall mass as reported in the scaled model chapter is around 100g, but as it is almost impossible to respect both scaling the mass and the natural frequencies of the scaled model, Usually it has to be decided which one is more important to observe. As the natural frequencies of the system influence directly the dynamic behavior of the system, in the design of the blade and also other components it is important to observe the natural frequencies rather than the mass of the components, in case that is impossible to respect both of them.

4.1 Blade and Hub Layout

In this section we will propose 2 different layout designs for the wind turbine blade and hub. As the design of the blade and hub in the wind turbine are dependent on each other, we have decided to propose for each blade layout a hub that is more compatible with the blade design. One important parameter in the design of the blade is the load acted on the system that has to be transferred to the hub and then to the tower, so the first step in our design is to calculate all of the components of the force acted on the wind turbine to take in consideration of the layout design.

4.1.1 Blade Loads

As it is important that all of the blade components (Motor, Gearbox, Fixing Components and, etc.) resist the load of the aerodynamic force and the weight of the blade itself, we have to calculate the forces that are acted on the blade and verify one by one the strength of the components to these forces. The first component is the motor and gearbox. The limitation of the axial and radial force of the gearbox are respectively 170N and 150N as reported in the gearbox catalog in the APPENDIX B. The torsional moment has been verified in Chapter 3. The problem is the bending moment that the motor does not give any indication, so it has to be verified if the gearbox shaft can resist the bending moment or not.

4.1.2 Aerodynamic Load on the Blade

We have used the blade sections defined in Chapter 3 and calculated the overall blade lift and drag force. It has been reported below the table containing all of the information relative to the lift and drag coefficients, the dimension of the blade sections and the relative velocity of the blade in the rated wind velocity of 25m/s and in the rated rotational velocity of the rotor(For the full scale model).

Table 4.1. Blade Characteristics used to calculate the load on the blade.

	<i>Distance</i>	<i>Distance From HUB</i>	<i>chord</i>	<i>Section</i>	<i>Lift Coefficient</i>	<i>Drag Coefficient</i>
<i>Sec 1</i>	4,4	2,8	3,5	10,1	1,9	1,86
<i>Sec 2</i>	7,1	5,6	3,8	10,5	1,9	1,86
<i>Sec 3</i>	9,8	8,3	4,2	11,4	1,9	1,86
<i>Sec 4</i>	13,2	11,7	4,5	15,6	1,9	1,86
<i>Sec 5</i>	17,3	15,8	4,6	19,1	1,9	1,86
<i>Sec 6</i>	21,4	19,9	4,4	18,3	1,9	1,86
<i>Sec 7</i>	25,5	24,0	4,2	17,4	1,9	1,86
<i>Sec 8</i>	29,7	28,1	4,0	16,4	1,9	1,86
<i>Sec 9</i>	33,7	32,2	3,7	15,4	1,9	1,86
<i>Sec 10</i>	37,8	36,3	3,5	14,3	1,9	1,86
<i>Sec 11</i>	41,9	40,4	3,2	13,3	1,9	1,86
<i>Sec 12</i>	46,0	44,5	3,0	12,3	1,9	1,86
<i>Sec 13</i>	50,1	48,6	2,7	11,3	1,9	1,86
<i>Sec 14</i>	54,2	52,7	2,5	10,3	1,9	1,86

Sec 15	57,6	56,1	2,3	7,9	1,9	1,86
Sec 16	60,4	58,9	2,0	5,7	1,9	1,86
Sec 17	63,1	61,6	1,4	3,9	1,9	1,86

	<i>Air Dencity</i>	<i>Relative Velocity</i>	<i>Lift Force</i>	<i>Drag Force</i>	<i>Bending Moment</i>
Sec 1	1,2	25,6	7865,2	7589,6	34345,3
Sec 2	1,2	26,5	8786,0	8478,1	62381,0
Sec 3	1,2	27,9	10499,5	10131,5	103244,4
Sec 4	1,2	30,1	16682,0	16097,4	221037,1
Sec 5	1,2	33,3	24974,2	24098,9	433301,8
Sec 6	1,2	36,9	29447,5	28415,5	631648,9
Sec 7	1,2	40,9	34434,1	33227,3	879790,6
Sec 8	1,2	45,1	39524,9	38139,8	1171916
Sec 9	1,2	49,5	44546,3	42985,2	1503439
Sec 10	1,2	54,1	49617	47878,2	1878003
Sec 11	1,2	58,7	54415,7	52508,8	2282741
Sec 12	1,2	63,5	58749,6	56690,8	2705422
Sec 13	1,2	68,3	62425,7	60238,1	3130653
Sec 14	1,2	73,1	65251,1	62964,5	3539876
Sec 15	1,2	77,2	55681,1	53729,8	3210946
Sec 16	1,2	80,5	43662,1	42132,0	2637196
Sec 17	1,2	83,8	32185,0	31057,1	2031949

The overall lift force, drag force and bending moment is respectively the sum of the last 3 columns of the table. Obviously these values should be scaled using the force scaling factor and torque scaling factor defined in the Chapter 2. The final values for the scaled model are:

Lift Force=59.5N

Drag Force=57.4N

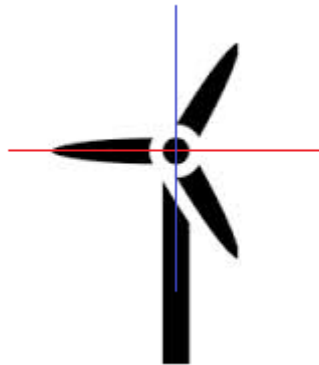
The resulting force is equal to

$$F = \sqrt{F_{Lift}^2 + F_{Drag}^2} = 82.7N \quad (4.1)$$

The bending moment of the resulting force is equal to 42.5Nm

4.1.3 Blade Weight

If we consider the case that we will not respect the mass scaling law of the blade (As mentioned before the reason) and rather than using the 100g limitation of the scaling law we use 500g as the overall weight of the blade, we will have that in case that the blade is aligned with the blue line in the figure below. The total weight will influence the axial component of the shaft and in case that the blade is aligned with the red line the mass will influence purely the radial component.



So in the worst case the mass of the blade can influence the shaft of the gearbox with the following component.

Axial Force=5N

Radial Force=5N

Bending Moment=2.6Nm

Putting together the component due to the weight of the blade and the aerodynamic force we have:

Total Axial Force=5N

Total Radial Force=87.7N

Total Bending Moment=45.1Nm

4.2 Blade First Layout Configuration

In the Figure 4.1 it has been reported the primary layout of the blade. The length of the blade is 1.06 m and the diameter of the cylindrical part of the blade that contains the components inside the blade is around 6cm the length of the cylindrical part should be at least 9cm to contain all of the components that are used inside the blade.



Figure 4.1. Blade Layout.

4.2.1 Blade Fixing Components

Below is reported the 2 main components that connect the motor, gearbox and the encoder to the blade. The blade fixing component is connected to the blade and it will be connected with 6 bolts to the component reported in Figure 4.2 (Pitch Motor Fixing Component) .the package of gearbox motor and encoder will be connected with 3 bolts to the pitch motor fixing component.



Figure 4.2. Pitch Motor Fixing Component

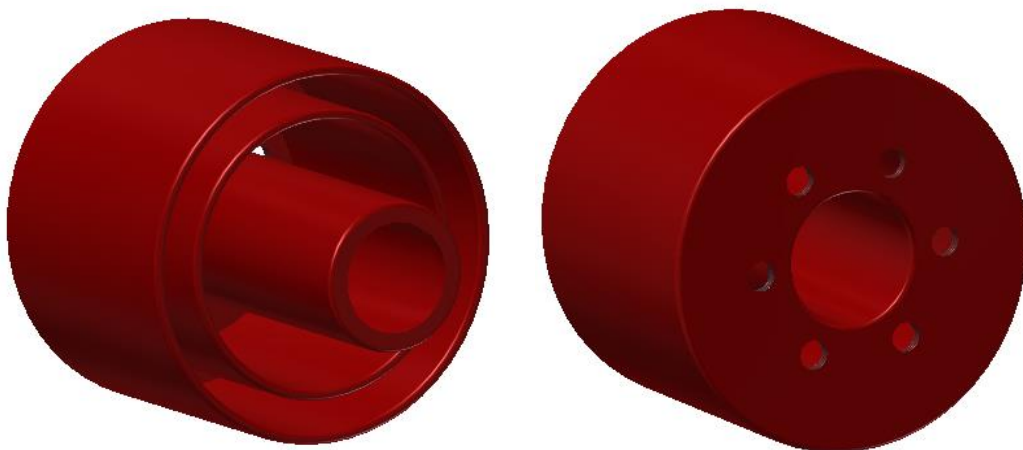


Figure 4.3. Blade Fixing Component

As reported in Figure 4.1 all of the Axial force, Radial force and the bending moment due to the aerodynamic force and the weight of the blade is acted on the shaft of the gearbox that will transfer it to the Hub. As discussed before the Gearbox can resist the axial and radial force of the load, but it has been verified that the gearbox shaft cannot resist the bending moment. To overcome this problem we have proposed the B.M.A (Bending Moment Absorber) that will be discussed in the next section.

4.2.2 Blade Bending Moment Absorber

To solve the problem of bending moment that is acted on the gearbox shaft we have designed a component to absorb the bending moment of the shaft and transfer it to the Hub. We have called this component B.M.A or Bending Moment Absorber. In Figure 4.4 is reported the design of be B.M.A, this component is connected to the secondary shaft trough a bearing that has been selected before (Chapter 4), the bearing is connected to the rotating shaft. As the deformation of the B.M.A is less than the shaft, it resists to the deformation of the shaft and absorbs the load from the motor.

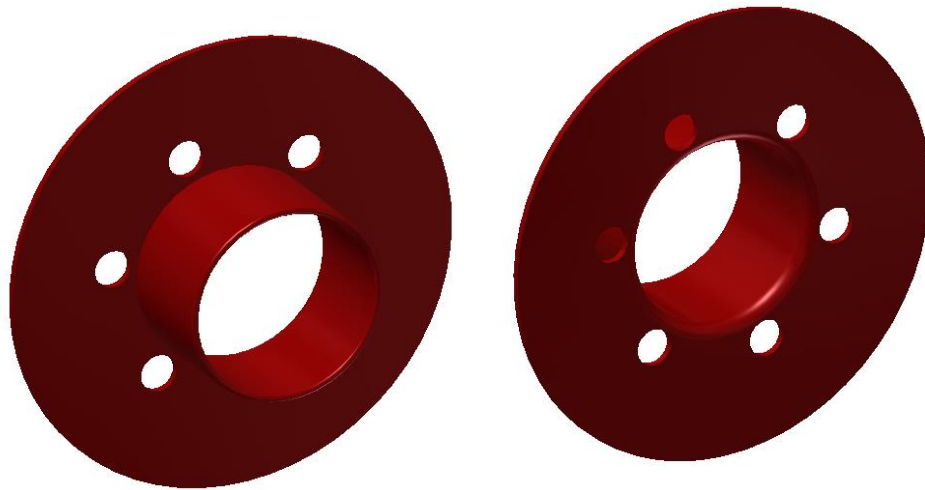


Figure 4.4. Blade bending moment absorber layout.

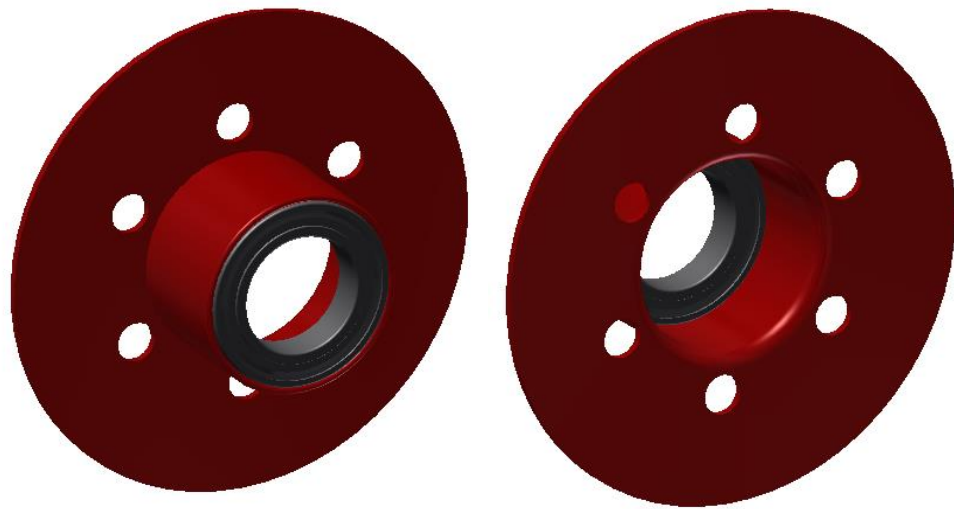


Figure 4.5. In this figure is reported the B.M.A connected to the bearing that will be connected to the secondary shaft

To the shaft of the blade is connected a secondary shaft that has a diameter equal to 15mm (9mm more than the gearbox shaft). As the B.M.A is designed in such a way to have higher inertia with respect to the gearbox shaft (less deformation and more rigidity), the load is transferred to the hub trough the B.M.A rather than the shaft of the gear box. Below is reported the B.M.A the bearing and the secondary shaft that connected the hub to the blade bypassing the loads from the motor.

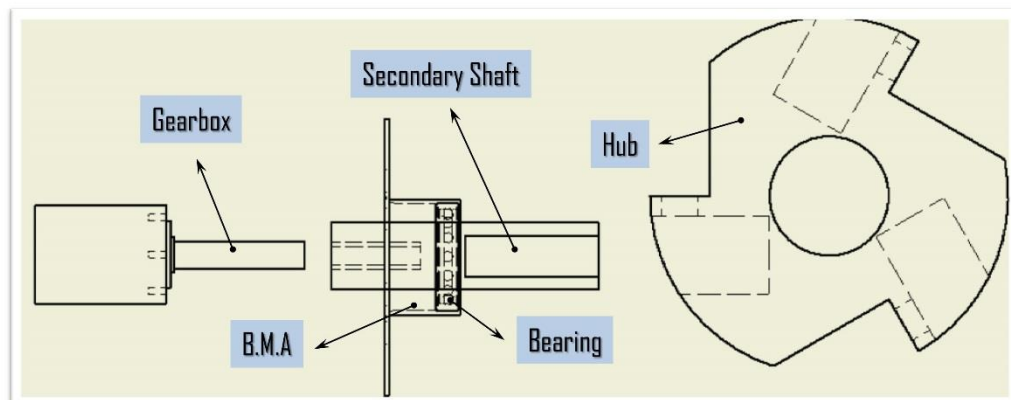


Figure 4.6 Gearbox, B.M.A, Secondary shaft, Hub connection

4.2.3 FEM Analysis

As the most excited components of our blade are the B.M.A and the secondary shaft that transfer the aerodynamic load to the Hub, it has to be done a FEM analysis to verify if these 2 components can resist to the loads that are calculated in the blade load section.

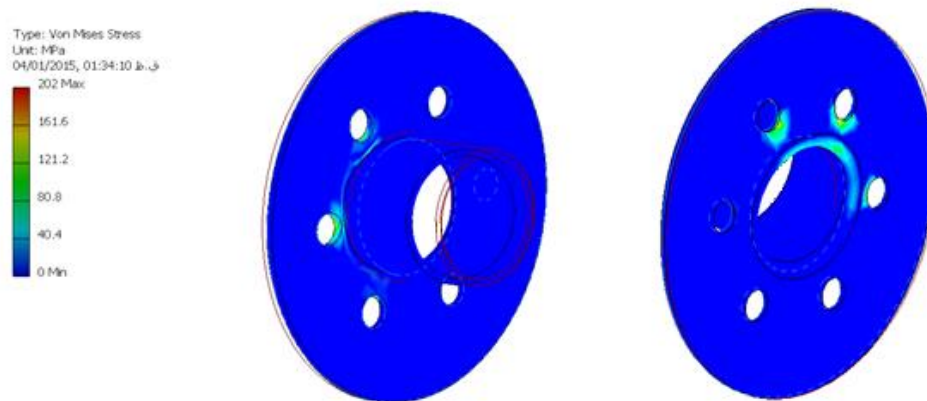
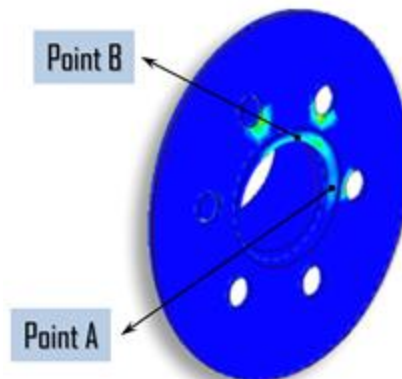


Figure 4.7. FEM analysis of the B.M.A

As shown in the figure the most excited section of the B.M.A is the circular section of the tube near to the bolts. Below it has been reported the values of the tensions in two different points of the circular section.



The tension of the point A and point B of the B.M.A has been reported Below. The σ_{tot} is due to the sum of the Bending moment and the axial force acted on the blade. As in the point A the bending moment component is zero the only contribute is due to axial force that is 5N. In the point B the value of bending

moment is not zero (because of the distance from the CM) for this reason the value of the σ_{tot} is higher than point A

Point A

$$\sigma_{tot} = 0.3 \text{ MPa}$$

$$\tau_{xy} = 1.3 \text{ MPa}$$

Point B

$$\sigma_{tot} = 49.7 \text{ MPa}$$

$$\tau_{xy} = 0 \text{ MPa}$$

Now using the Von Mises Criteria for the point B we have

$$\sigma_o = \sqrt{(\sigma^2 + 3\tau^2)} = 49.7 \text{ MPa}$$

This value is less than the limitation of the steel with a very good security factor so we don't have structural problems due to the aerodynamic loads and the weight of the blade.

The second component that has to be verified is the secondary shaft that is the component connected to the hub and transfers the bending moment from the B.M.A to the hub. Again we have considered two points on the section of the shaft one on the center of mass of the shaft (Point A) and one on the surface of the shaft (Point B) then we have calculated the tension for both of the points and the result has been reported below:

Point A

$$\sigma_{tot} = 0.3 \text{ MPa}$$

$$\tau_{xy} = 1.98 \text{ MPa}$$

Point B

$$\sigma_{tot} = 132 \text{ MPa}$$

$$\tau_{xy} = 0 \text{ MPa}$$

Now using the Von Mises Criteria for the point B we have

$$\sigma_o = \sqrt{(\sigma^2 + 3\tau^2)} = 132 \text{ MPa}$$

4.2.4 Blade Layout with the B.M.A

The layout of the blade containing the B.M.A is reported in the following figure, we have proposed this layout as an optional layout in case that the bending moment of the blade is relevant with respect to the limitation of the gearbox shaft. It can easily be assembled to the blade and disassembled in case that is not necessary.

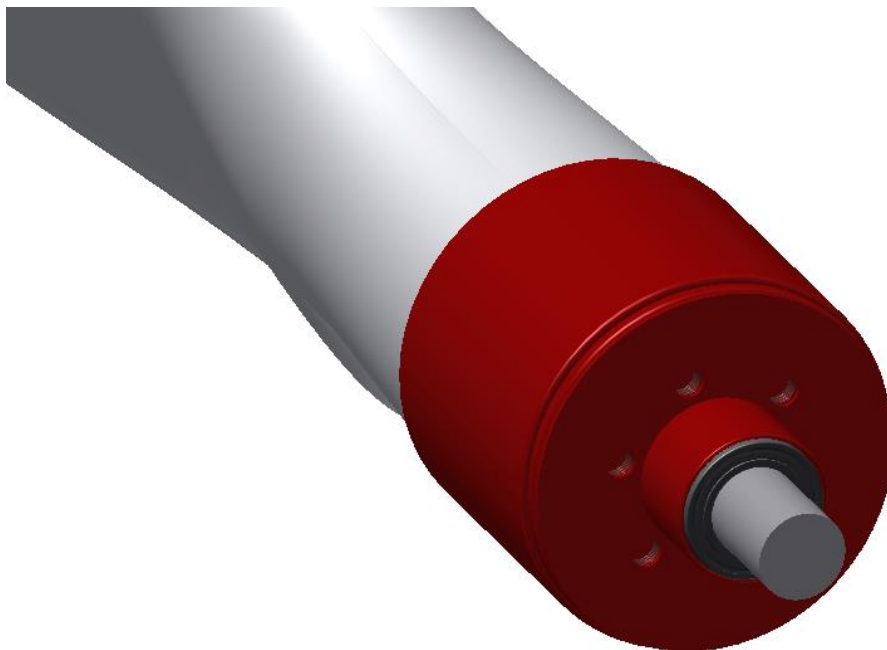


Figure 4.8. Blade layout with the B.M.A

4.2.5 Blade Components

As shown in the figure the blade contains 8 main components, the first component from the left side is the blade itself the material of the blade is composite and the weight as reported in the previous chapters should be around 100 g. The second component is the encoder that is one of the main parts for the control system. The encoder will measure the rotational angle of the blade that will be used for the pitch control. The third components from left and right side are the fixing components used to fix the motor gearbox and the encoder to the blade. These 3 components rotate with the blade, so there is no relative velocity between the blade and the components inside the blade. The only component that has relative velocity with respect to the blade is the shaft of the gearbox that is connected to the secondary shaft and will be connected to the Hub. The components in the middle are the motor and gearbox that will provide the motion for the rotation of the blade(chosen in Chapter 3) the last 2 components are the B.M.A and a bearing used to absorb the bending moment. The dimensions of all of the components used and designed has been reported in Appendix C.

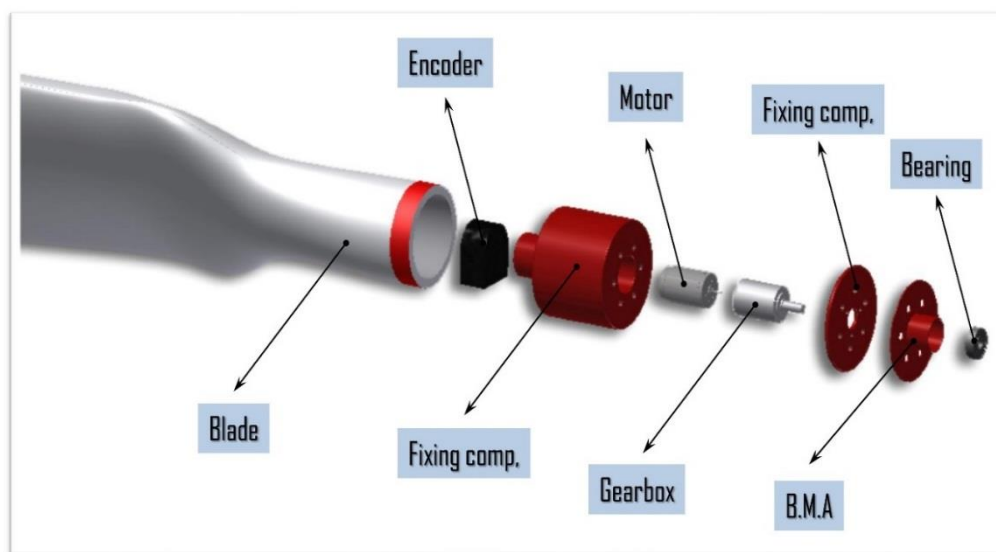


Figure 4.9. Blade Components.

4.3 Hub Layout for the first blade configuration

The dimension of the Hub is important due to the fact that if the dimensions are higher than the one defined in Chapter 2, it can influence the overall mass of the wind turbine, furthermore the diameter of the hub can influence the overall length of the blade that should be 1.06m. The hub is one of the main components in any wind turbine because it has to transfer the load (the energy coming from the wind) to the drivetrain. For the first blade layout we have proposed the following Hub layout. The details on the dimension of the Hub is reported in Appendix C.

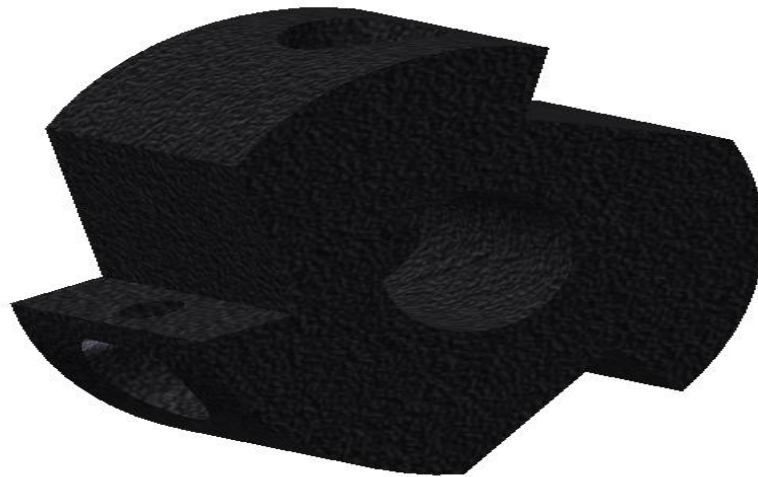


Figure 4.10. Hub of the scaled model.

In the following figures it has been reported the blade mounted on the Hub. The secondary shaft enters to the bore designed on the Hub and is fixed trough 3 bolts that are orthogonal to the direction of the shaft and prevent rotation of the shaft inside the Hub. The shaft of the Drivetrain enters from the back side of the hub and is fixed to the Hub.



Figure 4.11.a Hub layout using the blade with the B.M.A

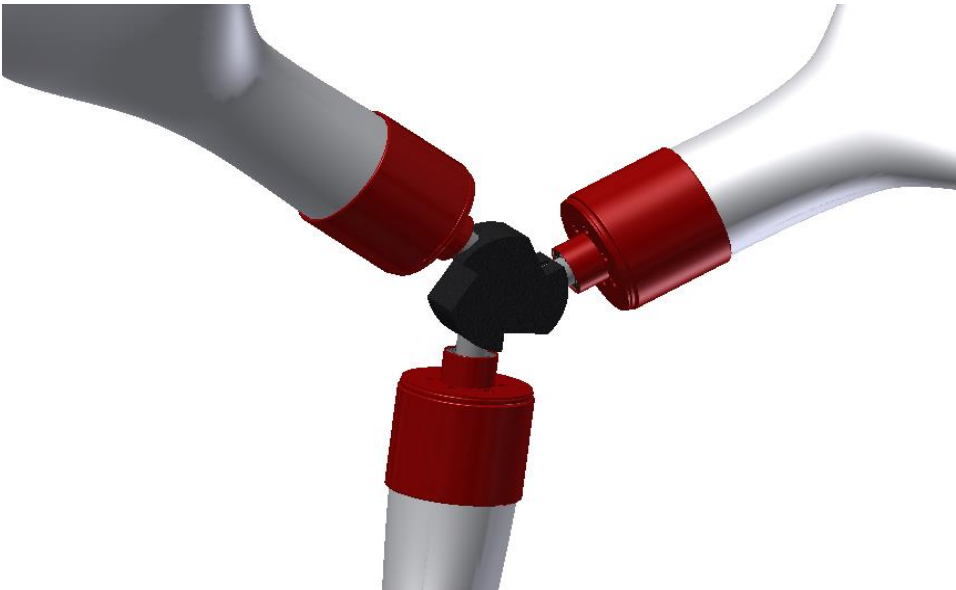


Figure 4.11.b. Hub layout using the blade with the B.M.A

In the following figure it has been reported the layout of the blade with the B.M.A connected to the Hub.

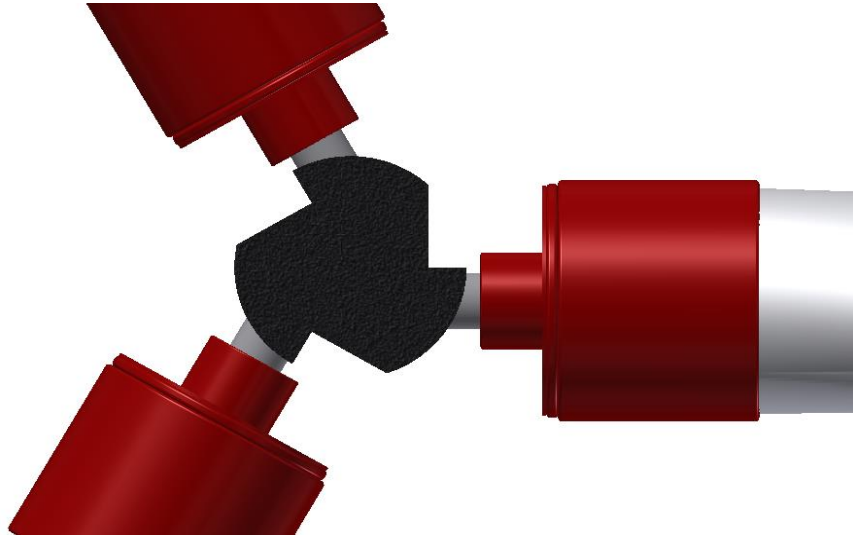


Figure 4.11.c. Hub layout using the blade with the B.M.A.

4.4 Blade Second Layout Configuration

The second configuration uses a thrust bearing that is connected directly to the Hub and can transfer directly the bending moment to the Hub rather than using the B.M.A. the layout of the blade has been reported in the following Figure 4.12.

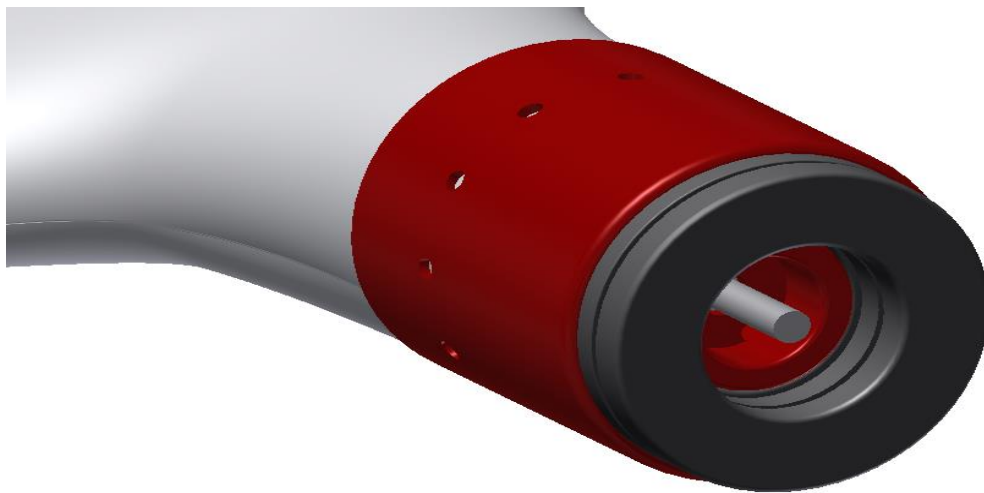


Figure 4.12. Blade layout using the thrust bearing

4.4.1 Blade second Layout Fixing Components

The first fixing component of the blade has been reported in Figure 4.13. The gearbox is connected rigidly by 3 bolts to this component. The external diameter of this component is equal to the internal diameter of the blade so the whole component will enter in the blade and will be connected to the blade trough 12 bolts that are on the surface of the cylinder.

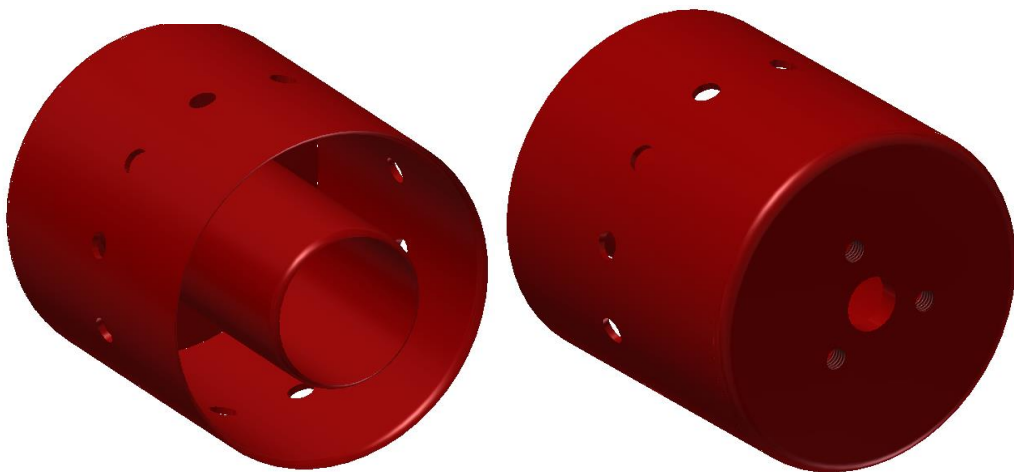


Figure 4.13. Motor fixing component for the second blade layout

The second fixing component as reported in the following figure is connected to the blade and the first fixing component trough 12 bolts that are on the surface of the cylinder. The internal diameter of the cylinder is 60mm so the blade will be fixed in between these 2 components. In the right side of this component will enter the rotating side of the bearing that will connect to the Hub. Both of these components and the gearbox will rotate with the blade. The fixing components don't have any connection to the gearbox shaft that is directly connected to the Hub.



Figure 4.14. Second fixing component for the second blade layout

4.4.2 Blade Second Configuration Hub Layout

As shown in the following figure the Hub in this case is triangular rather than cylindrical. From one side of the Hub the rotor shaft enters to the Hub and from the other side 3 bolt prevent the rotation of the gearbox shaft that enters inside the Hub. The blade is connected to the Hub trough a thrust bearing. The fixed side of the bearing is connected to the Hub and the rotating side of the bearing is connected to the blade. The dimensions of the Hub is reported in Appendix C.

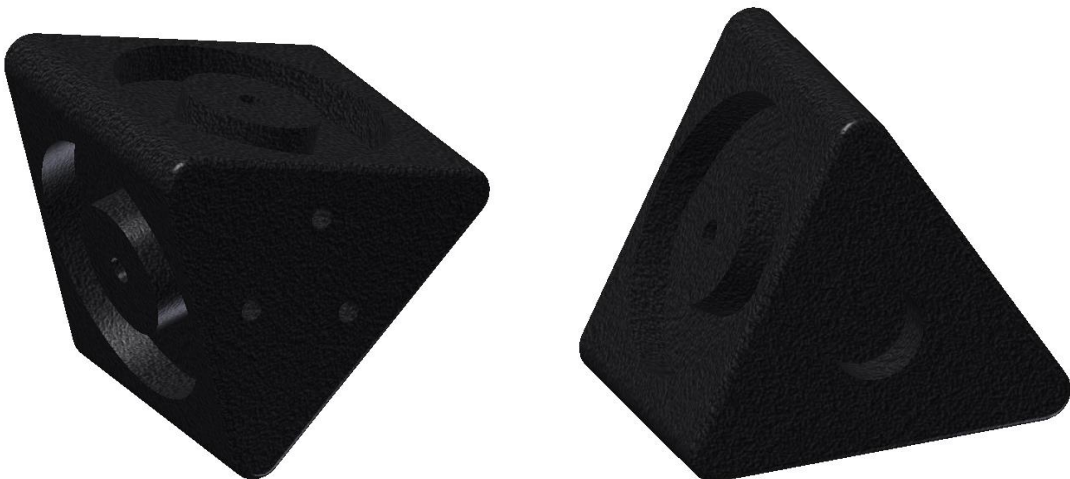


Figure 4.15. Second blade configuration Hub.

In the following figure it has been reported the Layout of the blade connected to the rotor.

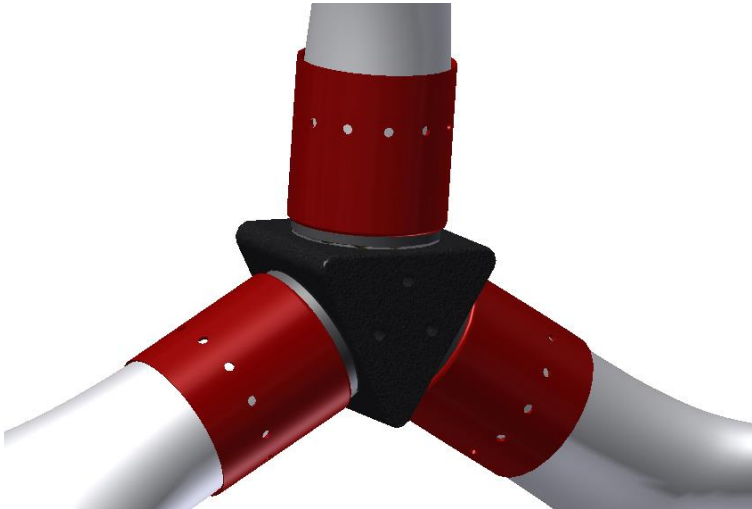


Figure 4.16. Second blade configuration rotor design

This configuration presents less stress on the fixing components, because the diameter of the fixing component is equal to 60mm, rather than 25mm. having higher values of inertia the stress on the components reduces.

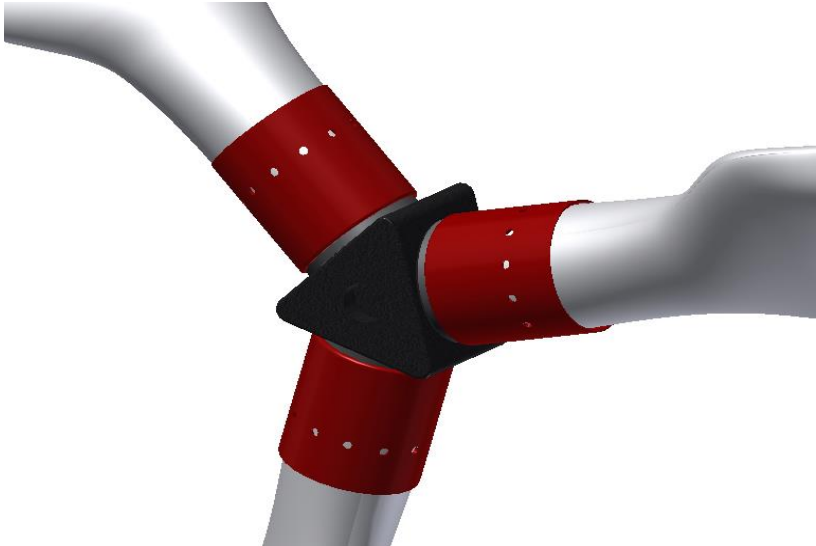


Figure 4.17. Second blade configuration rotor design

4.4.3. Blade Second Configuration Components

Below it has been reported the details of the components connected to the blade. The encoder and motor are connected to the gearbox and don't suffer any load. The gearbox is connected to the fixing components. The bearing is connected to the hub and the fixing component and transfers the load from the blade directly to the hub. The gearbox shaft does not have any connection with the fixing components and is directly fixed to the hub.

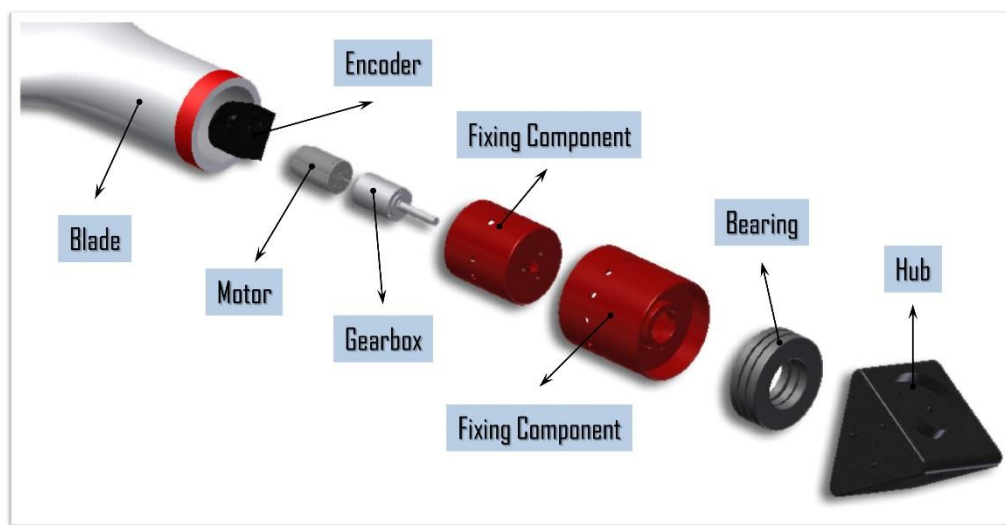


Figure 4.18. Second blade configuration components

4.5 Nacelle and Drivetrain Layout

One of the important points in the project of a wind turbine or any other mechanical system is the layout, because of the fact that it has to be chosen once, and usually it is not easy to change it when the system is produced because the layout itself imposes important restrictions on the system that can limit further modifications of the system later on when the model is produced. Small modifications can influence other components making it more complicated. For this reason the choice of the layout has to be done once accurately considering the benefits and weakness of each model and deciding the best model that fits with the objectives of the project.

We have proposed 2 different layouts for our scaled wind turbine, the first model is more similar to other scaled models using a simple Nacelle with a motor that has been based at the end of the drivetrain, the second layout is a more complicated model having its benefits due to the fact that in the first layout and in the other similar works the motor has been based at the end of the tower. So there are different mechanical and electrical components in between of the motor and the rotor these components can influence the dynamic behavior of the system adding undesired components on the response of the system. Another effort to solve this problem is using a motor inside the tower and transmit the motion using two perpendicular gears [37] as shown in the figure below, but also this can introduce undesired influence on the system because of the matching problems usual in the perpendicular gears, even if the only component in between the motor and the rotor is the perpendicular gearbox.



Figure 4.19. Perpendicular gearbox configuration.

An example of using a layout configuration using the perpendicular gear is reported in the following figure.

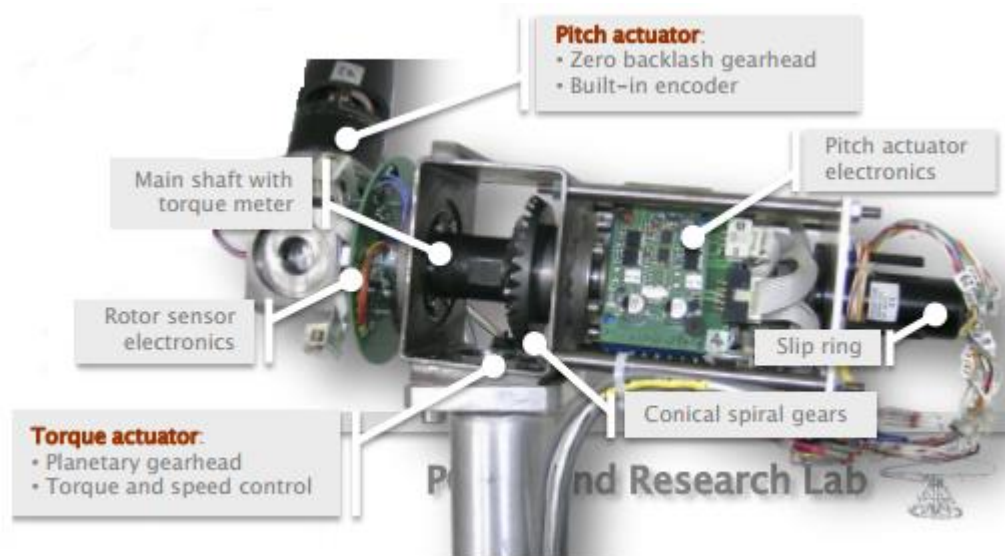


Figure 4.20. Scaled model using the motor in the tower and transferring the motion to the drivetrain through a perpendicular gearbox [14].

4.5.1 First Configuration

The first layout proposed, uses a simple Nacelle that is easily producible with low cost because it uses simple components (3 sheets and 4 Tubes with dimensions indicated in the Appendix) in which the motor is at the end of the Nacelle coupled directly to the gearbox, the gearbox is linked to the Nacelle with 4 bolts. The slip ring has to be a through pass slip ring and is near the rotor, minimizing the length of the wires. As the slip ring is going to transfer data and electricity to the pitch motors this can reduce the complexity of the wires and data transfer, in the middle of the motor and the slip ring if it is desired to have the electronic components onboard, there is sufficient area for the electronic equipment to be installed. In this case there has been used a single shaft that starts from the motor and arrives to the hub reducing the complexity and using multi shaft layouts maintaining the problem of the fact that the motor is far from the rotor and the components in between can add undesired influence on the dynamic behavior of the system.

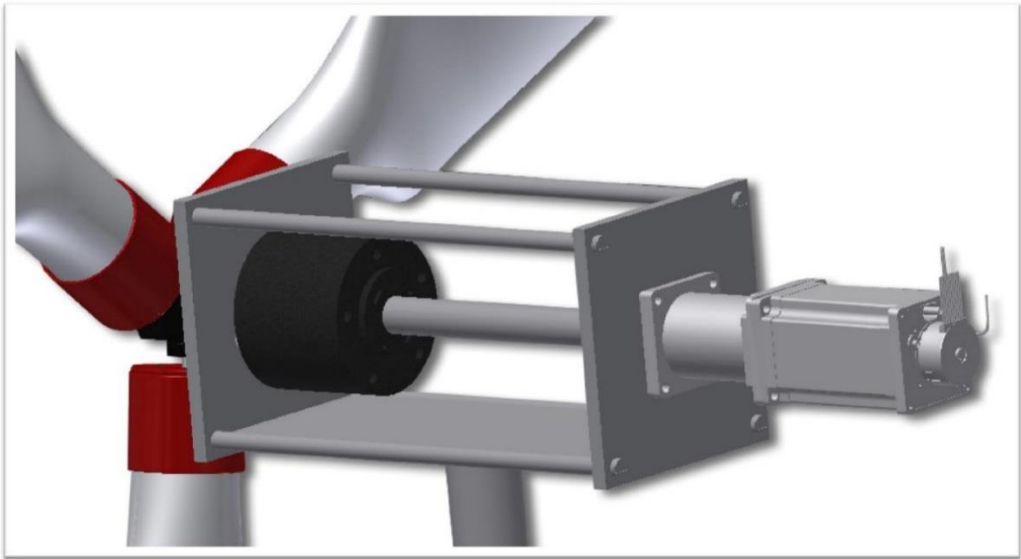


Figure 4.21. View of the scaled model wind turbine layout (First configuration).

As shown in the figure the drivetrain is connected to the Nacelle through 2 ball bearings one near to the gear box and another near to the blade. In the following figure it has been reported the bearing beside the gearbox.

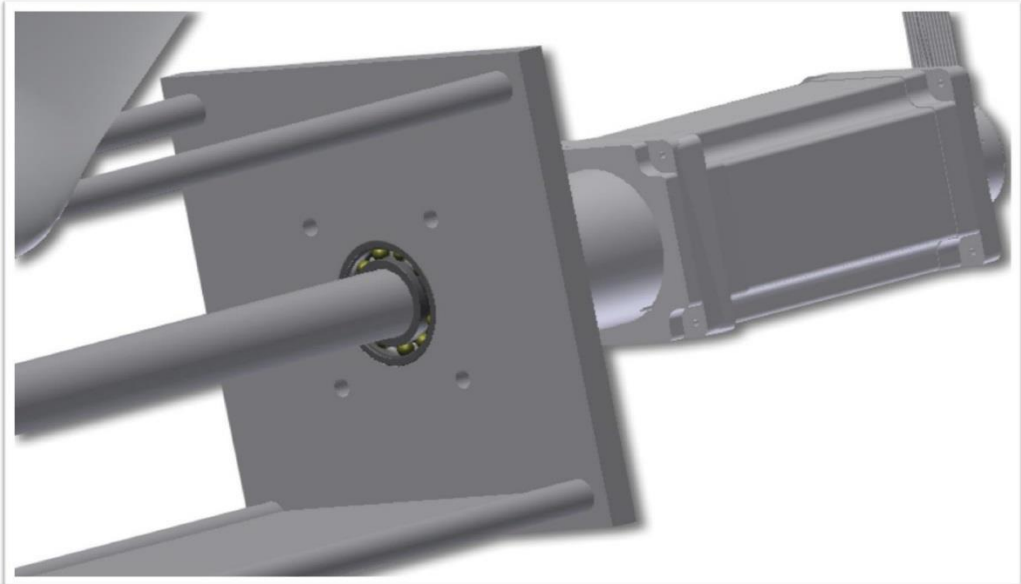


Figure 3 View of the bearing position of the scaled model wind turbine (First configuration).

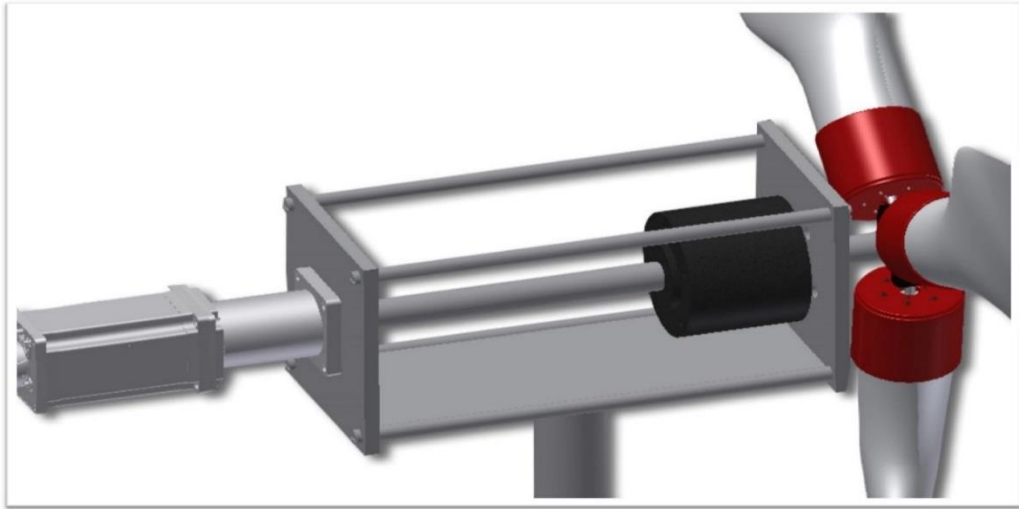


Figure 4.23. View of the scaled model wind turbine layout (First configuration)

In the following figure it is shown the drivetrain of the First configuration layout of the wind turbine. As shown in the figure the components from the left to the right of the drivetrain are respectively motor that is connected to the Bear box. The drivetrain is connected rigidly to the Nacelle trough 2 deep groove ball bearings one near to the motor and one near to the blade. In this configuration we have one shaft that connects the rotor to the hub. The slip ring is the component near to the blade.

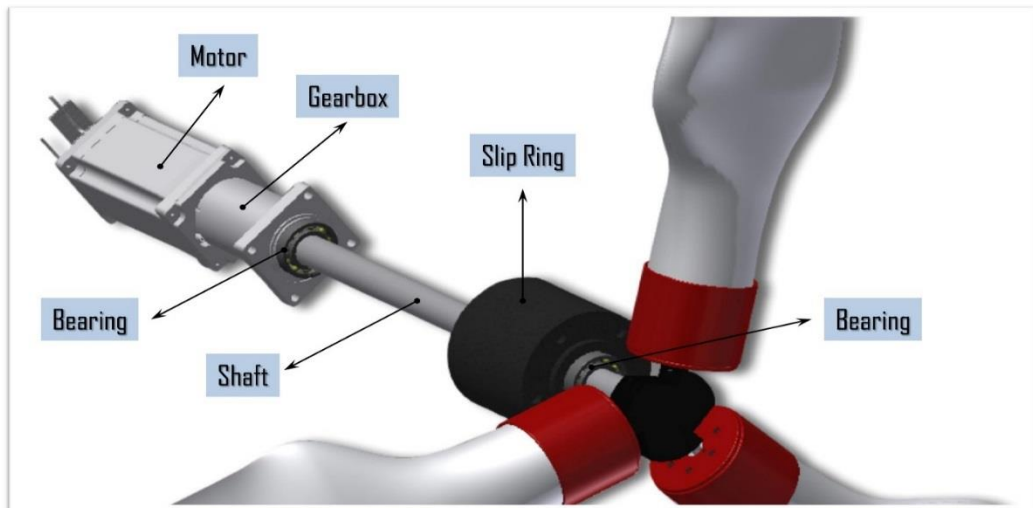


Figure 4.24. Components of the scaled wind turbine drivetrain (First layout).

4.5.2 Second Configuration

In the second layout as shown in the following figures we have the motor that is the first component near to the rotor, this can have benefits, because there is no other component in-between that can produce any influence on the response of the motor. We have used the B1515 motor of the Portescap company with two gear heads that have to be used for the both sides of the motor to guarantee the same rotational speed in both sides, we have used two shafts in the left and right side of the motor, the first one is a short shaft to connect the motor to the rotor and the second shaft is the one to connect the motor to the slip ring [38]. In this layout configuration the only way to connect the slip ring to the pitch actuator is to have a bore inside the whole shaft and transfer wires from inside of the shaft. This fact makes the model more complicated and costly but if we want to obtain the best dynamic behavior of the system, the best choice is the following layout. Another problem in this case is because of the addition of the second gearbox. This can influence the system adding mass and inertia on the system but as it is not in the side of the blade it does not add much influence on the response of the motor. Anyway it can be compensated using smaller shaft and changing the slip ring. As in this case the slip ring at the end of the drivetrain can be used with slip rings without through bore that usually have less inertia with respect of the actual slip ring chosen for our model.

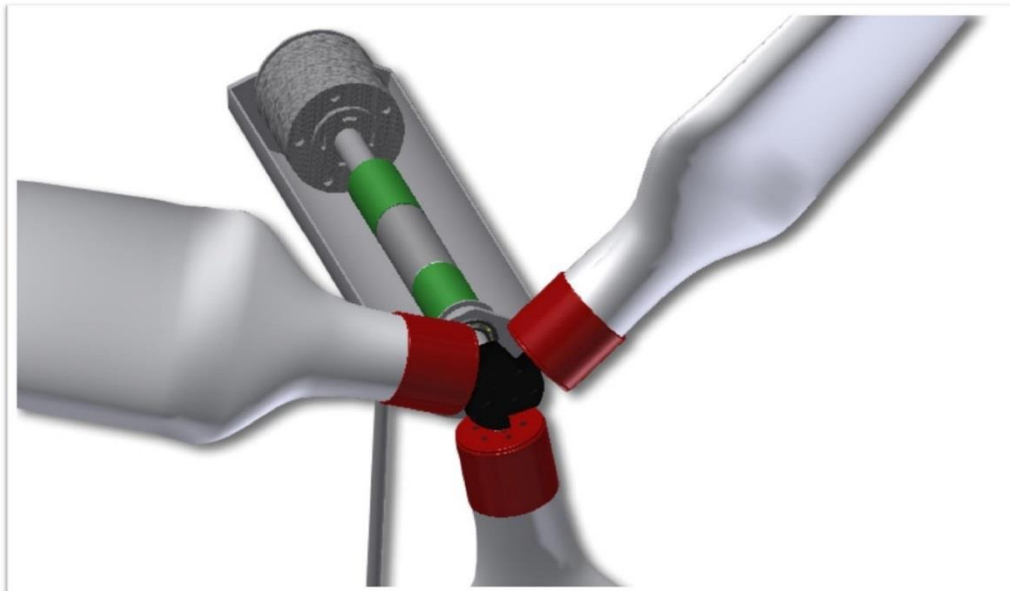


Figure 4.25. Wind turbine scaled model layout (second configuration)

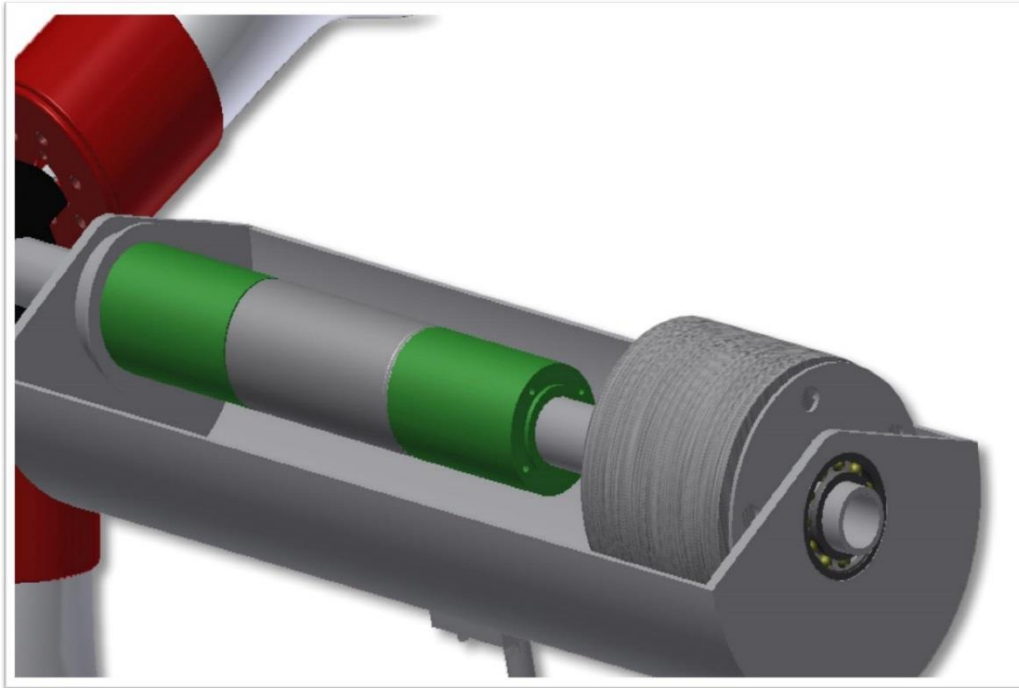


Figure 4.26. Wind turbine Nacelle view (second configuration).

In the figure reported below it is all the components shown without the nacelle base to show the position of each component. The first component from the left side is the ball bearing that is connected to the Nacelle rigidly. The next component is the slip ring with 56 channels after the gray component is the motor that will generate the motion of the rotor and the 2 green components in the sides of the motor are the gearboxes that reduces the rotational velocity of the motor to achieve the rotational velocity required from the control system, between the motor and the blades .The only component is the ball bearing that is again connected to the Nacelle.

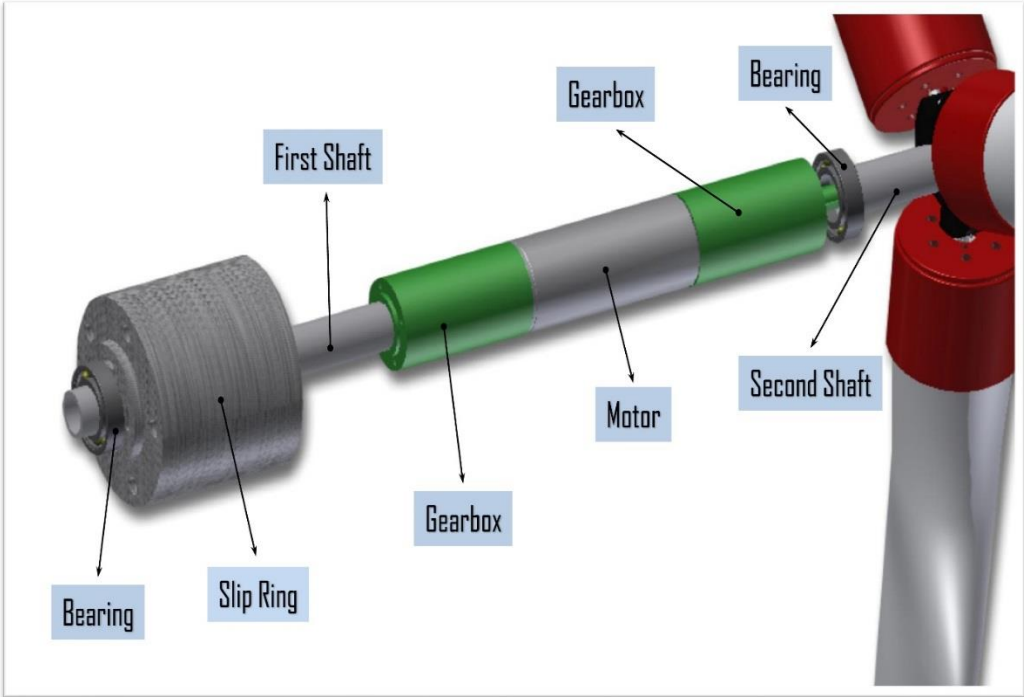


Figure 4.27. Wind turbine components (second layout).

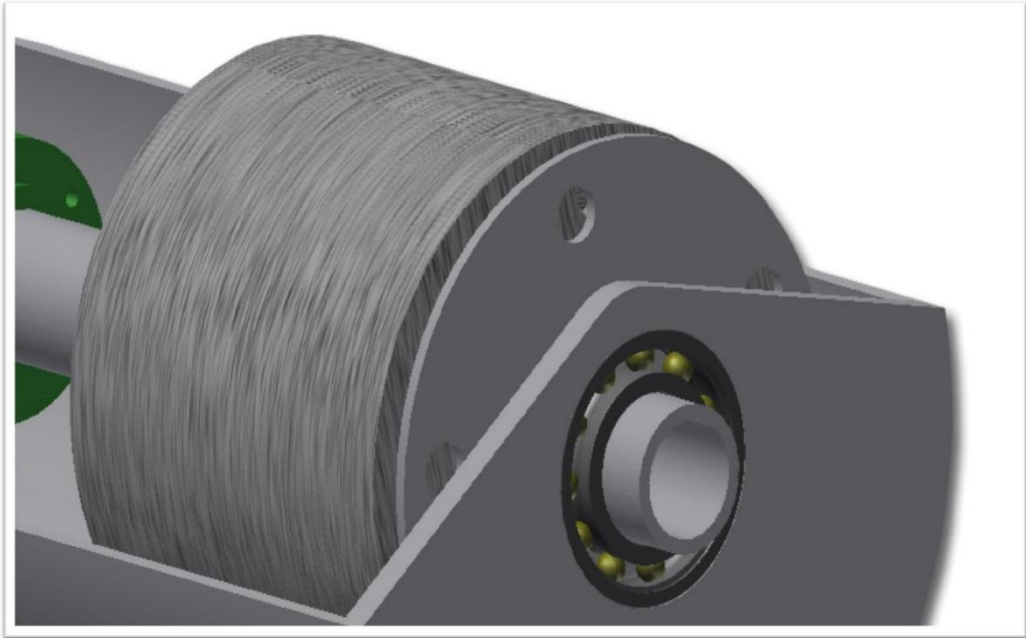


Figure 4.28. Wind turbine Nacelle and drivetrain connection view.

CHAPTER 5

WIND TURBINE CONTROL SYSTEM

Modern large wind turbines are variable-speed machines. When the wind speed is below rated, generator torque is used to control the rotor speed in order to capture as much power as possible. The most power is captured when the tip speed ratio is held constant at its optimum value (typically 6 or 7). This means that as wind speed increases, rotor speed should increase proportionally. The difference between the aerodynamic torque captured by the blades and the applied generator torque controls the rotor speed. If the generator torque is lower, the rotor accelerates, and if the generator torque is higher, the rotor slows down. Below rated wind speed, the generator torque control is active while the blade pitch is typically held at the constant angle that captures the most power, fairly flat to the wind. At above rated wind speed, the generator torque is typically held constant while the blade pitch is active. In this Chapter we will design both the generator power control and the pitch control for our scaled model.

5.1 Generator Power Control

The generator torque is computed as a tabulated function of the generator speed, incorporating five control regions [39]. 1, 1.5, 2, 2.5 and 3. Region 1 is a control region before cut in wind speed, where the generator torque is zero and no power is extracted from the wind. Instead, the wind is used to accelerate the rotor for startup. Region 2 is a control region for optimizing power capture. Here, the generator torque is proportional to the square of the filtered generator speed to maintain a constant (optimal) tip speed ratio. In Region 3, the generator power is held constant so that the generator torque is inversely proportional to the filtered generator speed. Region 1.5, a start-up region, is a linear transition between

Region 1 and 2. The width of this region should be as less as possible considering the limitation of the motor for generating the required torque variation. Region 2.5 is a linear transition between Region 2 and 3 with a torque slope corresponding to the slope of an induction machine. In the Figure 5.1 it is reported the ideal and real generator torque that we have to obtain from our motor.

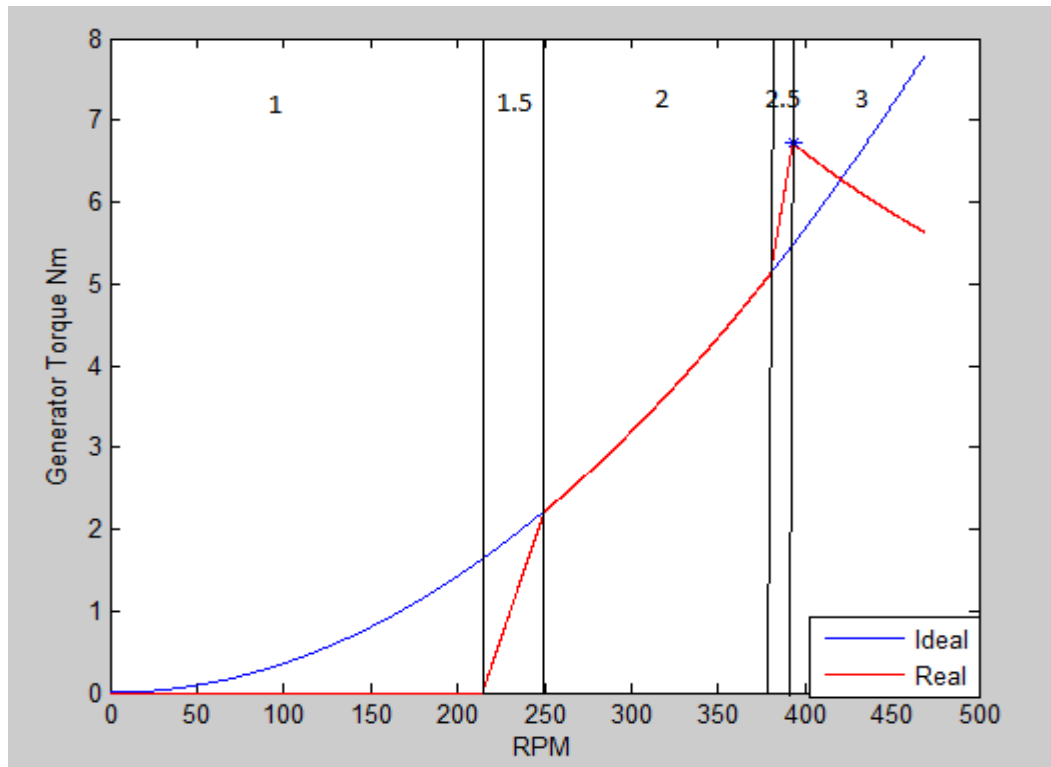


Figure 5.1. Generator torque in different rotational speed (Scaled model).

To compare with the full scale model we have reported below the full scale generator torque behavior (Figure 5.2) to have an indication of the difference between the full scale and scaled model.

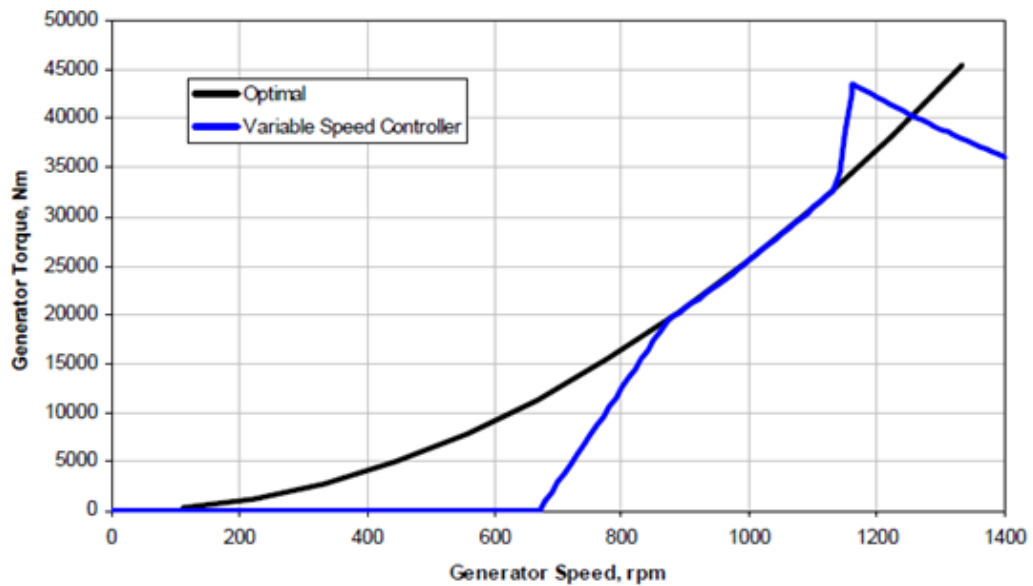


Figure 5.2. Generator torque in different rotational speed (Full scale model) [9].

5.1.1 Generator Power Control Formulation

The equation for the ideal torque is:

$$T = 0.000035469\omega^2 \quad (5.1)$$

The equations for the real torque is reported below

Region 1 is defined in the range of 0 and 214.3 rpm and the generator torque in this range is zero.

Region 1.5 is defined in the range of 214.3 and 250 rpm and the torque in this range is:

$$T = 0.06227(\omega - 214.3) \quad (5.2)$$

Region 2 is defined in the range of 250 and 380 rpm and the torque in this range is:

$$T = 0.000035469\omega^2 \quad (5.3)$$

Region 2.5 is defined in the range of 380 and 393 rpm and the torque in this range is:

$$T = 0.124(\omega - 380) + 5.119 \quad (5.4)$$

Region 3 is defined in the range of 393 and 469 rpm and the torque in this range is:

$$T = \frac{276.47}{\omega \frac{\pi}{30}} \quad (5.5)$$

The torque table is generated by the following Simulink scheme:

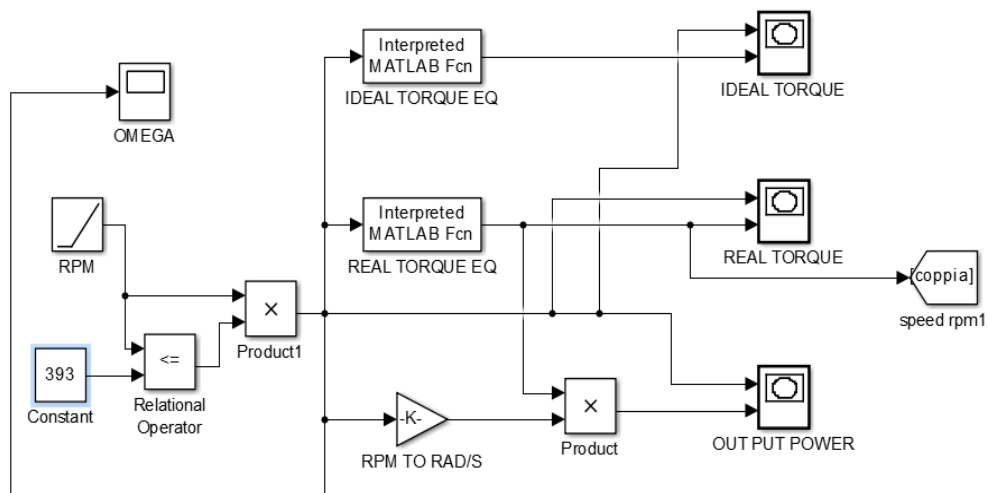


Figure 5.3. Generator power control Simulink scheme.

The model gets as input the velocity of rotation and as output gives the generator torque table and generator power table using the interpreted Matlab functions used in the Simulink scheme [40]. The generator power is reported below:

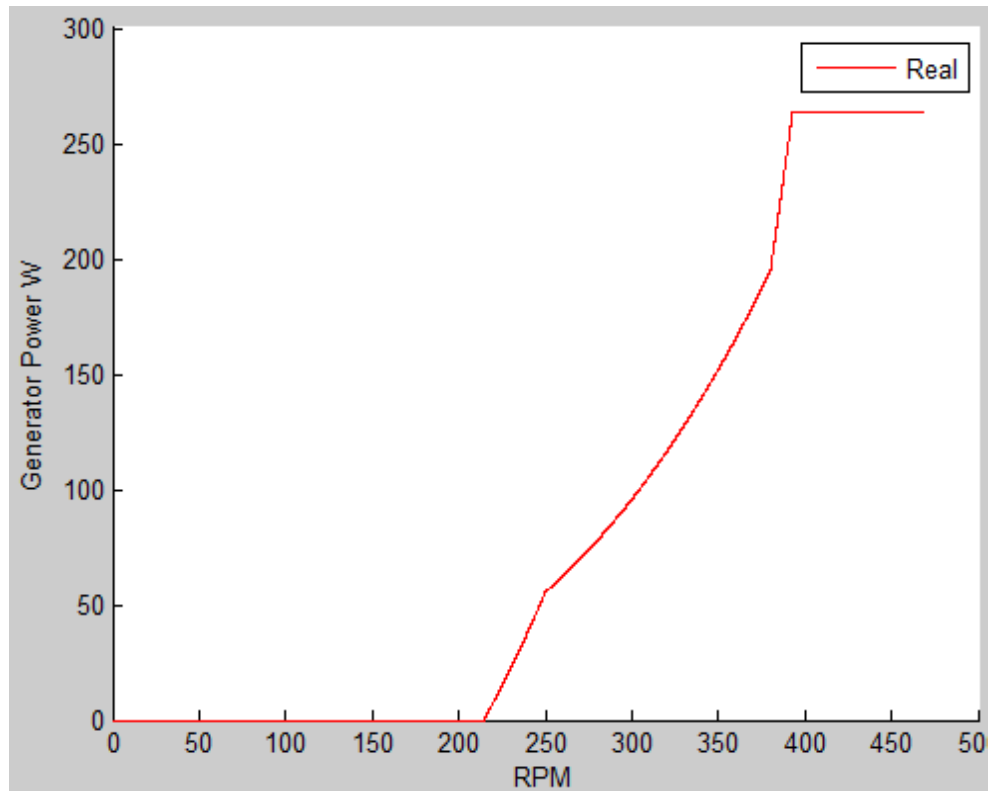


Figure 5.4. Generator Power in different rotational speed (scaled model).

5.2 Pitch Control

Wind turbine pitch control system can change incidence of rotor blades in a wind power generation system based on real time wind speed (or rotor speed) for the purpose of adjusting output power, achieving higher utilization efficiency of wind power and providing protection for rotor blades. When wind speed is not higher than the rated speed, the blade incidence stay near the angle 0° (highest power point), which is similar to that of a generator with constant pitch, generating an output power that changes along with wind speed. When wind speed is higher than the rated speed, the pitch control mechanism changes blade incidence so that the output power of generator is within the allowed range.



5.2.1 Pitch Control Formulation

The first control that we are going to investigate is the control proposed by [41] in which in region 3 (pitch control region) the full scale rotor blade pitch angle commands are computed using gain scheduled proportional integral (PI) control [42] on the speed error between the filtered generator speed and the rated generator speed (393 rpm). It has been used a single degree of freedom (single DOF) model of the wind turbine. Because the goal of the blade pitch control system is to regulate the generator speed, this DOF is the angular rotation of the shaft. To compute the control gains, it is beneficial to study the equation of motion of this single DOF system. From a simple free body diagram of the drivetrain, the equation of motion is [43]:

$$T_{Aero} - N_{Gear}T_{Gen} = (I_{Rotor} + N_{Gear}^2 I_{Gen}) \frac{d}{dt}(\Omega_0 + \Delta\Omega) = I_{Drivetrain} \Delta\dot{\Omega} \quad (5.6)$$

T_{Aero} is the low speed shaft aerodynamic torque. T_{Gen} is the high speed shaft generator torque, N_{Gear} is the high speed to low speed gearbox ratio $I_{Drivetrain}$ is the drivetrain inertia cast to low speed shaft, I_{Rotor} is the rotor inertia, I_{Gen} is the generator inertia relative to the high speed shaft, Ω_0 is the rated low speed shaft rotational speed, $\Delta\Omega$ is the small perturbation of low speed shaft rotational speed

about the rated speed, $\Delta\dot{\Omega}$ is the low speed shaft rotational acceleration, and t is the simulation time.

Because the generator torque controller maintains constant generator power in Region 3 as seen in previous section, the generator torque in Region 3 is inversely proportional to the generator speed, or

$$T_{Gen}(N_{gear}\Omega) = \frac{P_0}{N_{gear}\Omega} \quad (5.7)$$

Where P_0 is the rated mechanical power and Ω is the low speed shaft rotational speed.

Similarly, assuming negligible variation of aerodynamic torque with rotor speed, the aerodynamic torque in Region 3 is

$$T_{Aero}(\theta) = \frac{P(\theta, \Omega_0)}{\Omega_0} \quad (5.8)$$

Where P is the rated mechanical power and θ is the full span rotor blade pitch angle.

Using a first order Taylor series expansion of the last two equations, one can see that

$$T_{Gen} \approx \frac{P_0}{N_{gear}\Omega_0} - \frac{P_0}{N_{gear}\Omega_0^2} \Delta\Omega \quad (5.9)$$

And

$$T_{Aero} \approx \frac{P_0}{\Omega_0} + \frac{1}{\Omega_0} \left(\frac{\partial P}{\partial \theta} \right) \Delta\theta \quad (5.10)$$

$\Delta\theta$ is a small perturbation of the blade pitch angles about their operational point. With proportional integral derivative (PID) control, this is related to the rotor speed perturbation by

$$\Delta\theta = K_P N_{Gear} \Delta\Omega + K_I \int_0^t N_{gear} \Delta\Omega dt + K_D N_{Gear} \Delta\dot{\Omega} \quad (5.11)$$

K_P , K_I and K_D are the blade pitch controller proportional, integral and derivative gains, respectively.

By setting $\dot{\phi} = \Delta\Omega$, combining the above expressions, and simplifying, the equation of motion for the rotor speed error becomes

$$\begin{aligned} & \left[I_{Drivetrain} + \frac{1}{\Omega_0} \left(-\frac{\partial P}{\partial \theta} \right) K_D N_{Gear} \right] \ddot{\phi} + \left[\frac{1}{\Omega_0} \left(-\frac{\partial P}{\partial \theta} \right) K_P N_{Gear} - \frac{P_0}{\Omega_0^2} \right] \dot{\phi} \\ & + \left[\frac{1}{\Omega_0} \left(-\frac{\partial P}{\partial \theta} \right) K_I N_{Gear} \right] \phi = 0 \end{aligned} \quad (5.12)$$

One can see the idealized PID controlled rotor speed error will respond as a second order system with the natural frequency $\omega_{\phi n}$ and damping ratio $\zeta_{\phi n}$ equal to

$$\omega_{\phi n} = \sqrt{\frac{K_\phi}{M_\phi}} \quad (5.13)$$

And

$$\zeta_{\phi n} = \frac{C_\phi}{2\sqrt{K_\phi M_\phi}} = \frac{C_\phi}{2M_\phi \omega_{\phi n}} \quad (5.14)$$

In an active pitch wind turbine, the sensitivity of aerodynamic power to the rotor collective blade pitch angle ($\frac{\partial P}{\partial \theta}$) is negative in Region 3. With positive control gains, then, the derivative term acts to increase speed error (to maintain constant

power) in Region 3, one can see that the generator torque controller introduces a negative damping in the speed error response (introduced by $-\frac{P_0}{\Omega_0^2}$ term). This negative damping must be compensated by the proportional term in the blade pitch controller.

In the design of the blade pitch controller the [44] recommends neglecting the derivative gain, ignoring the negative damping from the generator torque controller, but in our model represented below we have considered also this component. The other information from the reference is to consider the $\zeta_{\varphi n} = 0.6$ to 0.7 and $\omega_{\varphi n} = 0.6 \text{ rad/s}$ for the full scale wind turbine. For the scaled model the $\zeta_{\varphi n}$ remains the same and the $\omega_{\varphi n} = 19.48 \text{ rad/s}$. This expression leads to direct expression for choosing appropriate PI gains once the sensitivity of aerodynamic power to rotor collective blade pitch ($\frac{\partial P}{\partial \theta}$) is known:

$$K_P = \frac{2I_{Drivetrain}\Omega_0 \zeta_{\varphi n}\omega_{\varphi n}}{N_{Gear} \left(-\frac{\partial P}{\partial \theta}\right)} \quad (5.15)$$

And

$$K_I = \frac{2I_{Drivetrain}\Omega_0\omega_{\varphi n}^2}{N_{Gear} \left(-\frac{\partial P}{\partial \theta}\right)} \quad (5.16)$$

5.2.2 Blade Pitch Sensitivity

The blade pitch sensitivity ($\frac{\partial P}{\partial \theta}$) is an aerodynamic property of the rotor that depends on the wind speed, rotor speed, and blade pitch angle. The reference has calculated it for the NREL offshore 5MW baseline wind turbine by performing a linearization analysis in FAST with AeroDyn at a number of given, steady, and uniform wind speeds, at the rated rotor speed ($\Omega_0 = 12.1 \text{ rpm}$) and at the corresponding blade pitch angles that produce the rated mechanical power ($P_0 = 5.296610 \text{ MW}$) the linearization analysis involves perturbing the rotor collective

blade pitch angle at each operating point and measuring the resulting variation in aerodynamic power. In Table 5.1 the result of the linearization has been reported:

Table 5.1. Pitch sensibility table of the wind turbine in different wind speed and rated rotational velocity of the blade (Full scale model) [9].

Wind Speed (m/s)	Rotor Speed (rpm)	Pitch Angle (degree)	$\frac{\partial P}{\partial \theta}$ (watt/rad)
11.4	12.1	0	-28.24E+6
12	12.1	3.83	-43.73E+6
13	12.1	6.6	-51.66E+6
14	12.1	8.7	-58.44E+6
15	12.1	10.45	-64.44E+6
16	12.1	12.06	-70.46E+6
17	12.1	13.54	-76.53E+6
18	12.1	14.92	-83.94E+6
19	12.1	16.23	-90.67E+6
20	12.1	17.47	-94.71E+6
21	12.1	18.7	-99.04E+6
22	12.1	19.94	-105.90E+6
23	12.1	21.18	-114.30E+6
24	12.1	22.35	-120.20E+6
25	12.1	23.47	-125.30E+6

As designing the blade is not one of the objectives of this Thesis, we will adapt the same linearization results for our scaled model. Using the scaling laws for the scaled model we have:

Table 5.2. Pitch sensibility table of the wind turbine in different wind speed and rated rotational velocity of the blade model (Scaled model).

Wind Speed (m/s)	Rotor Speed (rpm)	Pitch Angle (degree)	$\frac{\partial P}{\partial \theta}$ (watt/rad)
6.38	393	0	-1.47E+3
6.7	393	3.83	-2.28E+3
7.3	393	6.6	-2.70E+3

7.8	393	8.7	-3.05E+3
8.4	393	10.45	-3.36E+3
9.0	393	12.06	-3.67E+3
9.5	393	13.54	-4.00E+3
10.0	393	14.92	-4.38E+3
10.6	393	16.23	-4.73E+3
11.2	393	17.47	-4.94E+3
11.8	393	18.7	-5.17E+3
12.3	393	19.94	-5.53E+3
12.9	393	21.18	-5.97E+3
13.4	393	22.35	-6.28E+3
14	393	23.47	-6.54E+3

We have used the following linear interpolation to interpolate the results of the information coming from the linearization. In particular the variation of the pitch sensitivity for different pitch angles in rated rotational velocity is:

$$\frac{\partial P}{\partial \theta} = -215.6\theta - 1261 \quad (5.17)$$

As shown in the Figure 5.5 there is a slight error between the linear interpolation result and the results of the linearization coming from FAST. This error can influence slightly the results of the control system. This error can be reduced using also higher order interpolations but it is not possible to eliminate completely from the results.

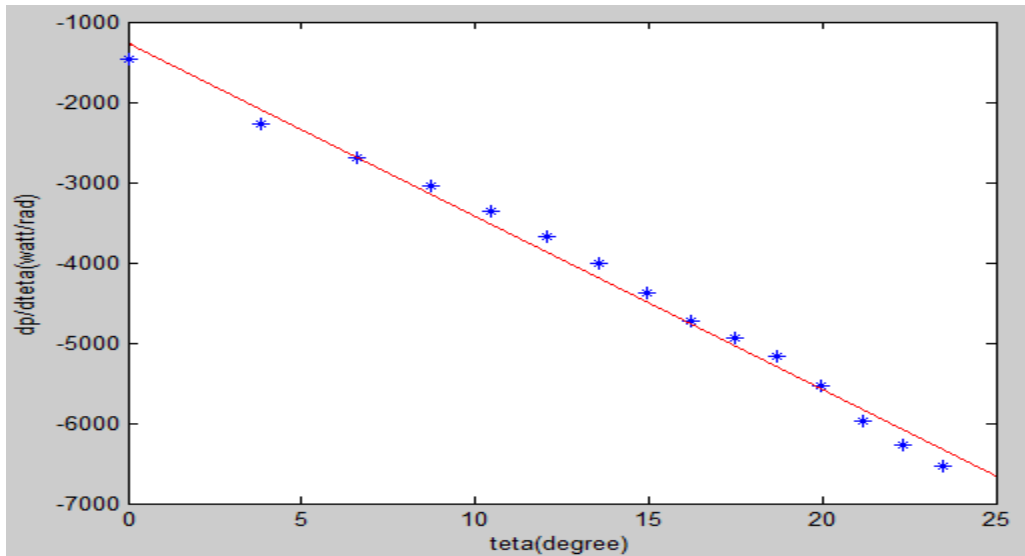


Figure 5.5. Pitch sensitivity variation with respect of the blade pitch angle. Red line is the interpolation of the linearization results (blue points)

The only variable in the formula of the K_P, K_I is $\frac{\partial P}{\partial \theta}$, so as reported in the following figure they have a decrease for higher values of $\frac{\partial P}{\partial \theta}$.

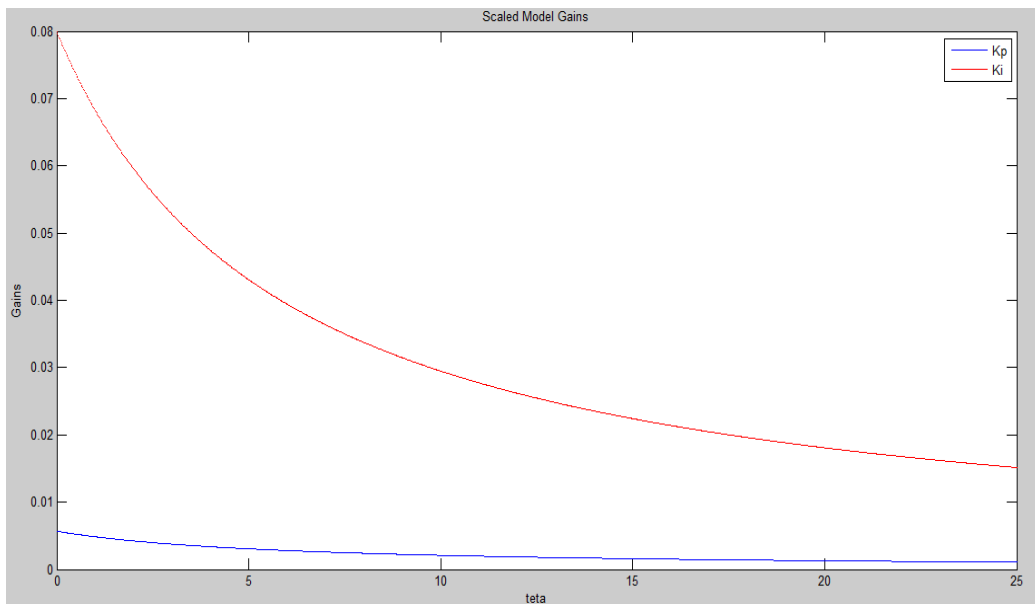


Figure 5.6. Integral and proportional gains of the scaled model

Below are reported the gains for the full scale model. The gains for the scaled model are different from the full scale model because of the difference in the inertia of the rotor and the difference in the blade pitch sensitivity ($\frac{\partial P}{\partial \theta}$) and other constants of the equation.

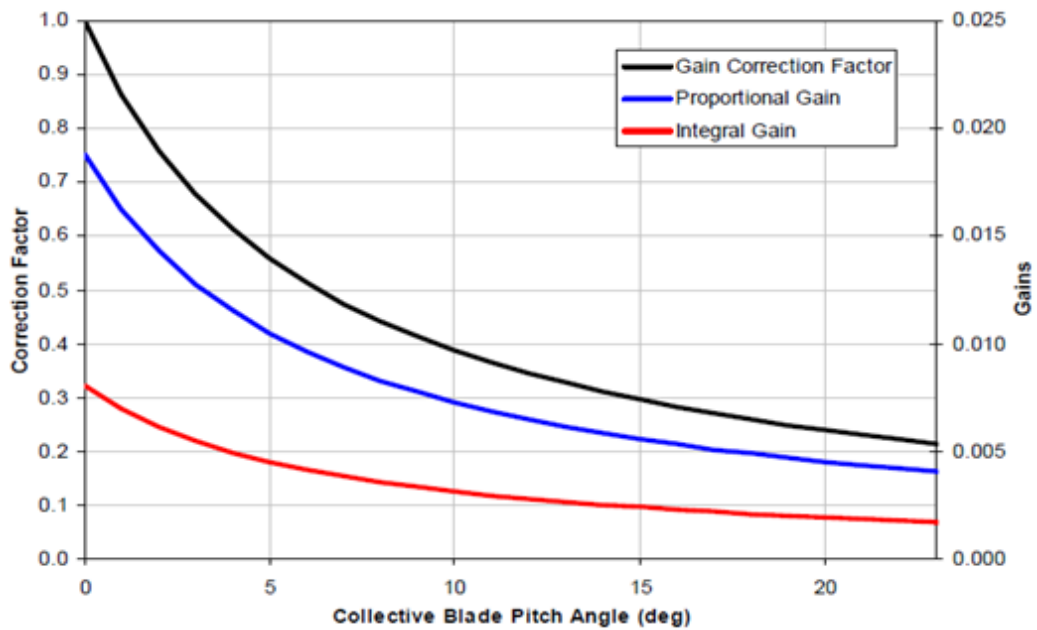


Figure 5.7. Integral and proportional gains of the full scale model [9].

5.3 Feedforward Control System Design

In this Chapter we will study 2 different control system designs for the pitch angle of the blade. In the first model we have feedback on the rotational velocity of the rotor but the control on the angle of the blade pitch is a feed forward control so we measure the wind velocity for each blade and having the data of the equation reported below we calculate for each wind speed the angle for which the wind turbine in the steady condition rotates with the rated rotational velocity. The input of our Simulink model is the wind speed that is converted to the pitch angle using the following relationship that is the equation that interpolates the data coming from the Fast linearization (Calculating the pitch angle for different wind

velocities) reported before. We have used a 2nd order equation as the relation in not linear.

$$\theta = -0.21V^2 + 7.05V - 34.5 \quad (5.18)$$

Where:

θ =Pitch angle & V =wind speed

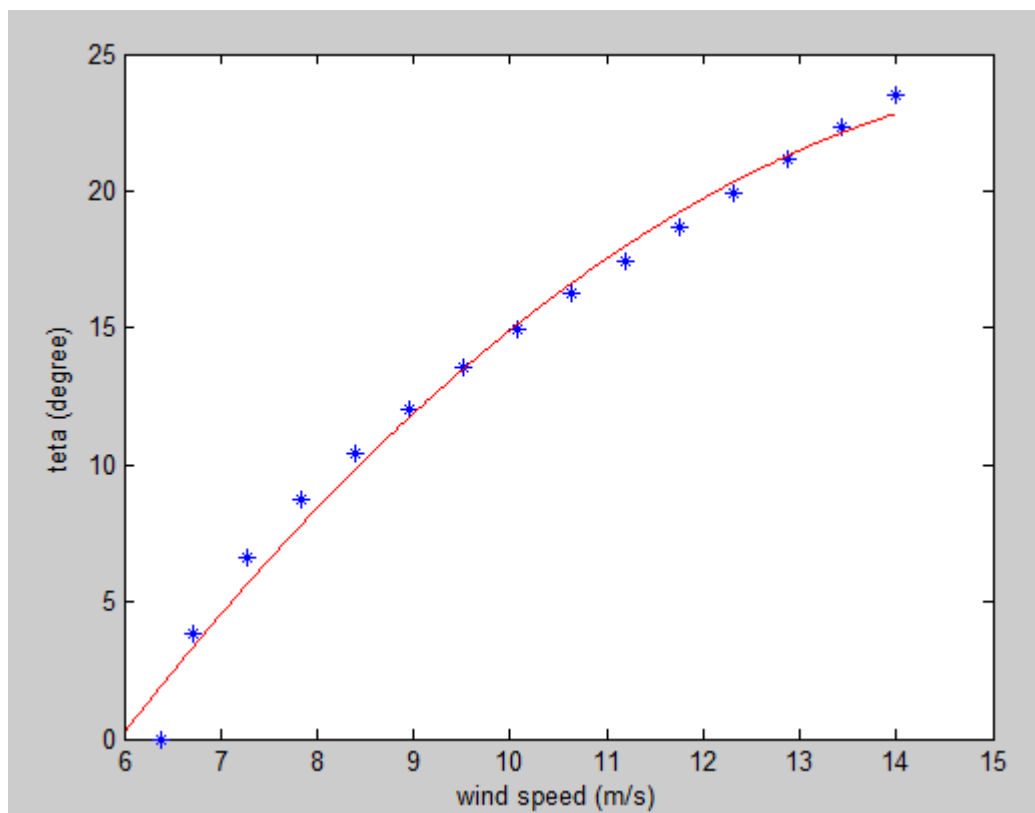


Figure 5.8. Blade pitch angle variation with respect to the wind speed for the scaled model (Stationary condition). The Red line is the second order interpolation of the FAST linearization results (Blue points) using the first column and third column of the Table 5.2.

As it's shown in Figure 5.8 the error in the low wind speed is higher than high wind speed so we expect a slight error in the low speed wind (Rated).

The Simulink scheme of the feedforward pitch control is reported below.

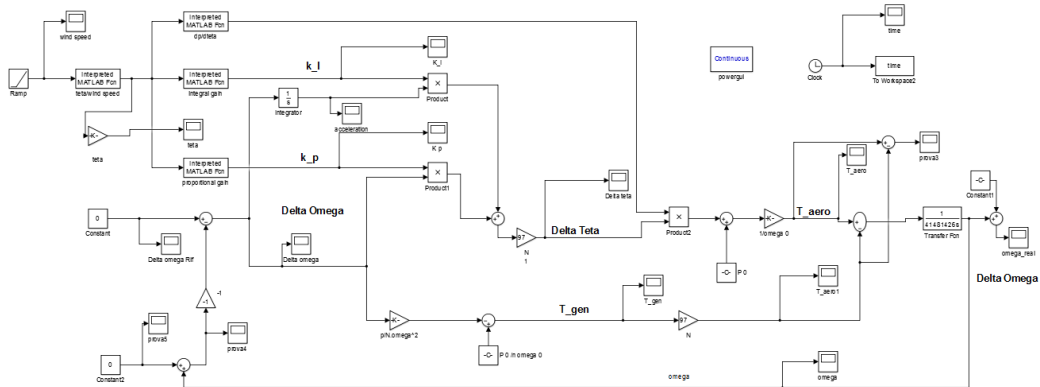


Figure 5.9. Feedforward pitch control Simulink scheme

In the Simulink model the input is the wind velocity that in real case is measured with the sensors. The wind velocity is the input of the first interpreted matlab function. this function calculates the pitch angle for each wind speed that stabilizes the rotor of the turbine in 393rpm(the procedure is explained before).in the next step the pitch angle is the input of 3 other interpreted matlab functions that calculate for each pitch angle(wind speed) the blade pitch sensitivity ($\frac{\partial P}{\partial \theta}$), proportional and integral gains of the control system (as the gains are not constant). the integral and proportional gains are acted to signal coming from the rotors rotational velocity and calculate the effective variation of the pitch angle $\Delta \theta$. This value then is used to calculate the aerodynamic torque and then is compared with the generator torque (the generator torque is calculated as explained in the torque generator control chapter).the control system acts to minimize this difference cause if the difference is not convergent to zero the rotor rotational velocity diverges and the system is going to be instable

5.3.1 Simulation Results (Full Scale)

First of all we will study the influence of the feed forward pitch control on the full scale wind turbine and then compare the results with the scaled model. To see the behavior and the results of the pitch control we give as input a ramp on the wind speed that starts from the wind speed equal to 11.4 m/s with a slope of 0.5, and a simulation time equal to 25 second the resulting input is reported in the following figure:

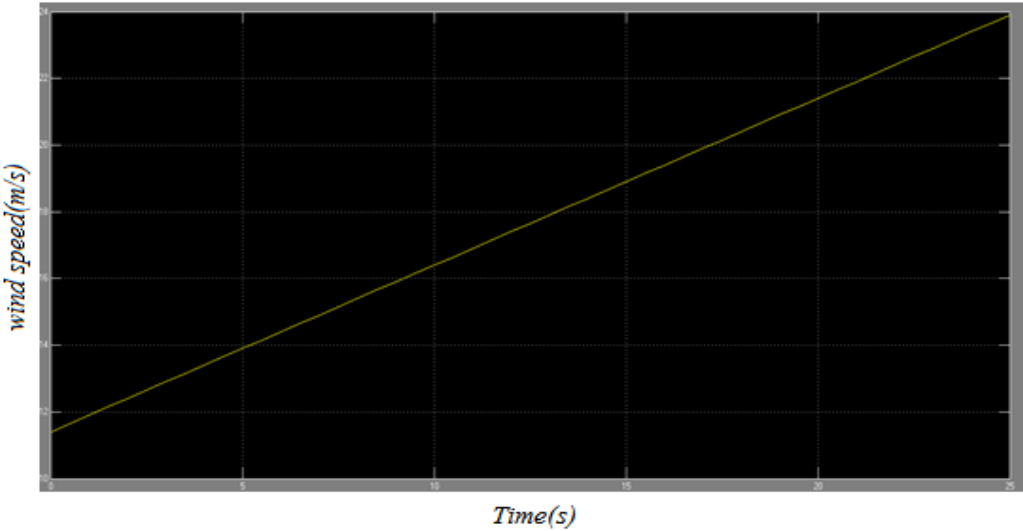


Figure 5.10. Wind speed variation in 25 seconds from.

Then using the equation reported before we calculate the pitch angle in each time step (degree), as shown below in the rated speed we have an error of almost two degrees this error can be minimized choosing another interpolation equation.

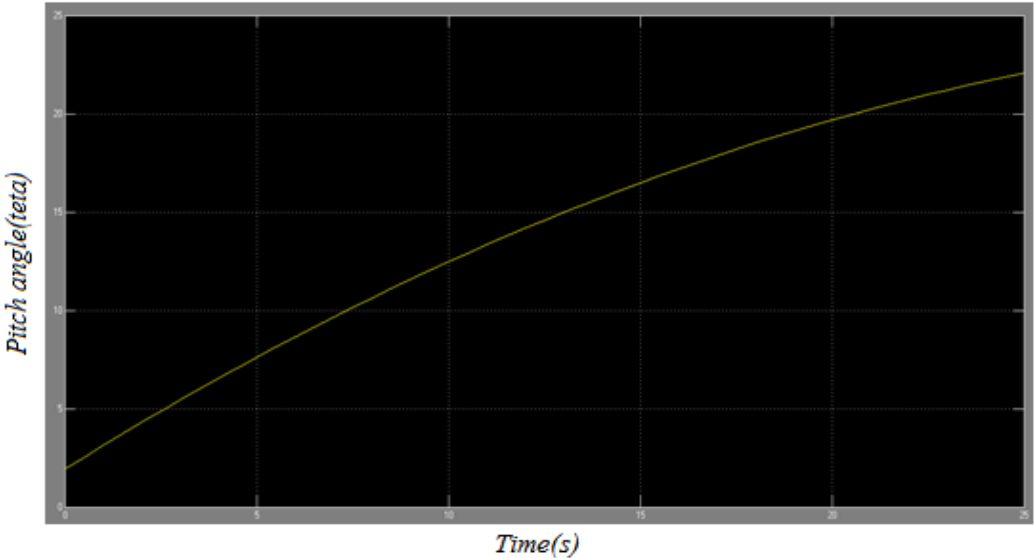


Figure 5.11. Pitch angles in stationary condition due to wind speed variation.

The resulting gains for the angles in each time step is reported below, the first plot is the integral gain K_i , the second plot is the K_p and the third plot is the pitch sensitivity ($\frac{\partial P}{\partial \theta}$) that is used for the dynamic model and also as denominator (as the sole variable) in both of the gains.

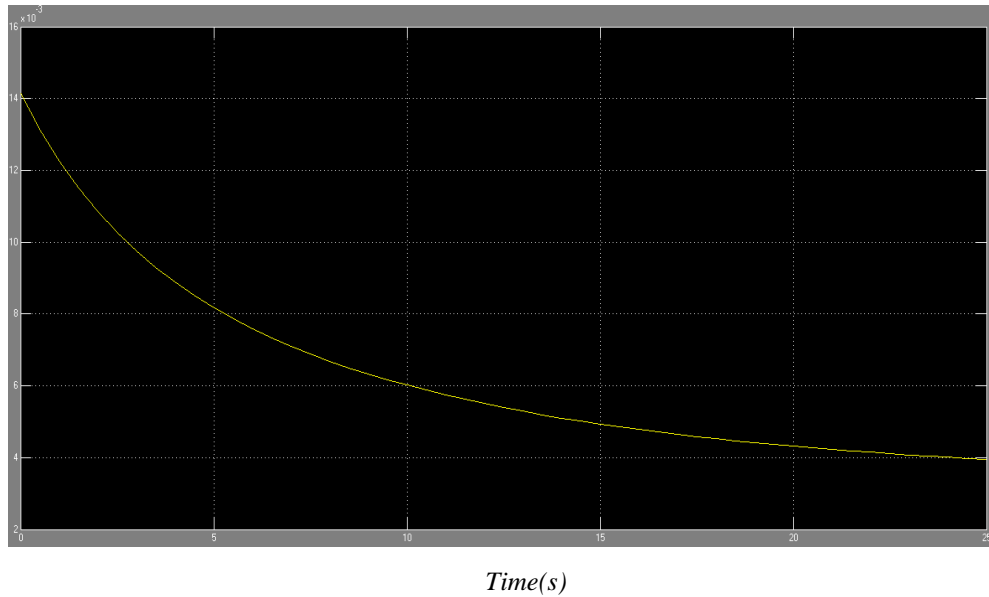


Figure 5.12. Integral gain variation in time.

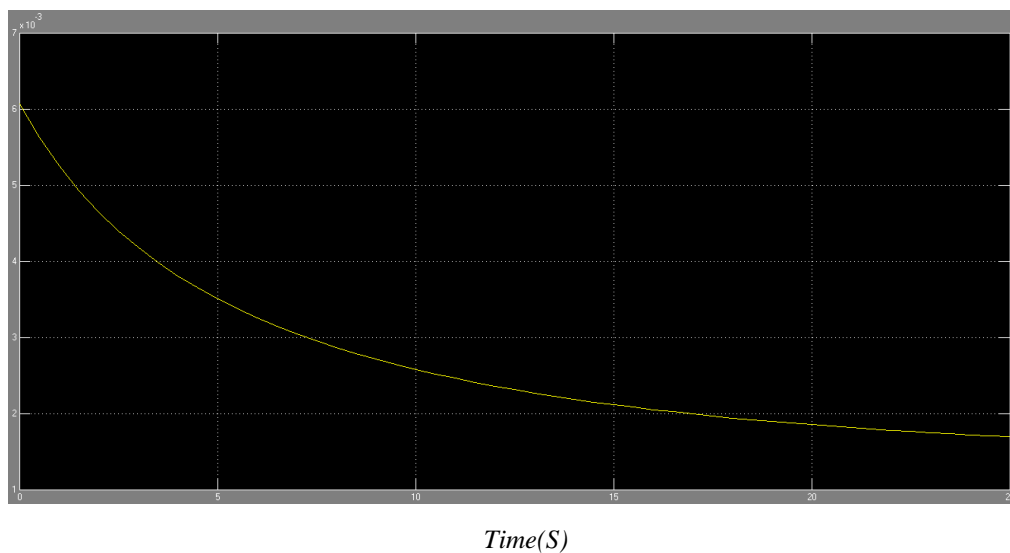


Figure 5.13. Proportional gain variation of the control system.

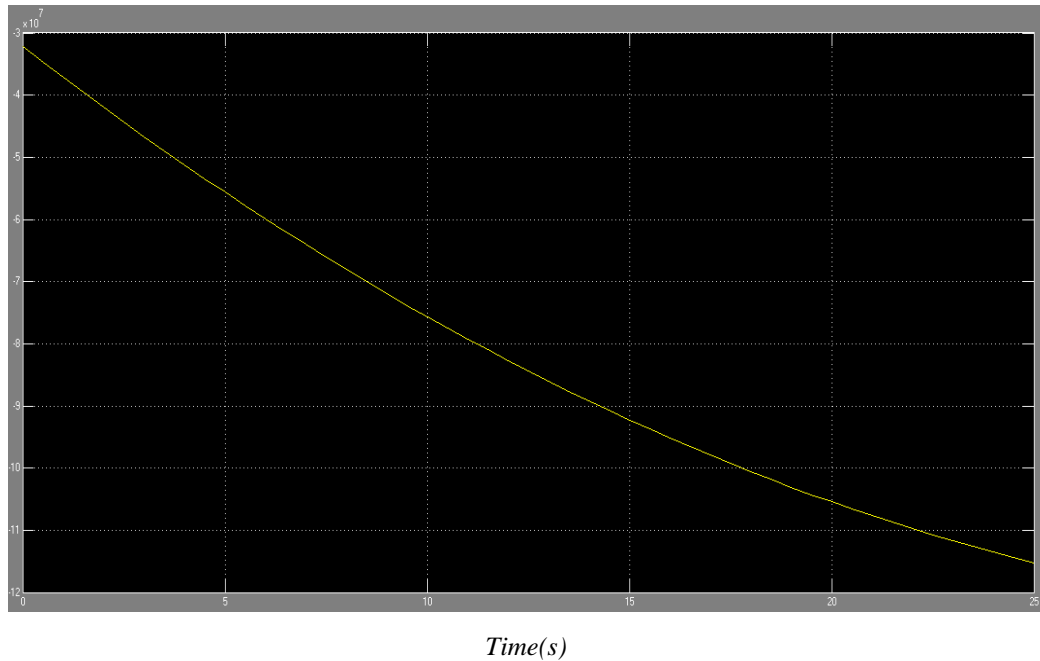


Figure 5.14. Pitch sensitivity variation in time.

As a result the variation of the rotational speed $\Delta\Omega$ remains equal to zero even if we insert an input different from zero the control system can compensate this difference if it is small but if this variation is not small as the equation $\theta = -0.21V^2 + 7.05V - 34.5$ is defined for the constant rotational velocity equal to 12.1 rpm the pitch control will insert bigger error in the pitch angle calculation and the system may diverge.

5.3.2 DC Motor Simulink Scheme

Now we will do the same simulation for our scaled model with the only difference that for the scaled model we have designed a DC motor Simulink model that inserts the dynamics of the motor in our model to have a more realistic model that considers also the motor as one of the parameters that can add errors in the system the model of the DC motor is reported below using the real data of our motor chosen before with the position control of the motor. The gains used for the motor can be changed to have a better behavior of the control

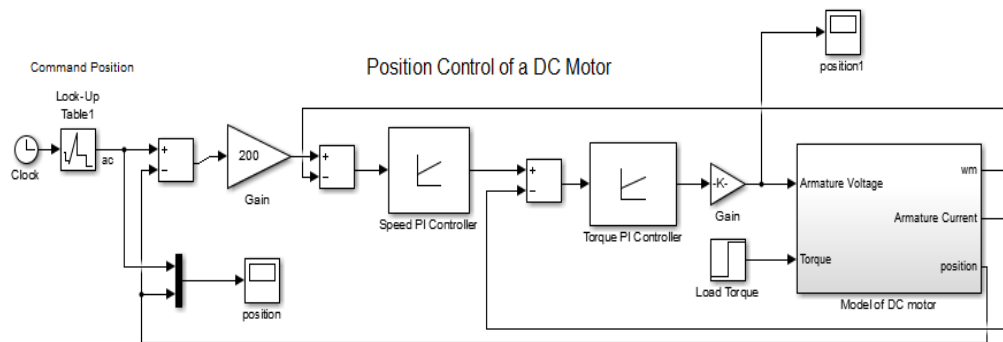


Figure 5.15. DC Motor Simulink Scheme

The input in this model is the pitch angle of the motor as we use a gearhead we have to consider also the gearhead in the model. To show the behavior of the model and the efficiency of the gains that we have chosen for the position control we have inserted as input a table of positions to see the behavior of the motor and the control system to follow the required position θ (degree).

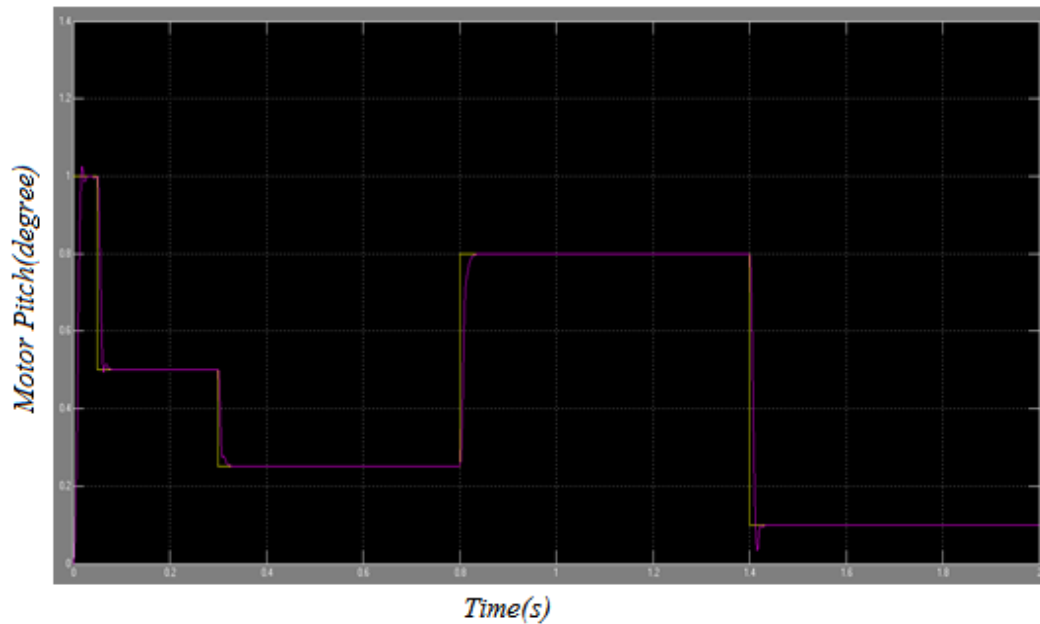


Figure 5.16. DC motor transition behavior with the gains used for the position control of the motor. Yellow: requirement of the control system. Red response of the motor.

So our model for the feed forward scaled model becomes

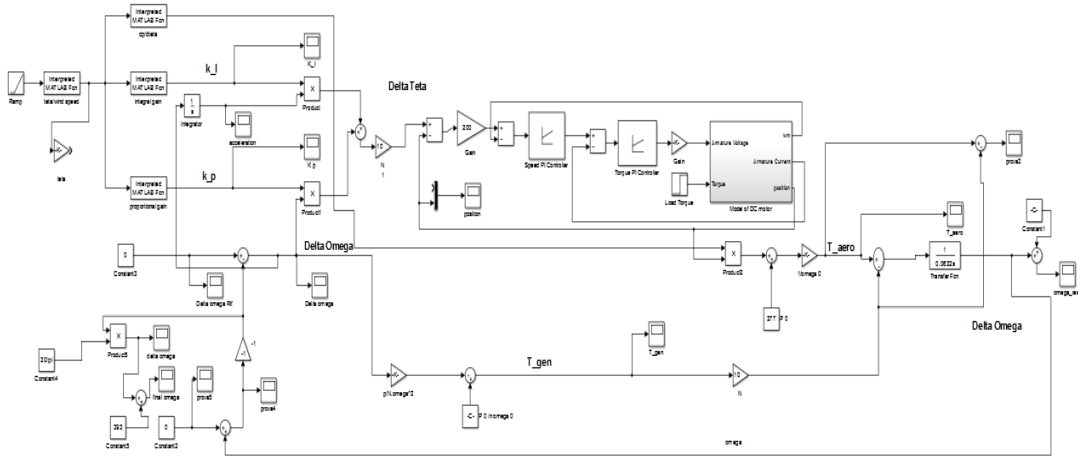


Figure 5.17. Simulink scheme of the Feedforward control, for the scaled model with the DC Motor model for the pitch control.

5.3.3 Simulation Results (Scaled Model)

The input (wind speed) is in range of 6.4 and 14 m/s and then as the full scale model the Simulink file calculates the pitch angle. The rotor velocity is 393 rpm. The simulation time is 15 seconds.

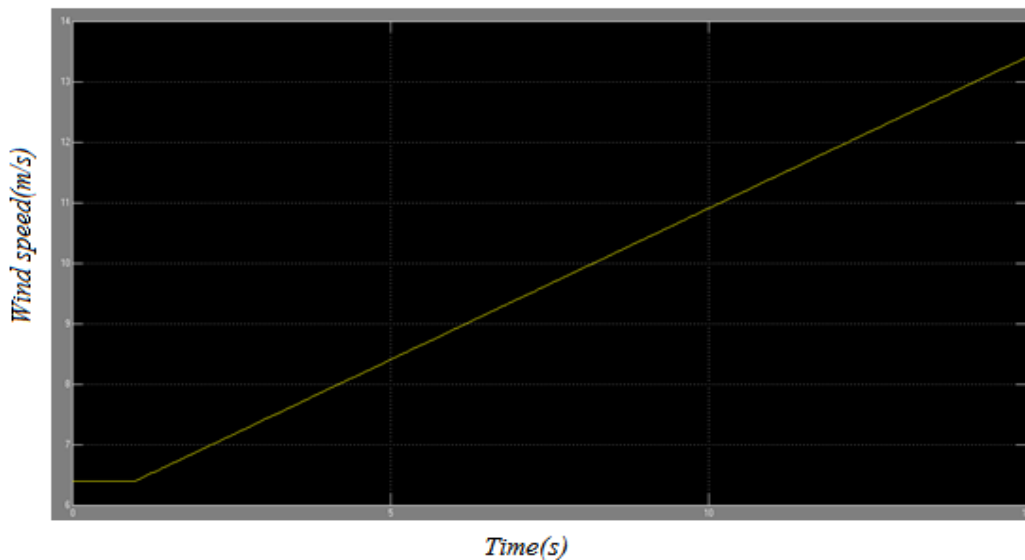


Figure 5.18. Wind speed in the scaled model.

The resulting angles that we obtain for the following wind speed behavior is:

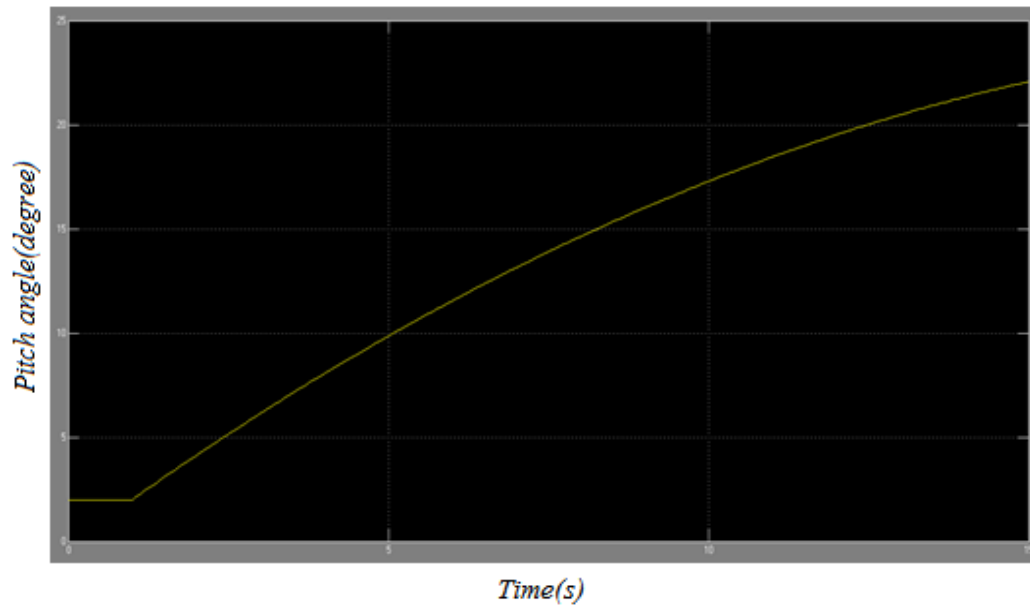


Figure 5.19. Blade Pitch angles due to the input wind speed.

In the next step the integral and proportional gains are calculated to compensate the influence of the variation of wind speed on the rotor speed. So as a result we expect that by changing the wind velocity the pitch angle increases and the gains decreases (as shown before). The first plot is the integral gain K_i and the second plot is the proportional gain. The last figure is the pitch sensitivity $\left(\frac{\partial P}{\partial \theta}\right)$.

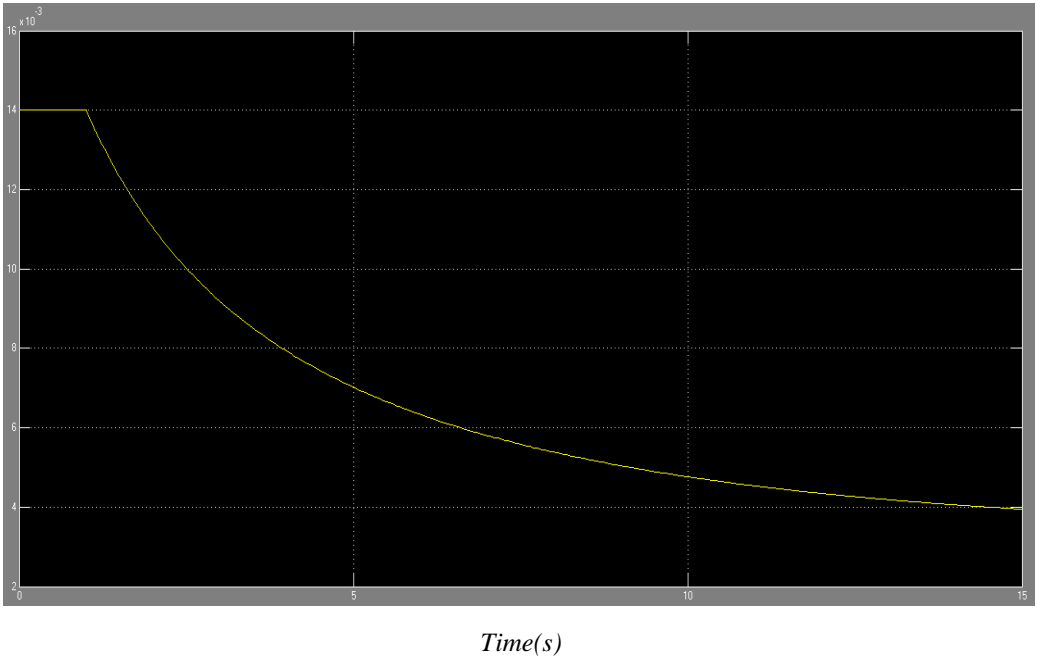


Figure 5.20. Integral Gains.

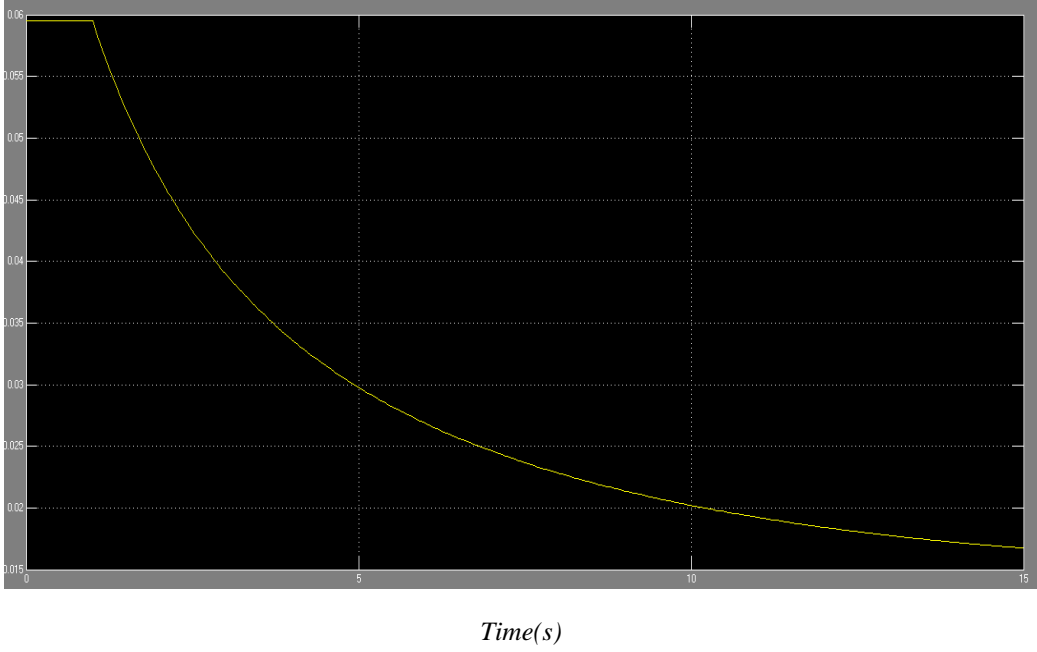


Figure 5.21. Proportional Gains.

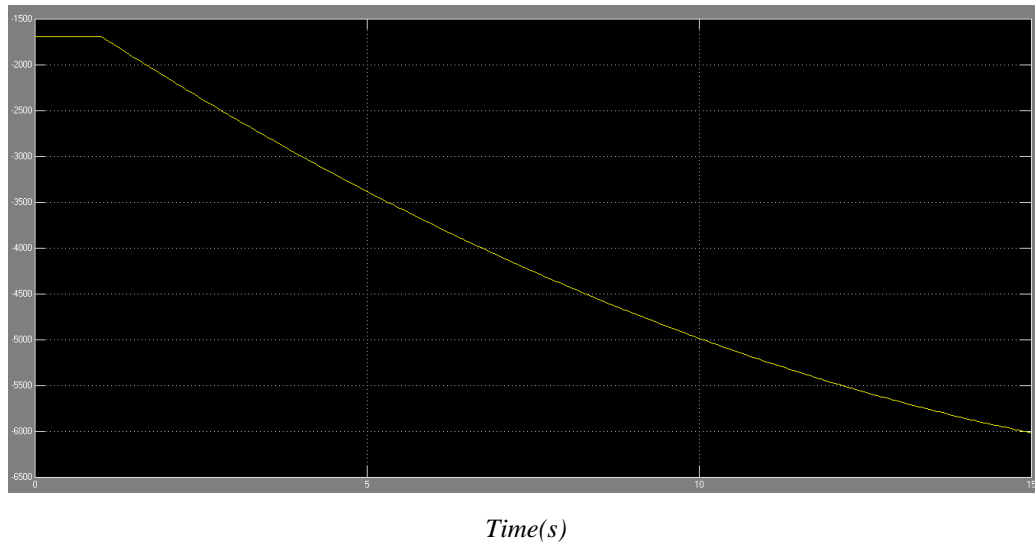


Figure 5.22. Blade pitch sensitivity.

As a result the control keeps constant the rotational velocity of the rotor that is the aim of the control. As shown in the figure below the system has oscillation around the rated rotational speed $\Delta\Omega$. This oscillation is because of the very fast dynamics of the scaled model. But as the amplitude is very low and not divergent the result is acceptable.

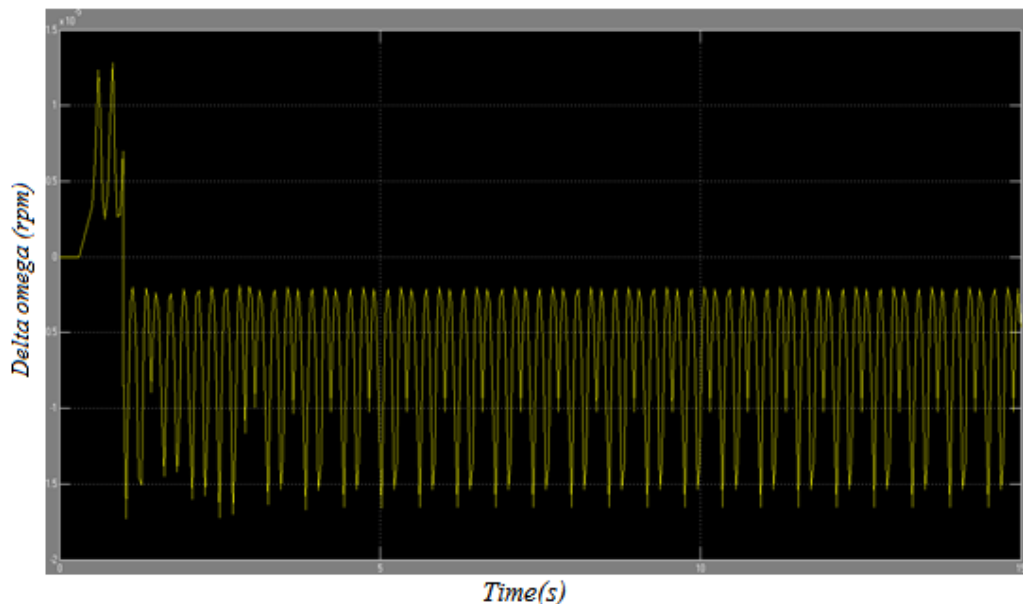


Figure 5.23. Rotor rotational velocity.

5.4 Feedback Control System Design

The second control has a feedback on the pitch angle and gets the angle from previous controller step time to calculate the gain at the next step. Else of calculating the pitch angle considering the wind speed so in this case the sole input for the control system is the rotor rotational velocity. The Simulink scheme for this controller has been reported below

5.4.1 Simulation results (Full Scale)

As shown in the figure we introduce an impulse of 0.3(rad/s) to the velocity of the full scale model reported in the following figure this impulse influences the whole system and control system acts to make the velocity turn back to the nominal value that is 12.1(rpm). The simulation time for the full scale model is 20 seconds and the impulse width is 0.1 second.

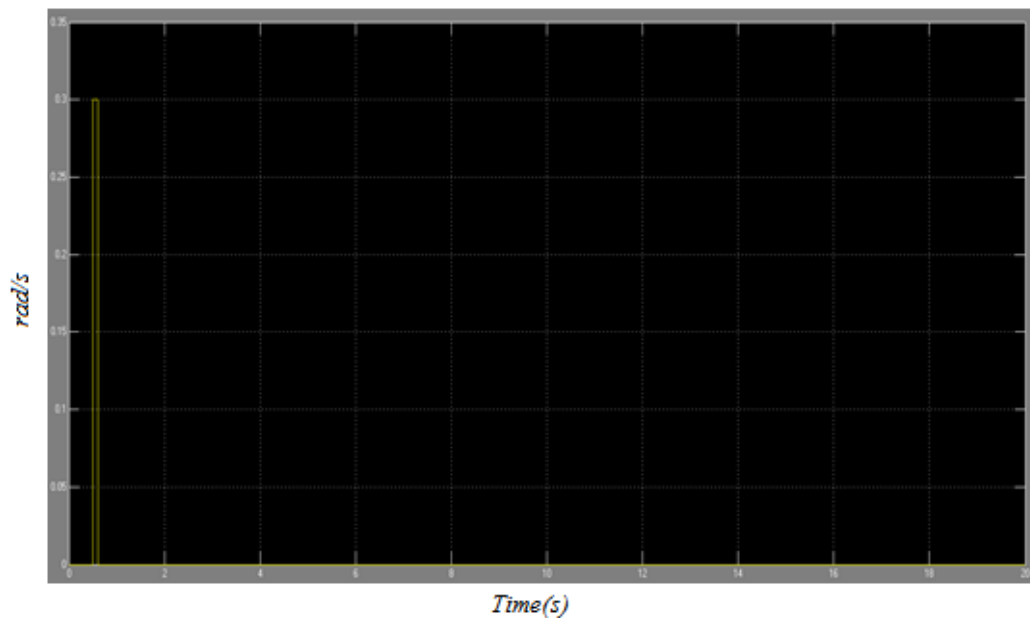
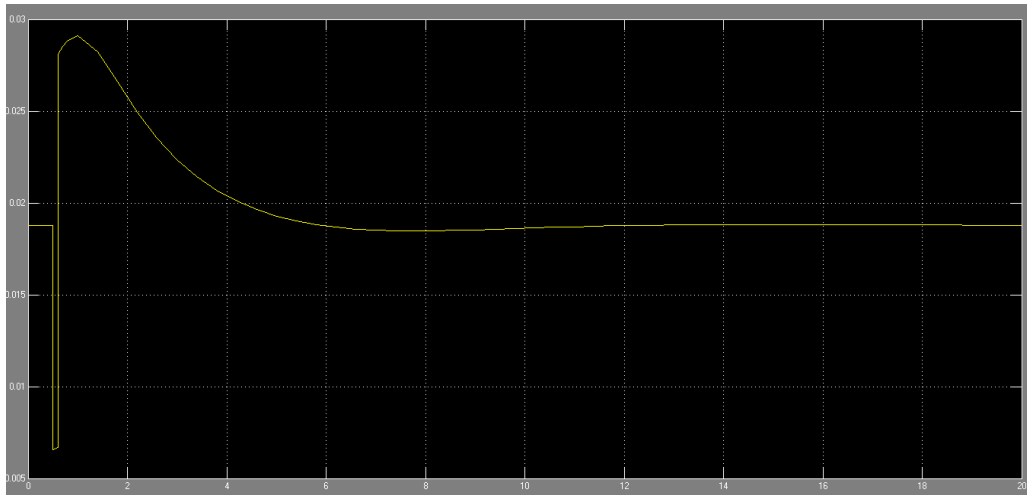


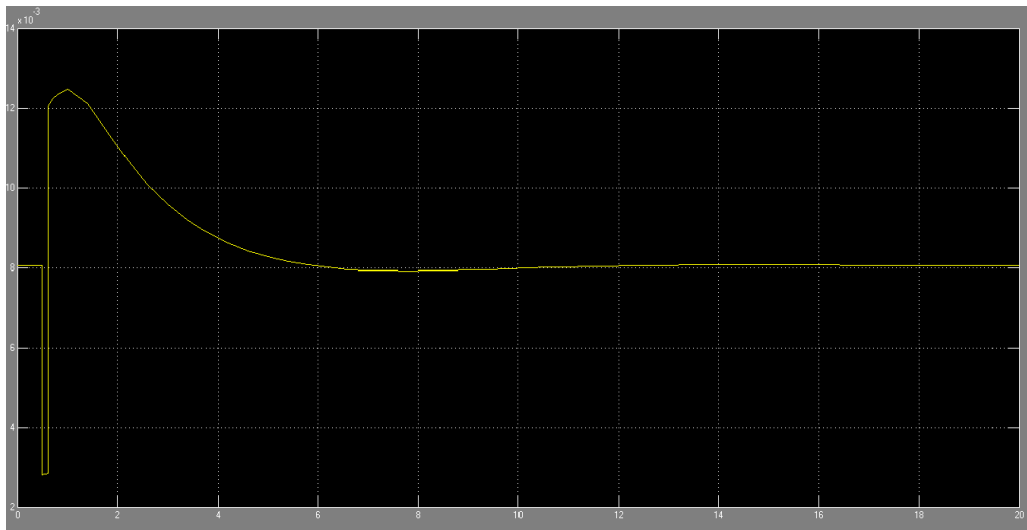
Figure 5.24. Impulse imposed to the rotational velocity of the rotor.

As a result we will have that the control system acts with the following gains to compensate the variation of the rotational speed that is the parameter that the control system acts to keep constant in the following figures the first figure is the gains of the integral controller and in the second figure it is reported the integral and proportional gains for each second.



Time(s)

Figure 5.25. Integral Gain.



Time(s)

Figure 5.26. Proportional gain.

As a result the PI controller change the pitch angle to stabilize the system, below is reported the $\Delta\theta$ for each time step of the simulation. (unit in degree).

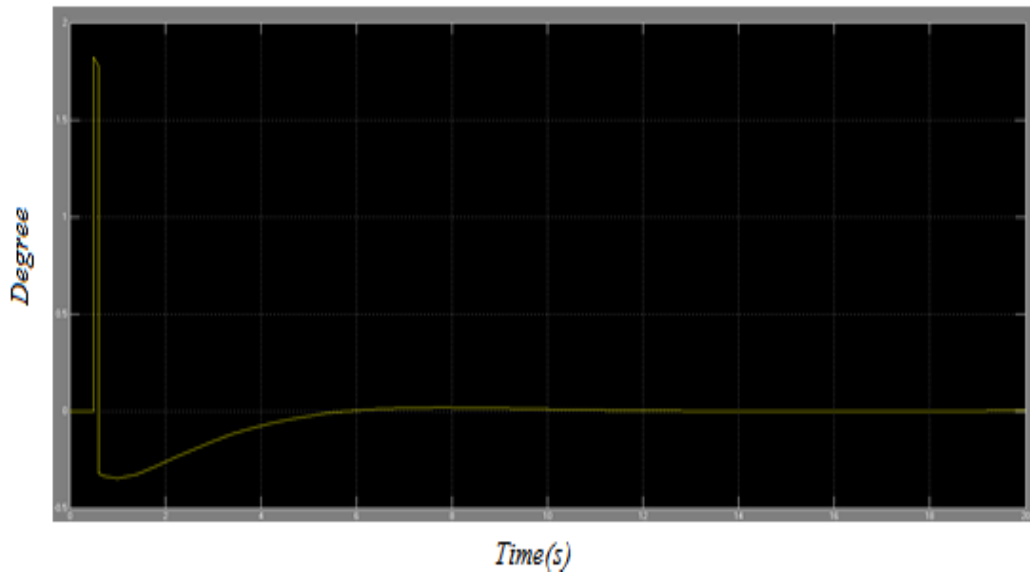


Figure 5.27. Pitch angle variation.

The aerodynamic torque and the generator torque are also reported in the following figures the value of both of the torques are decreased when the impulse is imposed and then the control system forces the system to turn to the rated value (Nm)

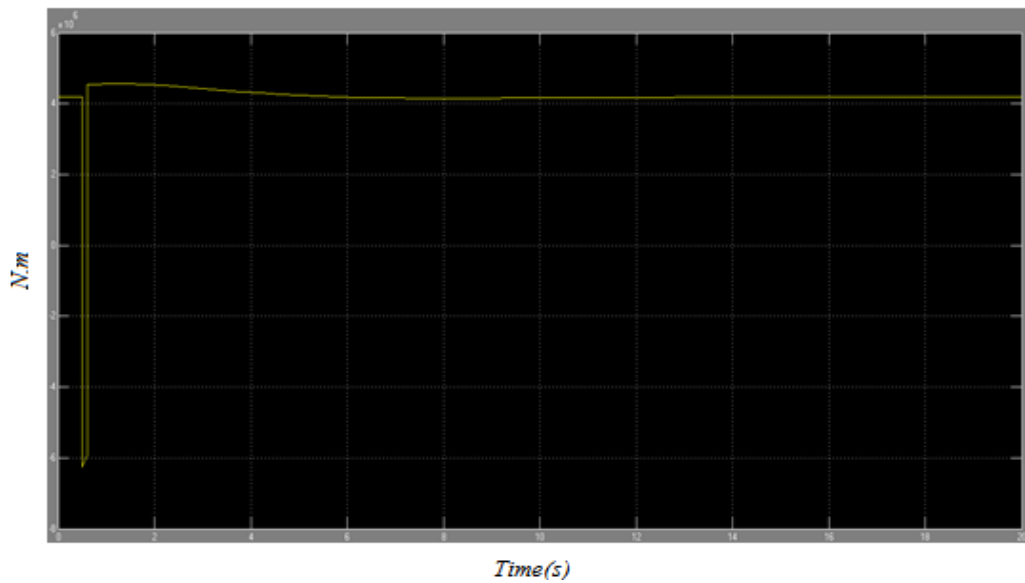


Figure 5.28. Aerodynamic torque of the blade.

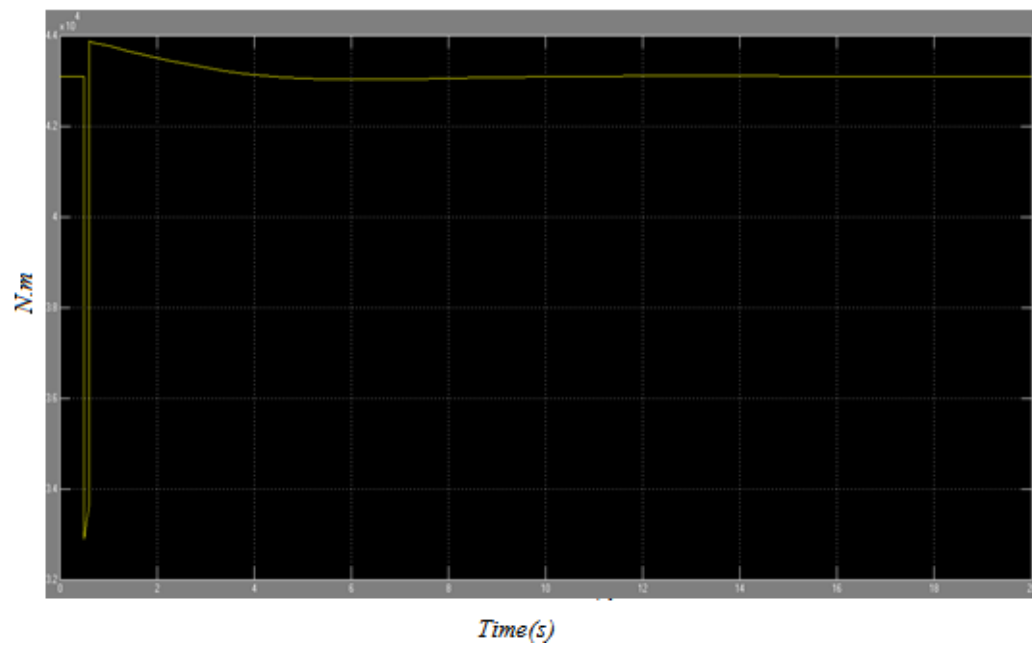


Figure 5.29. Generator torque due to power generator control.

As we know the dynamic of the full scale model is very slow because of huge inertia of the system so the control takes almost 12 seconds to turn back to

the nominal value and the first part of the plot else of being completely vertical as we saw before is slightly inclined. Below in the figure is reported the variation of the nominal velocity Ω around the nominal value that is 12.1 (rpm)

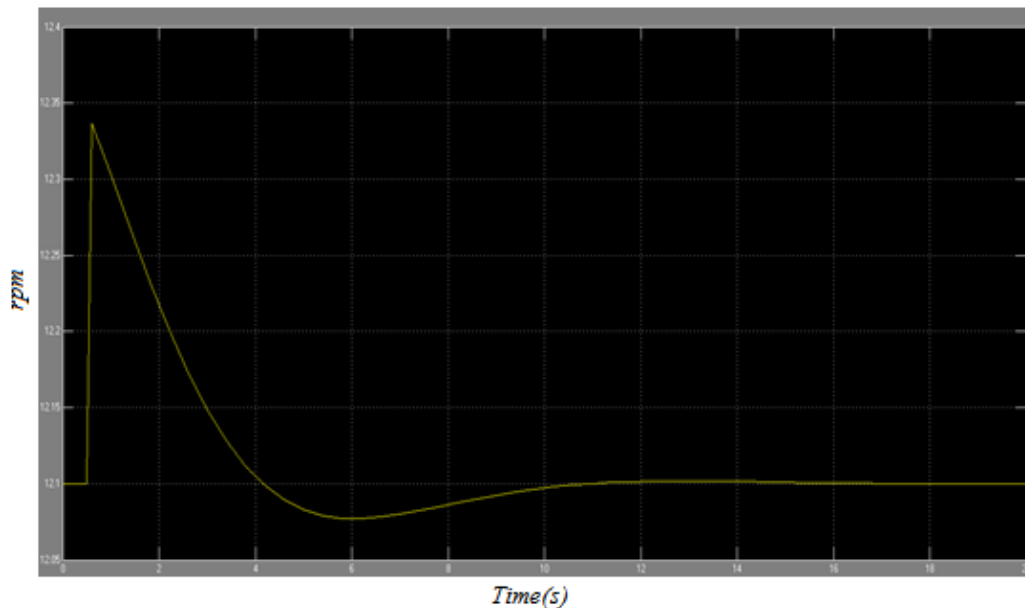


Figure 5.30. Full scale controlled system rotor rotational velocity.

In the real case we have to put a limitation that does not let the pitch angle to go in the negative values of pitch angle but to have a better view of the dynamic of the system we did not put this limitation.

5.4.2 Simulation results (Scaled Model)

Now we will see the same simulation for our scaled model wind turbine we expect the system to be faster because of the fast dynamic of the system and slight variation around the nominal values. That can be solved putting filters on the signals of the high frequency that we are not interested in. Again we impose an impulse with the amplitude equal to 0.3 and width of 0.1 second as reported in the following figure.

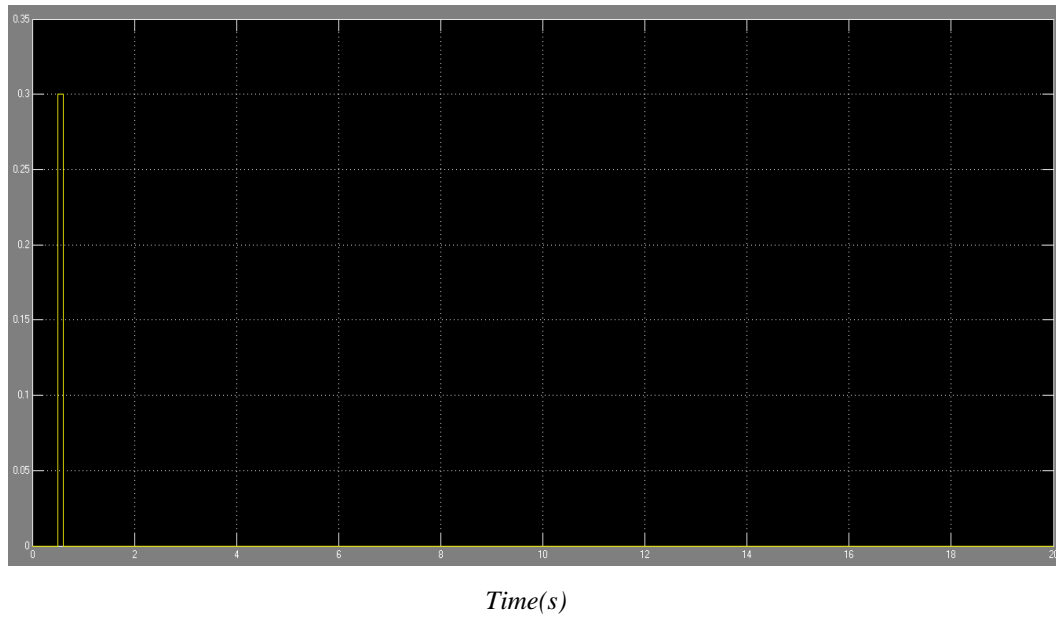


Figure 5.31. Impulse imposed on the rotational velocity of the rotor (rad/s).

The dynamic of the scaled model is faster than the full scale model so as shown in the figure imposing the same impulse the control system can make the system to turn back to the rated velocity in few milliseconds. Below is reported in the first figure the variation of the nominal velocity $\Delta\Omega$ and in the second figure the variation of Ω around the nominal value that is 393 (rpm).

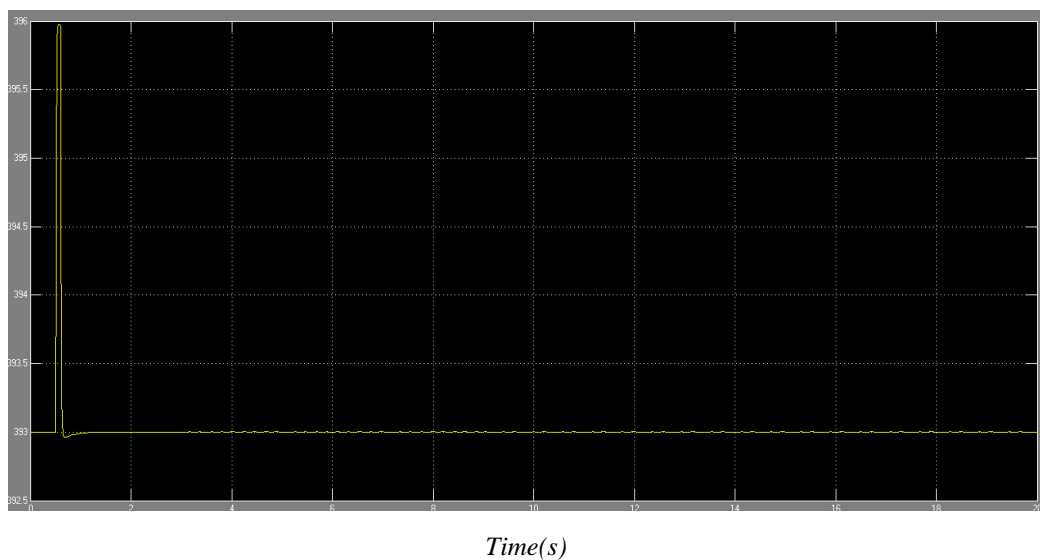


Figure 5.32. Rotor rotational velocity of the controlled system at 393 rpm.

CONCLUSIONS

The purpose of this Thesis is to design with high level of detail a 1/58th scale model wind turbine based on the NREL 5 MW reference model for the purpose of construction and future tests in the GVPM wind tunnel .

This has been motivated by the fact that simulation is the key of the design and optimization of wind energy systems, while model validation and calibration is the key for ensuring that the predictions generated by simulation models are reliable. Although wind tunnel testing cannot exactly reproduce full scale conditions nor can it substitute field testing, it may play an important role in the validation of models and in the evaluation of new concepts and ideas.

This thesis presents not only the scaling methodologies used for scaling the reference wind turbine to create a rigid scaled model, but also proposes the best components that fit with the scaled model dimensions and requirements reporting the methodologies used for this aim. There has been also proposed different layouts for the Blade, Rotor, Drivetrain, Nacelle, Tower and the connections in between. Some of the layouts proposed have never been used in previous works giving huge benefits in the design of the scaled wind turbines. This has been possible because of being in contact with the producers of different companies to find the best solutions to solve the problems of the previous scaled model layouts and to find the flexibility of the producers in modifying standard products for specific applications.

At the end there has been designed the control system adapting the control laws designed by references to our scaled model, and it has been created the control systems in the Simulink environment that can be useful for future academic studies.

Further works can be done on the Control system design of the model as it is a field that the innovation influences a lot on the efficiency and the cost effectiveness of wind turbines. As an example the IPC control

that has not been implemented on our model (but has been verified that the motors chosen are adequate for this type of control system) is a future work that can be done on the model. In variable pitch control, the wind speed in the axis of the blade is used as the reference wind speed for wind blade synchronous control. In fact, the wind speed is changing with the height. With the increasing of the wind turbine capacity, the difference of the blade wind speed in different spin high degree is gradually increasing, making the loads of the blades tend to gradually increase, which has seriously affected the wind turbine life. Blade pitch control has primarily been used to limit aerodynamic power in above rated wind speeds. In order to keep the turbine within its design limits and to optimize energy capture at below rated conditions, collective pitch control techniques have been successfully utilized for this purpose (as we have implemented in Chapter 5). But as rotor size increases there is an increased interest in utilizing pitch control to alleviate loads experienced by wind turbines by pitching the blades individually.

APPENDIX A

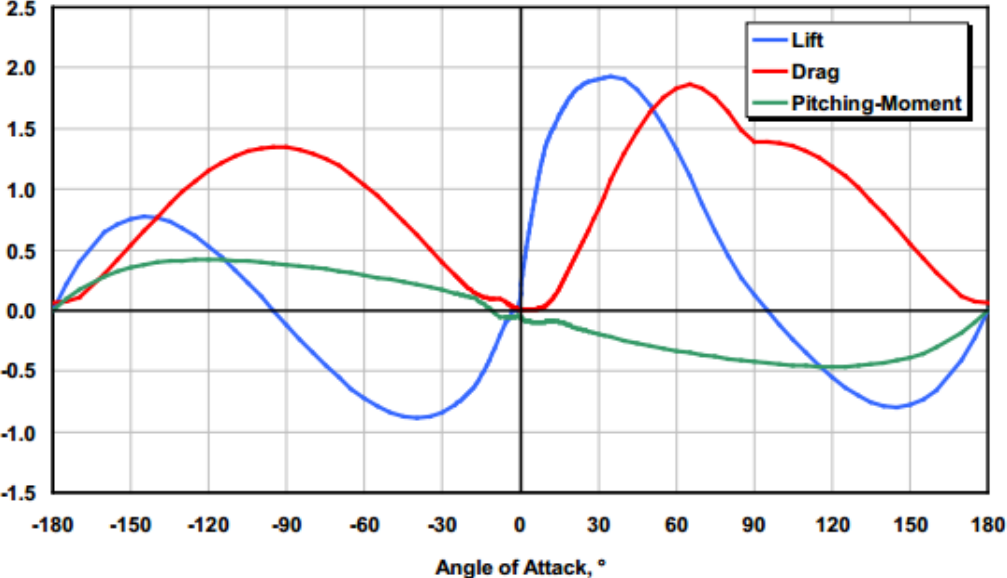


Figure A.1 Aerodynamic coefficients of DU40 airfoil

Elevation (m)	HtFract (-)	TMassDen (kg/m)	TwFASTif (N·m ²)	TwSSStif (N·m ²)	TwGJStif (N·m ²)	TwEASTif (N)	TwFAlner (kg·m)	TwSSIner (kg·m)	TwFAcgOf (m)	TwSScgOf (m)
0.00	0.0	5590.87	614.34E+9	614.34E+9	472.75E+9	138.13E+9	24866.3	24866.3	0.0	0.0
8.76	0.1	5232.43	534.82E+9	534.82E+9	411.56E+9	129.27E+9	21647.5	21647.5	0.0	0.0
17.52	0.2	4885.76	463.27E+9	463.27E+9	356.50E+9	120.71E+9	18751.3	18751.3	0.0	0.0
26.28	0.3	4550.87	399.13E+9	399.13E+9	307.14E+9	112.43E+9	16155.3	16155.3	0.0	0.0
35.04	0.4	4227.75	341.88E+9	341.88E+9	263.09E+9	104.45E+9	13838.1	13838.1	0.0	0.0
43.80	0.5	3916.41	291.01E+9	291.01E+9	223.94E+9	96.76E+9	11779.0	11779.0	0.0	0.0
52.56	0.6	3616.83	246.03E+9	246.03E+9	189.32E+9	89.36E+9	9958.2	9958.2	0.0	0.0
61.32	0.7	3329.03	206.46E+9	206.46E+9	158.87E+9	82.25E+9	8356.6	8356.6	0.0	0.0
70.08	0.8	3053.01	171.85E+9	171.85E+9	132.24E+9	75.43E+9	6955.9	6955.9	0.0	0.0
78.84	0.9	2788.75	141.78E+9	141.78E+9	109.10E+9	68.90E+9	5738.6	5738.6	0.0	0.0
87.60	1.0	2536.27	115.82E+9	115.82E+9	89.13E+9	62.66E+9	4688.0	4688.0	0.0	0.0

Figure A.2 Distributed tower property of the NREL 5MW wind turbine

Appendix B



Planetary Gearheads

0,7 Nm

For combination with
DC-Micromotors
Brushless DC-Motors
Stepper Motors

Series 22/7

	22/7
Housing material	metal
Geartrain material	steel
Recommended max. input speed for:	
- continuous operation	4 000 rpm
Backlash, at no-load	≤ 1 °
Bearings on output shaft	ball bearings, preloaded
Shaft load, max.:	
- radial (10 mm from mounting face)	≤ 170 N
- axial	≤ 150 N
Shaft press fit force, max.	≤ 150 N
Shaft play	
- radial (10 mm from mounting face)	≤ 0,03 mm
- axial	≤ 0,1 mm
Operating temperature range	- 30 ... + 100 °C

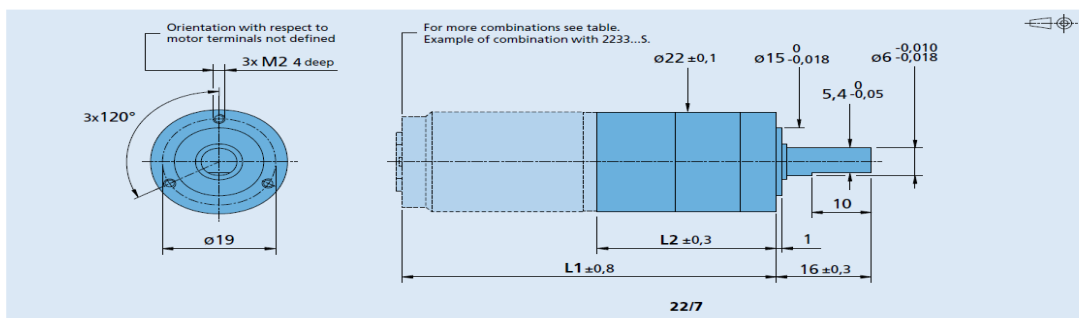
Specifications

	1	2	3	4	5
Number of gear stages	1	2	3	4	5
Continuous torque	200	300	700	700	700
Intermittent torque	400	600	1 000	1 000	1 000
Mass without motor, ca.	68	63	76	88	102
Efficiency, max.	88	80	70	60	55
Direction of rotation, drive to output	=	=	=	=	=
Reduction ratio ¹⁾ (rounded)	3,71:1	9,7:1 14:1	43:1 66:1	94:1 112:1 134:1 159:1 190:1 246:1	415:1 592:1 989:1 1 526:1
L2 [mm] = length without motor ²⁾	27,9	34,1	40,3	46,4	52,6
L1 [mm] = length with motor					
2224U...SR	48,2	54,4	60,6	66,7	72,9
2230U...S	54,0	60,2	66,4	72,5	78,7
2232U...SR	56,2	62,4	68,6	74,7	80,9
2233U...S	56,6	62,8	69,0	75,1	81,3
2237S...CXR	64,9	71,1	77,3	83,4	89,6
2342S...CR	69,9	76,1	82,3	88,4	94,6
2232S...BX4(S)	61,7	67,9	74,1	80,2	86,4
2250S...BX4(S)	79,7	85,9	92,1	98,2	104,4
2444S...B	71,9	78,1	84,3	90,4	96,6
AM2224...-10	55,6	61,8	68,0	74,1	80,3

¹⁾ The reduction ratios are rounded, the exact values are available on request or at www.faulhaber.com.

²⁾ L2 - 3,9 mm, in combination with 2224U...SR, 2230U...S, 2232U...SR, 2233U...S and AM2224.

Note: Reduction ratio 3,71:1 with motor types 2224U...SR, 2230U...S, 2232U...SR, 2233U...S and AM2224 shall be ordered as 22/7 3,71:1 - K288.



For notes on technical data and lifetime performance refer to "Technical Information".
Edition 2014

© DR. FRITZ FAULHABER GMBH & CO. KG
Specifications subject to change without notice.
www.faulhaber.com

DC-Micromotors

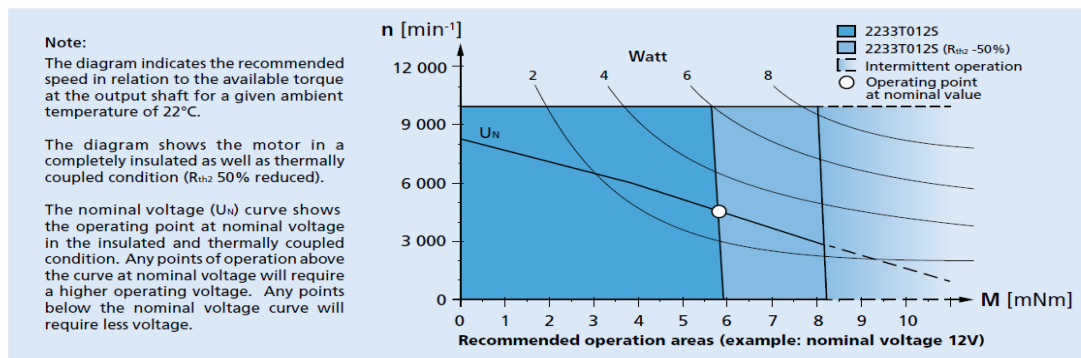
Precious Metal Commutation

5,9 mNm

8 W

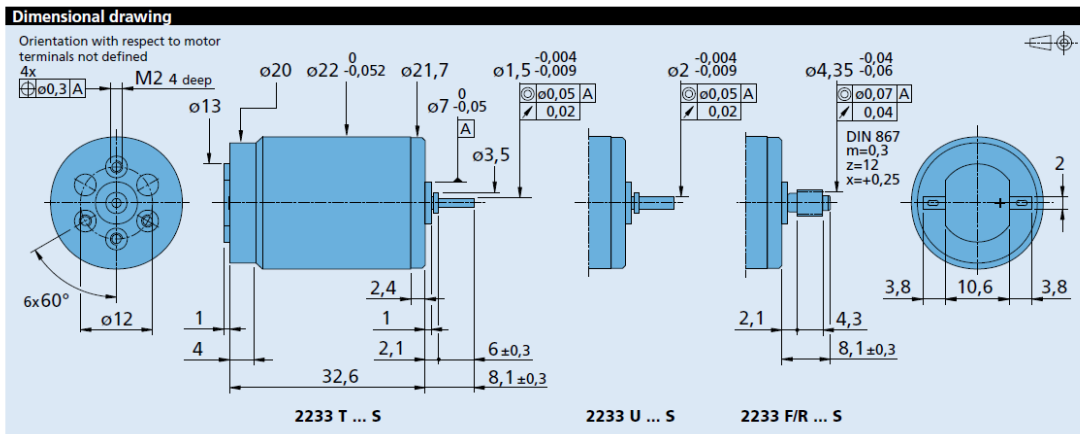
Series 2233 ... S

Values at 22°C and nominal voltage	2233 T	4,5 S	006 S	012 S	018 S	024 S	030 S	
1 Nominal voltage	U_N	4,5	6	12	18	24	30	V
2 Terminal resistance	R	1,2	2,7	9,6	25	52	97	Ω
3 Output power	$P_{2nom.}$	4,48	3,23	3,69	3,19	2,75	2,26	W
4 Efficiency, max.	$\eta_{max.}$	86	85	85	83	83	81	%
5 No-load speed	n_0	8 500	7 700	8 200	9 000	8 400	8 700	min ⁻¹
6 No-load current, typ. (with shaft \varnothing 1,5 mm)	I_0	0,02	0,014	0,007	0,005	0,004	0,003	A
7 Stall torque	M_H	20,2	16	17,3	13,4	12,4	9,9	mNm
8 Friction torque	M_R	0,1	0,1	0,1	0,1	0,1	0,1	mNm
9 Speed constant	k_n	1 895	1 296	684	508	354	293	min ⁻¹ /V
10 Back-EMF constant	k_E	0,528	0,772	1,46	1,97	2,82	3,41	mV/min ⁻¹
11 Torque constant	k_M	5,04	7,37	14	18,8	27	32,6	mNm/A
12 Current constant	k_i	0,198	0,136	0,072	0,053	0,037	0,031	A/mNm
13 Slope of n-M curve	$\Delta n/\Delta M$	421	483	472	676	678	877	min ⁻¹ /mNm
14 Rotor inductance	L	60	120	440	800	1 600	2 400	μ H
15 Mechanical time constant	τ_m	11,5	10	11	17	11	12,9	ms
16 Rotor inertia	J	2,6	2	2,2	2,5	1,6	1,4	gcm ²
17 Angular acceleration	$\alpha_{max.}$	77	80	78	54	78	71	$\cdot 10^3$ rad/s ²
18 Thermal resistance	R_{th1} / R_{th2}	4 / 27						K/W
19 Thermal time constant	τ_{w1} / τ_{w2}	4 / 660						s
20 Operating temperature range:								
- motor		-30 ... +85 (optional version -55 ... +125)						°C
- winding, max. permissible		+125						°C
21 Shaft bearings		sintered bearings (standard)			ball bearings, preloaded (optional version)			
22 Shaft load max.:								
- with shaft diameter		1,5			2			mm
- radial at 3 000 min ⁻¹ (3 mm from bearing)		1,2			8			N
- axial at 3 000 min ⁻¹		0,2			0,8			N
- axial at standstill		20			10			N
23 Shaft play								
- radial	\leq	0,03			0,015			mm
- axial	\leq	0,2			0			mm
24 Housing material		steel, zinc galvanized and passivated						
25 Mass		61						g
26 Direction of rotation		clockwise, viewed from the front face						
27 Speed up to	$n_{max.}$	10 000						min ⁻¹
28 Number of pole pairs		1						
29 Magnet material		AlNiCo						



For notes on technical data and lifetime performance refer to "Technical Information".
Edition 2015

© DR. FRITZ FAULHABER GMBH & CO. KG
Specifications subject to change without notice.
www.faulhaber.com



Options

Example product designation: **2233T012S-277**

Option	Type	Description
L	Twin Leads	For motors with twin leads (PVC), length 150 mm, red (+) / black (-)
4924	Twin Leads	For motors with twin leads (PVC), length 300 mm, red (+) / black (-)
X4924	Twin Leads	For motors with twin leads (PVC), length 600 mm, red (+) / black (-)
4925	Twin Leads	For motors with twin leads (PVC), length 150 mm, red (+) / black (-), with connector AMP 179228-2
X4925	Twin Leads	For motors with twin leads (PVC), length 300 mm, red (+) / black (-), with connector AMP 179228-2
Y4925	Twin Leads	For motors with twin leads (PVC), length 600 mm, red (+) / black (-), with connector AMP 179228-2
F	Single Leads	For motors with single leads (PTFE), length 150 mm, red (+) / black (-)
277	Bearings	2 preloaded ball bearings

Product Combination

Precision Gearheads / Lead Screws	Encoders	Drive Electronics
20/1	HEDS 5500	SC 1801
22E	HEDM 5500	SC 2402
22EKV	HEDS 5540	SC 2804
22/7	HEDL 5540	MCDC 3002
23/1		MCDC 3003
22/2		MCDC 3006
22/5		

For notes on technical data and lifetime performance refer to "Technical Information", Edition 2015

© DR. FRITZ FAULHABER GMBH & CO. KG
Specifications subject to change without notice.
www.faulhaber.com

Encoders

optical Encoder, digital outputs,
2 channels, 100 - 500 lines per revolution

For combination with
DC-Micromotors
Brushless DC-Motors

Series HEDS 5500

	HEDS 5500 C	HEDS 5500 A	
Lines per revolution	N	100	
Frequency range, up to ¹⁾	f	100	kHz
Signal output, square wave		2	Channels
Supply voltage	U _{DD}	4,5 ... 5,5	V
Current consumption, typical ²⁾	I _{DD}	17	mA
Pulse width	P	180 ± 45	°e
Phase shift, channel A to B	Φ	90 ± 20	°e
Logic state width	S	90 ± 45	°e
Cycle	C	360 ± 5,5	°e
Signal rise/fall time, max. (C _{LOAD} = pF)	tr/tf	0,25 / 0,25	µs
Inertia of code disc	J	0,6	gcm ²
Operating temperature range		-40 ... +100	°C

¹⁾ Velocity (rpm) = f (Hz) x 60/N

²⁾ U_{DD} = 5 V; with unloaded outputs

For combination with Motor

Dimensional drawing A	<L1 [mm]		
2230 ... S	52,8	3890 ... CR	112,1
2233 ... S	55,6	2036 ... B - K312	56,8
2342 ... CR	63,8	2057 ... B - K312	75,8
2642 ... CXR	64,8	2444 ... B - K312	64,9
2642 ... CR	64,8	3056 ... B - K312	76,1
2657 ... CXR	79,8	3564 ... B - K312	84,1
2657 ... CR	79,8	4490 ... B - K312	116,3
3242 ... CR	65,3	4490 ... B5 - K312	116,3
3257 ... CR	80,3		
3272 ... CR	95,3		
3863 ... CR	86,1		

Characteristics

These incremental shaft encoders in combination with the DC-Motors are designed for the indication and control of both shaft velocity and direction of rotation as well as for positioning.

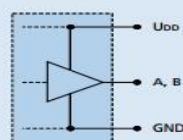
A LED source and lens system transmits collimated light through a low inertia metal disc to give two channels with 90° phase shift. The single 5 volt supply and the two or three channel digital output signals are interfaced with a 5-pin connector.

Motors with ball bearings are recommended for continuous operation at low and high speeds and for elevated radial shaft load.

Details for the Motors and suitable reduction gearheads are on separate catalogue pages.

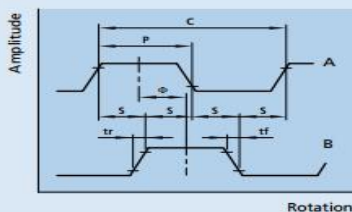
Circuit diagram / Output signals

Output circuit



Output signals

with clockwise rotation as seen from the shaft end



For notes on technical data and lifetime performance refer to "Technical Information".
Edition 2015

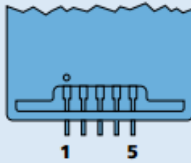
Page 1/2

© DR. FRITZ FAULHABER GMBH & CO. KG
Specifications subject to change without notice.
www.faulhaber.com

Connection information

No.	Function
1	GND
2	N.C.
3	Channel A
4	U ₀₀
5	Channel B

Connection Encoder



Option

- HEDS 5500 Interlocking connector, extension cables 300 mm length (Part No.: K798)

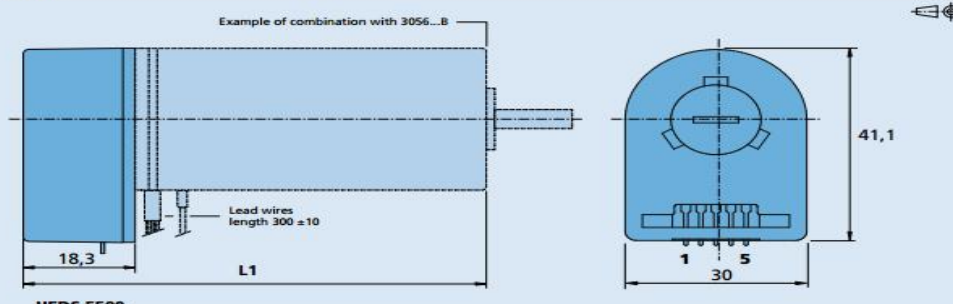
Recommended connector

AMP 103686-4/640442-5,
Molex 2695/2759
FCI 65039-032/4825x-000

Full product description

- Example:
2444S024B K312 HEDS5500C
3863H048CR HEDS5500A

Dimensional drawing A



Example of combination with 3056...B

Lead wires length 300 ± 10

18,3

L1

HEDS 5500

41,1

1 5 30



深圳市森瑞普电子有限公司

Senring Electronics Co., Limited.

SNH025 series(Through hole slip ring)

Through hole 25.4mm, OD: 86mm

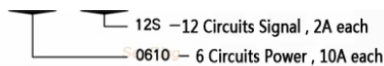
SNH025 series are standard through hole slip rings , through hole 25.4mm(suitable for <=25.4mm) , OD86mm, intergated structure with plastic & AL alloy,support signals(2A) , power 10A,circuitis no.*10A, voltage250VAC/VDC

Contact materials:precious metal + gold plating which ensures low torque,stable rotation, long life,low electrical noise and good transming performance.Compared to peer products , with advantages of higher rotation accuracy , more reliable performance and longer life

Typical application:automation equipment,working turntable,camera platform,robotics

Standard Part No.Description:

SNH025 - 0610 - 12S



For example :

SNH025-0610-12Smeans : through hole slip ring , hole size 25.4mm, OD 86mm, total 18circuits , 6circuits,10A each+ 12circuits,2A each (signal)

SNH025-0610through hole slip ring , hole size 25.4mm, OD 86mm,total 6circuits , 10A each

SNH025-12Smeans : through hole slip ring , hole size 25.4mm , OD 86mm,total 12circuits,2A each (signal)

* Remark: 10A circuits could be connected in parallel to be used as circuits no.*10A

* such as:two paralleling 10A circuits could be used as one 20A circuit

Technical Data

Circuits No	2~56(Pls refer to below table)	Current	standard 10A per circuit,2A(signal) per circuit, optional 20A per circuit
Voltage	440 VDC/VAC	Max speed	600RPM
Through hole size	25.4mm(or <=25.4mm)	OD	86mm
Housing material	AL alloy	Torque	0.1N.m;+0.03N.m/6 circuits
Working life	>80millions revolutions(depends on working speed,environment)	Contact material	Precious metal:gold-gold
Electrical Noise	<10mΩ @6VDC,50mA,5RPM	Contact Resistance	<20mΩ(AWG16#,300mm)
Dielectric Strength	800VDC@50Hz,10s	Lead wire Spec	UL Teflon@Awg22,3Awg16
Insulation Resistance	1000MΩ@600VDC,10s	Lead wire length	300mm
Work Temperature	-40°C to 85°C	IP grade	IP51
Mechanical vibration	MIL-SID-810E	Work Humidity	10% to 85% RH
Material	RoHS compliant	CE certificate	YES

Model no

Model no	Power circuits No.(10A)	Signal circuits No.S(5A)	Total circuits No.	L--Length(mm)
SNH025-0210	2	---	2	32
SNH025-0220	2	---	2	32
SNH025-024	2	---	2	36
SNH025-0310	3	---	3	36
SNH025-0320	3	---	3	36
SNH025-034	3	---	3	36
SNH025-0410	4	---	4	40
SNH025-0420	4	---	4	40
SNH025-044	4	---	4	40
SNH025-0210-02s	2	2	4	40
SNH025-0610	6	---	6	48
SNH025-0620	6	---	6	48
SNH025-064	6	---	6	48
SNH025-0210-04s	2	4	6	48
SNH025-0210-02s	2	4	6	48
SNH025-1210	12	---	12	72
SNH025-1220	12	---	12	72
SNH025-124	12	---	12	72
SNH025-0610-06s	6	6	12	72
SNH025-1810	18	---	18	96
SNH025-1820	18	---	18	96
SNH025-184	18	---	18	96
SNH025-0610-12s	6	12	18	96
SNH025-1210-06s	12	6	18	96
SNH025-2410	24	---	24	120
SNH025-2420	24	---	24	120
SNH025-244	24	---	24	120
SNH025-1210-12s	12	12	24	120
SNH025-0610-18s	6	18	24	120
SNH025-1010	10	---	30	144
SNH025-10s	---	30	30	144
SNH025-1810-12s	18	12	30	144
SNH025-1210-18s	12	18	30	144
SNH025-0610-24s	6	24	30	144
SNH025-3610	36	---	36	168
SNH025-36s	---	36	36	168
SNH025-2410-12s	24	12	36	168
SNH025-1210-24s	12	24	36	168
SNH025-48s	---	48	48	216
SNH025-36s	---	36	36	216

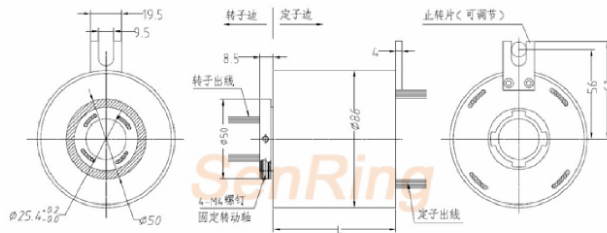
Tel: +86-755-29717812 Fax: +86-755-33250183 Email: Info@senring.com Website : www.senring.com



深圳市森瑞普电子有限公司

Senring Electronics Co., Limited.

Drawing



Lead Wire Color Code					
Ring no.#	Color	Ring no.#	Color	Ring no.#	Color
1	black	5	yellow	9	grey
2	brown	6	green	10	white
3	red	7	blue	11	pink
4	orange	8	purple	12	light blue

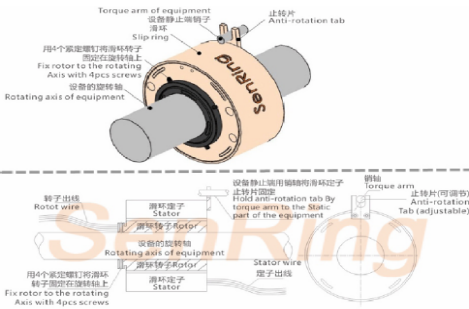
12 colors wires as a group, repeat from 13...24, each group wire marked with No. tube (1,2,3,4...)

Options

- ▲ Mounting flange
- ▲ Direction of lead wire exits
- ▲ support 1-56 circuits
- ▲ connectors and heat shrink tube
- ▲ Lead wire length
- ▲ Shield wire
- ▲ 500 MHz transmitting speed
- ▲ Transmit combined high speed data (Ethernet ,USB, Profibus)

- ▲ Combined with signal wires, coaxial wire and power wire
- ▲ Combined with thermocouple and signal
- ▲ Customize for high temperature, shockproof environment
- ▲ Combined with pneumatic, hydraulic
- ▲ Customize high temperature 250°C slip ring
- ▲ Customize high voltage, large current slip ring
- ▲ Military level
- ▲ IP65, IP68 Optional

Installation



Instructions :
 Since it is difficult to keep the rotor and stator concentric, suggest to fix the slip ring on the rotating shaft with four screws and insert the torque arm into the anti-rotation tab, do not force to fix anti-rotation tab which may cause damage and shorten working life

Caution :
 ■ Do not let slip ring to carry loads as well as lead wires
 ■ Protect lead wire to avoid any damages of insulation when intallation
 ■ As a precise component, slip ring should be operated in a dry, less dust environment. Pls take protect measurements if bad conditions

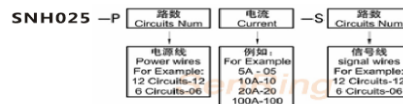
Customization

Customize based on this model

As one of domestic forthgoers in developing and manufacturing of slip rings, Senring has rich experiences in customizing slip rings for many industries, we have more than 10000 solutions and data sheets

How to customize?

Customized model no. description:



for example:
 if to order SNH025, support 67circuits*signals, model no. isSNH025-S67.
 if to order SNH025, support 13circuits*signals+2circuits*10A,, model no. SNH025-P0210-S13

Tel: +86-755-29717812 Fax: +86-755-33250183 Email: Info@senring.com Website : www.senring.com

BE Series Servo Motors

High-Torque Design, Low-Cost Package



Parker's BE Series brushless servo motors produce high continuous stall torque in a cost-saving and performance-enhancing package.



The BE Series is designed specifically as a very cost-effective alternative to comparably sized servos. The BE Series also provides exceptional torque with the design's increased number of magnetic poles. Comparably sized servos have four magnetic poles on the rotor, while BE Series motors have eight.

Unlike traditional servo motors, the BE Series does not have a separate metal housing. Instead, the motor stator laminations are not only used for performance, but provide both structural integrity and the motor shape. This design reduces both material costs and the time required to assemble the motor.

In addition to the manufacturing advantages, the exposed laminations reduce thermal resistance. This allows the heat generated by the motor to escape to the ambient surroundings more efficiently, thus improving time in the peak region and duty cycle.

Parker's wide range of Bayside® planetary gearheads are perfectly matched to the BE Series motor. Easy selection can be made using Parker's MotionSizer.

Features

- NEMA 16, 23, and 34 sizes
- From 1.4 to 46.8 in-lb (5.24 Nm) continuous torque
- Brushless construction
- Eight-pole open-lamination design provides increased torque and lower cost
- High torque density packaging
- Bridged stator design – quiet operation
- High performance neodymium magnets
- Thermoswitch protection on NEMA 23 and 34 sizes
- 2000 line encoder standard (8000 ppr post-quad)
- Resolver feedback option
- Several connector design choices
- Holding brake option available on size 34, custom order on size 23
- Custom modifications available
- Industry-leading 10-day delivery
- Two year warranty
- STP solid models and CAD (dxf) drawings available (free download at www.parkermotion.com)

Contact Information:

Parker Hannifin Corporation
Electromechanical Automation Division
5500 Business Park Drive
Rohnert Park, CA 94928
phone: 800.358.9068 / 707.584.7558
fax: 707.584.8029
email: emn_support@parker.com
www.parkermotion.com



ENGINEERING YOUR SUCCESS.

BE Series Servo Motors

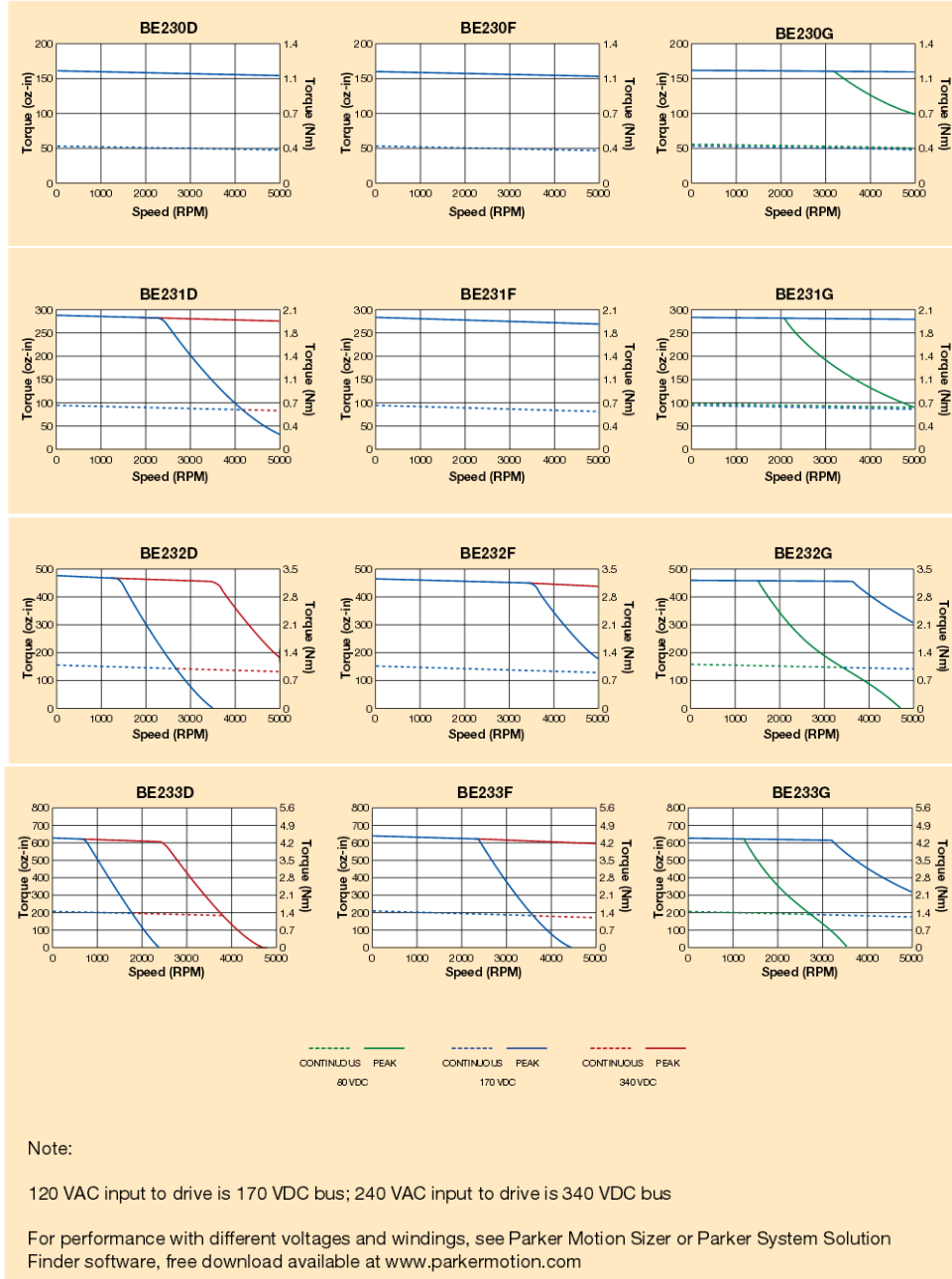
NEMA Size 23 Performance (Data at 240 VAC)

Model Size	Symbol	Units	BE230D	BE230F	BE230G	BE231D	BE231F	BE231G
Stall Torque Continuous ^{1,2,3}	T_{cs}	Nm	0.37	0.37	0.38	0.67	0.66	0.66
		in-lb	3.3	3.3	3.3	5.9	5.8	5.9
Stall Current Continuous ^{1,2,3}	$I_{cs(rms)}$	A_{rms}	2.2	4.3	5.3	1.9	3.8	5.3
		Nm	1.13	1.13	1.14	2.03	1.99	2.00
Peak Torque ⁸	T_{pk}	in-lb	10.0	10.0	10.1	18.0	17.7	17.7
Peak Current ⁸	$I_{pk(rms)}$	A_{rms}	6.6	12.8	16.0	5.8	11.3	15.9
Rated Speed ^{1,2,3,4}	S_r	rpm	4965	4965	4965	4965	4965	4965
		T_r	Nm	0.35	0.35	0.36	0.62	0.61
Rated Torque ^{1,2,3}	T_r	in-lb	3.1	3.1	3.2	5.5	5.4	5.4
		P_{out}	kW	0.18	0.18	0.19	0.32	0.32
Current @ Rated Speed ^{1,2,3}	I_r	Arms	2.1	4.1	5.2	1.8	3.6	5.0
Voltage Constant ^{4,7}	K_e	V_{ms}/k_{rpm}	10.37	5.32	4.35	21.14	10.74	7.67
Torque Constant ^{4,7}	$K_t(sine)$	Nm/A_{rms}	0.17	0.09	0.07	0.35	0.18	0.13
Resistance ^{4,7}	R	ohm	4.57	1.22	0.79	6.97	1.86	0.94
Inductance ^{5,7}	L	mH	15.49	4.04	2.69	28.52	7.43	3.79
Max DC bus Voltage ⁶	V_{mbus}	VDC _{max}	340	340	340	340	340	340
Max AC Voltage ⁶	V_s	VAC	240	240	240	240	240	240
Rotor Inertia ⁶	J	kg-m ²	5.20 ⁻⁶	5.20 ⁻⁶	5.20 ⁻⁶	9.04 ⁻⁶	9.04 ⁻⁶	9.04 ⁻⁶
		in-lb-sec ²	4.60 ⁻⁵	4.60 ⁻⁵	4.60 ⁻⁵	8.00 ⁻⁵	8.00 ⁻⁵	8.00 ⁻⁵
Motor Weight ⁶		kg	0.67	0.67	0.67	0.92	0.92	0.92
		lb	1.48	1.48	1.48	2.02	2.02	2.02

Model Size	Symbol	Units	BE232D	BE232F	BE232G	BE233D	BE233F	BE233G
Stall Torque Continuous ^{1,2,3}	T_{cs}	Nm	1.10	1.08	1.07	1.45	1.48	1.45
		in-lb	9.8	9.5	9.5	12.8	13.1	12.9
Stall Current Continuous ^{1,2,3}	$I_{cs(rms)}$	A_{rms}	2.0	3.8	5.5	1.8	3.5	5.6
		Nm	3.34	3.26	3.25	4.38	4.47	4.39
Peak Torque	T_{pk}	in-lb	29.6	28.9	28.7	38.8	39.6	38.9
Peak Current	$I_{pk(rms)}$	A_{rms}	5.9	11.5	16.4	5.3	10.4	16.8
Rated Speed ^{1,2,3}	S_r	rpm	4965	4965	4965	3741	4965	4965
		T_r	Nm	0.99	0.96	0.96	1.33	1.29
Rated Torque ^{1,2,3}	T_r	in-lb	8.8	8.5	8.5	11.8	11.5	11.2
		P_{out}	kW	0.51	0.5	0.5	0.52	0.67
Current @ Rated Speed ^{1,2,3}	I_r	Arms	1.8	3.5	5.0	1.6	3.1	5.0
Voltage Constant ^{4,7}	K_e	V_{ms}/k_{rpm}	34.14	17.18	12	50.42	26.19	15.85
Torque Constant ^{4,7}	$K_t(sine)$	Nm/A_{rms}	0.56	0.28	0.2	0.83	0.43	0.26
Resistance ^{4,7}	R	ohm	7.72	2.05	1.01	10.98	2.85	1.08
Inductance ^{5,7}	L	mH	35.8	9.66	4.73	51.71	13.95	5.02
Max DC bus Voltage ⁶	V_{mbus}	VDC _{max}	340	340	340	340	340	340
Max AC Voltage ⁶	V_s	VAC	240	240	240	240	240	240
Rotor Inertia ⁶	J	kg-m ²	1.70 ⁻⁵	1.70 ⁻⁵	1.70 ⁻⁵	2.37 ⁻⁵	2.37 ⁻⁵	2.37 ⁻⁵
		in-lb-sec ²	1.50 ⁻⁴	1.50 ⁻⁴	1.50 ⁻⁴	2.10 ⁻⁴	2.10 ⁻⁴	2.10 ⁻⁴
Motor Weight ⁶		kg	1.41	1.41	1.41	1.9	1.9	1.9
		lb	3.1	3.1	3.1	4.18	4.18	4.18

Note: These specifications are based on theoretical motor performance and are not specific to any amplifier.
¹ @ 25°C ambient, 125°C winding temperature, motor connected to a 10" x 10" x 1/4" aluminum mounting plate;
² @ 40°C ambient derate phase currents and torques by 6%.
³ Maximum winding temperature is 155 °C. Thermal protection device threshold may be at a lower temperature.
⁴ These ratings are valid for Parker drives. Other drives may not achieve the same ratings.
⁵ Maximum speed is 5000 PPM.
⁶ Measured line-to-line, ±10%, ±30%, line-to-line inductance bridge measurement @ 1Khz.
⁷ Reference only.
⁸ Total motor torque per peak of the sinusoidal amps measured in any phase, ±10%.
⁹ Initial winding temperature must be 60°C or less before peak current is applied.
⁹ Use servo drive thermal model for overtemp protection or lower peak current.

NEMA Size 23 Speed-Torque Performance



NE Nema Series: Lightweight, Compact and Low Friction



Parker Bayside's NEMA gearheads feature a high-efficiency spur-gear design, in a light, compact package. Designed to mount directly to the face of NEMA face stepper and servo motors, NEMA gearheads are ideal for applications requiring smooth operation and low starting torque. Ratios from 3:1 to 100:1 are available in NEMA 23, 34 and 42 frame sizes.

3 Frame Sizes

NE23
NE34
NE42

Ratios

3:1	20:1
5:1	30:1
8:1	50:1
10:1	100:1
15:1	



Performance Specifications

NE NEMA Series

	Units	Ratio	Frame Size		
			NE23	NE34	NE42
Nominal Output Torque, $T_{nom r}$	in-lb	3	16	64	123
	Nm		2	7	14
	in lb	5	27	107	205
	Nm		3	12	23
	in lb	8-10	40	142	250
	Nm		5	16	28
	in lb	15	46	170	300
	Nm		5	19	34
	in lb	20-100	50	180	350
	Nm		6	20	40
Max. Acceleration Output Torque, $T_{acc r}$	in lb	3	24	95	185
	Nm		3	11	21
	in lb	5	40	160	307
	Nm		5	18	35
	in lb	8-10	60	210	375
	Nm		7	24	42
	in lb	15	70	255	450
	Nm		8	29	51
	in lb	20-100	75	270	525
	Nm		9	31	59
Nominal Input Speed, $N_{nom r}$	RPM	All	4,000	4,000	4,000
Max. Input Speed, $N_{max r}$	RPM	All	5,500	5,000	4,500
Standard Backlash ⁽¹⁾	arc min	3, 5, 8, 10	30	25	25
	arc min	15-100	20	20	20
Low Backlash ⁽¹⁾	arc min	3, 5, 8, 10	15	15	15
	arc min	15-100	10	10	10
Efficiency at Nominal Torque	%	All	98%	98%	98%
Moment of Inertia	oz in sec ²	All	0.00007	0.0005	0.004
	gm cm sec ²		0.0051	0.0408	0.306
Maximum Weight	lb	All	1.0	3.0	6.0
	kg		0.5	1.4	3.0
Radial Load ⁽²⁾	lb	All	20	80	200
	N		90	350	890
Axial Load	lb	All	10	30	60
	N		45	135	265

(1) Measured at 2% of rated torque

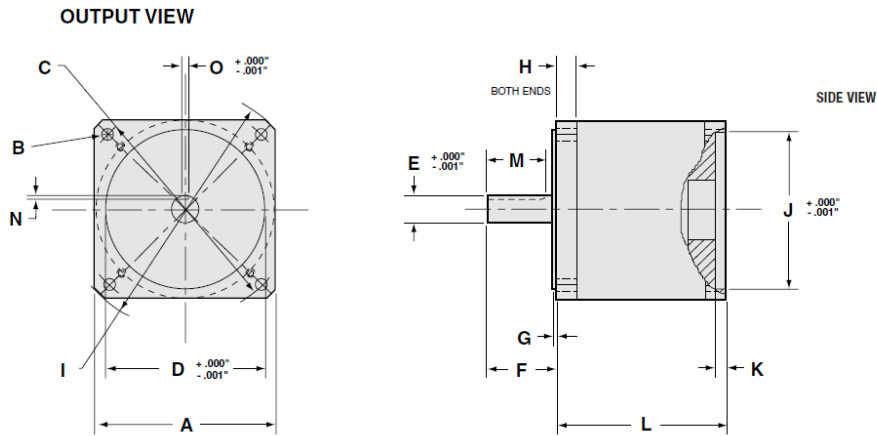
(2) Radial Loads are measured at 12.7mm (0.5in) from the gearhead mounting surface.
These ratings are based on gearhead making more than one revolution on output shaft.

Specifications are subject to change without notice

NE NEMA Series

Dimensions

OUTPUT VIEW

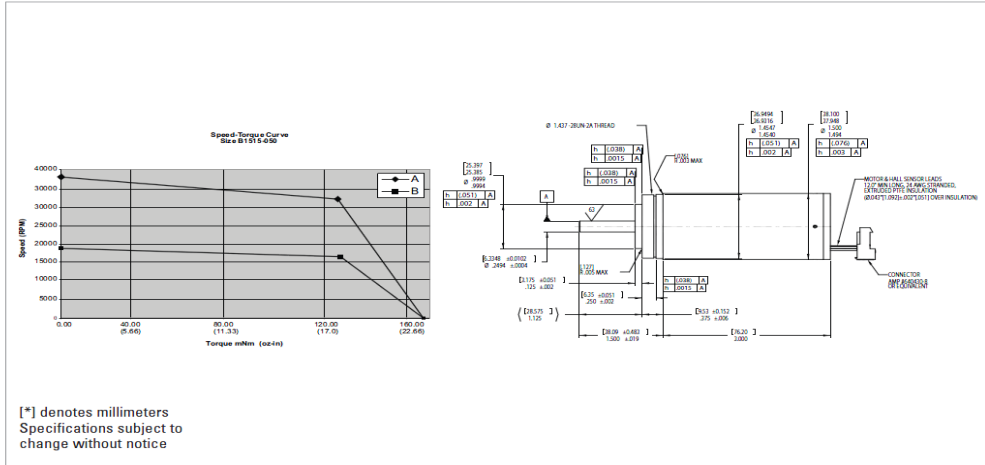


Frame Size	A Square Flange		B Bolt Hole		C Bolt Circle		D Pilot Diameter		E Output Shaft Diameter		F Output Shaft Length		G Pilot Thickness		H Flange Thickness	
	(in)	(mm)	(in)	(mm)	(in)	(mm)	(in)	(mm)	(in)	(mm)	(in)	(mm)	(in)	(mm)	(in)	(mm)
NE 23	2.27	58	0.195	5.0	2.625	66.7	1.500	38.1	0.375	9.5	1.00	25.4	0.062	1.6	0.19	5
NE 34	3.25	83	0.218	5.5	3.875	98.4	2.875	73.0	0.500	12.7	1.25	31.8	0.067	1.7	0.38	10
NE 42	4.20	107	0.281	7.1	4.950	125.7	2.187	55.5	0.625	15.9	1.50	38.1	0.093	2.4	0.50	13

Frame Size	I Housing Diameter		J Input Pilot Diameter		K Input Pilot Depth		L Housing Length		M Keyway Length		N Keyway Depth		O Keyway Width	
	(in)	(mm)	(in)	(mm)	(in)	(mm)	(in)	(mm)	(in)	(mm)	(in)	(mm)	(in)	(mm)
NE 23	3.00	76	1.501	38.13	0.125	3.2	2.30	58	0.75 flat	19 flat	0.015 flat	0.4 flat	—	—
NE 34	4.38	111	2.876	73.05	0.200	5.1	3.00	76	1.06	27	0.072	1.8	0.124	3.15
NE 42	5.63	143	2.188	55.58	0.187	4.7	3.75	95	1.13	29	0.108	2.7	0.187	4.75

B1515-150

Please contact us to learn about other available sizes: 8, 12, 13, 14 and custom



Size 15 Performance Data - Model: B1515-150

Symbol	Parameter	Units	A	B
T_{cs}	Max Cont Stall Torque	oz-in (mNm)	24.7 (174.6)	24.7 (174.6)
T_{pk}	Peak Torque	oz-in (mNm)	174.6 (1233.0)	86.0 (607.3)
P_{diss*}	Max Cont Pwr Dissipation	watt	24.1	24.1
W_{nl}	No Load Speed at 24 volts-25°C	rpm	38,560	18,360
I_{cs}	Max Cont Current	amp	4.70	2.28
K_m	Motor Constant	oz-in/watt ^{1/2} (mNm/watt ^{1/2})	5.04 (35.6)	5.12 (36.2)
K_t	Torque Constant	oz-in/amp (mNm/amp)	5.26 (37.1)	11.05 (78.0)
t_m	Mech Time Constant	msec	5.0	5.0
t_e	Elec Time Constant	msec	0.340	0.340
J_m	Rotor Inertia	oz-in-sec ² (kg-m ²)	9.00E-4 (6.36E-6)	9.00E-4 (6.36E-6)
K_d	Viscous Torque (Losses)	oz-in/krpm (mNm/krpm)	1.91E-2 (0.135)	1.91E-2 (0.135)
R_{th}	Thermal Resistance	°C/watt	5.40	5.40
T_f	Static Friction Torque	oz-in (mNm)	.330 (2.33)	.330 (2.33)
W	Motor Weight	oz (gm)	18.0 (510.0)	18.0 (510.0)

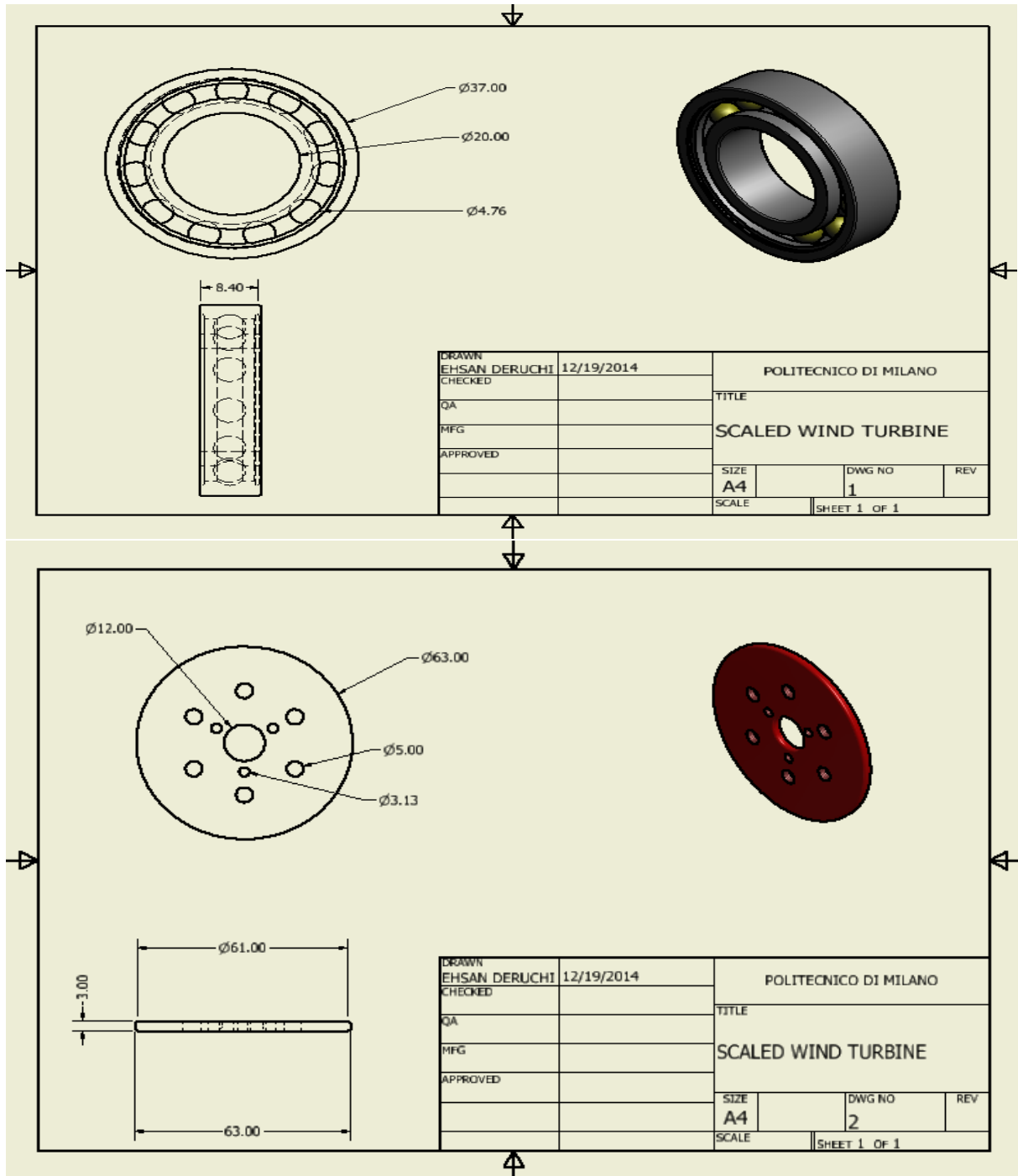
*Mounted on a 5.0" x 5.0" x 0.25" Aluminum Heat Sink

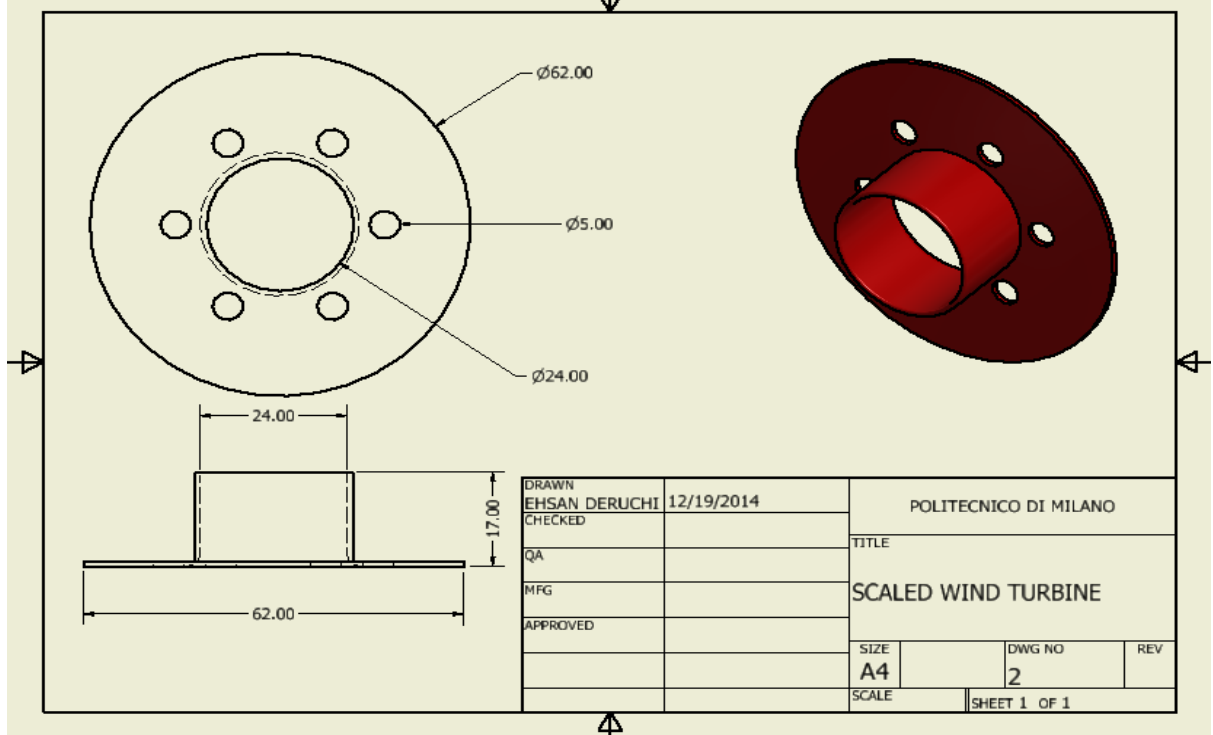
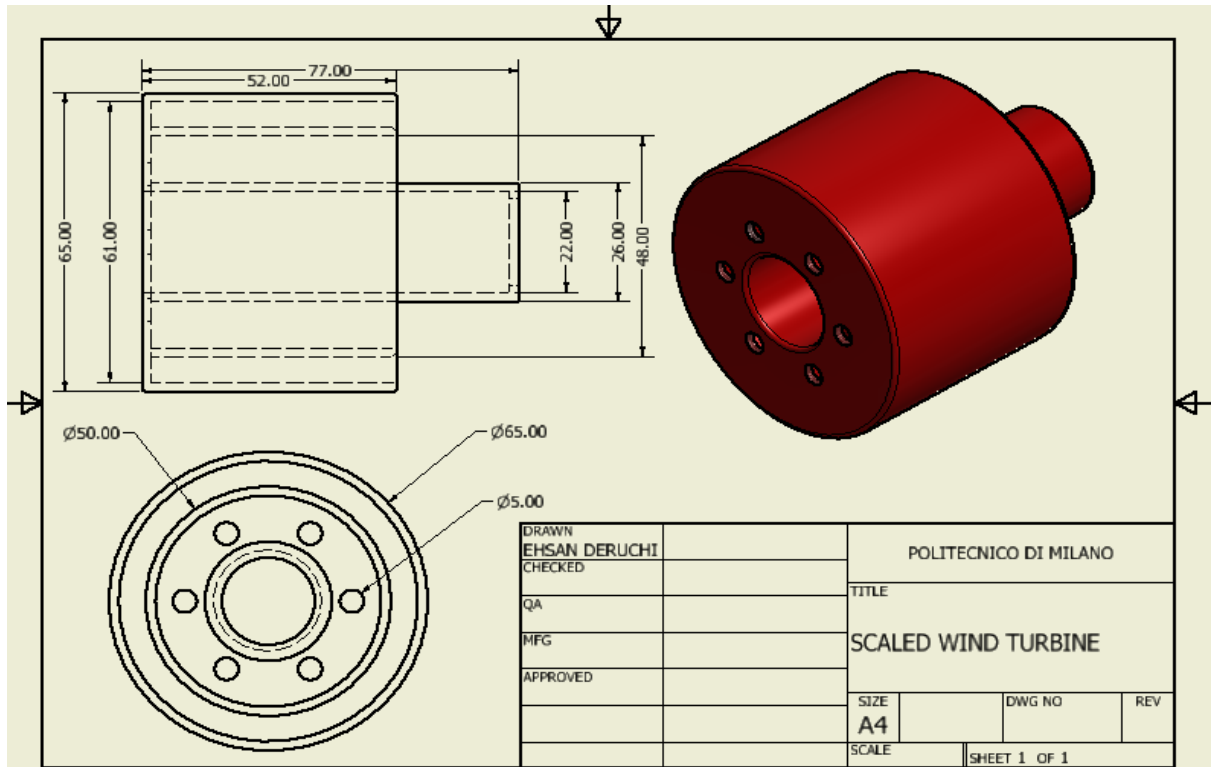
Size 15 Winding Data - Model: B1515-150

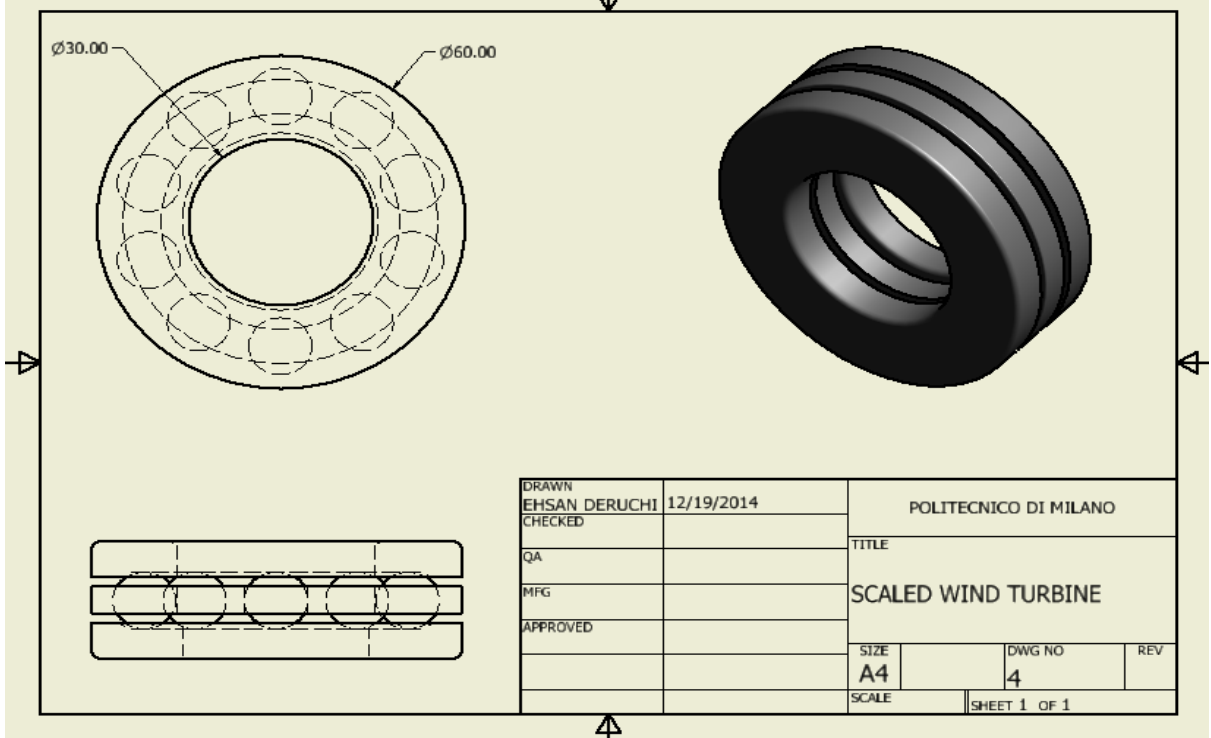
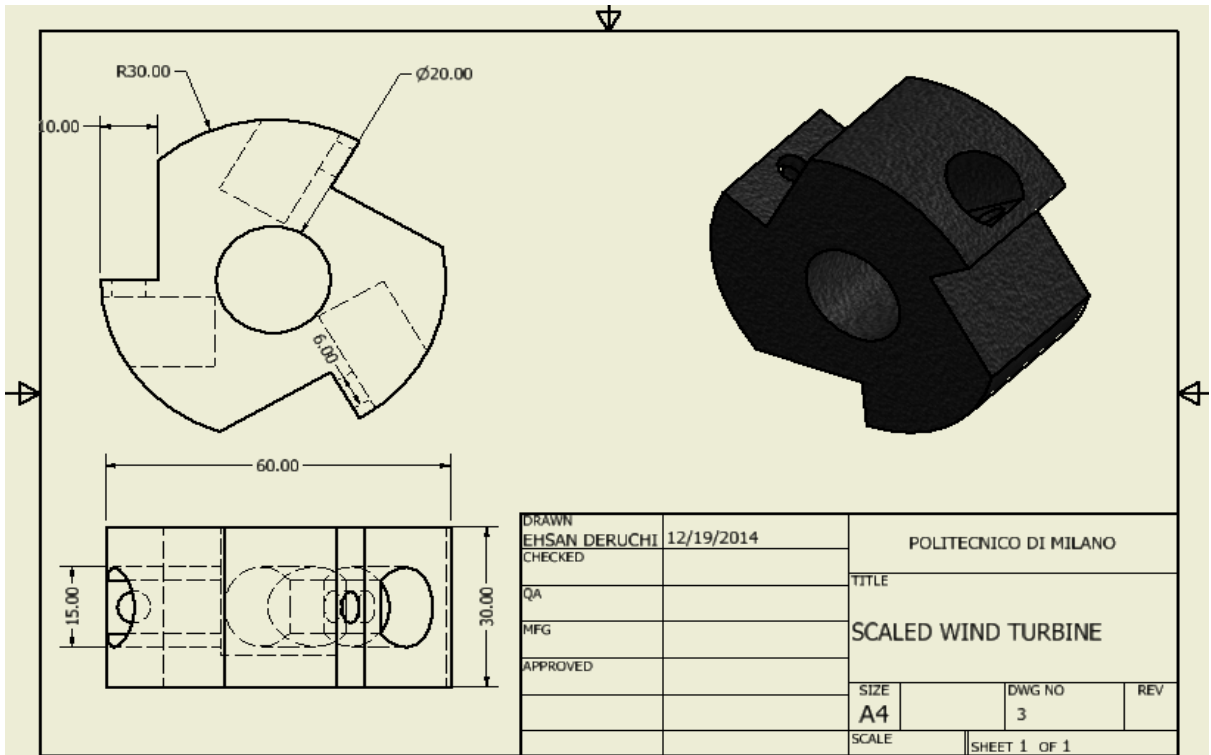
Symbol	Parameter	Units	A	B
V_r	Rated Voltage	VDC	150.0	150.0
I_{pk}	Peak Current	amp	33.2	7.78
K_e	Back EMF (Voltage) Constant	V/krpm	3.89	8.17
L	Inductance (Ph to Ph)	mH	0.370	1.62
R_c	Resistance (Ph to Ph)	Ω	1.09	4.65

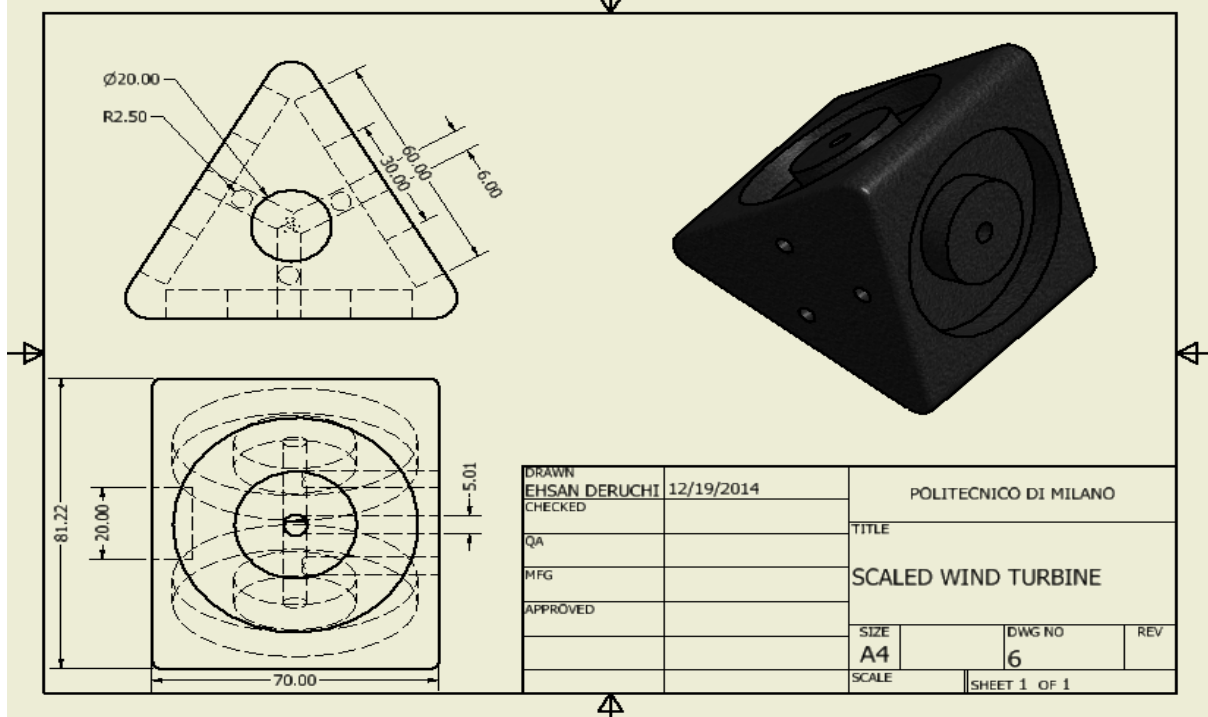
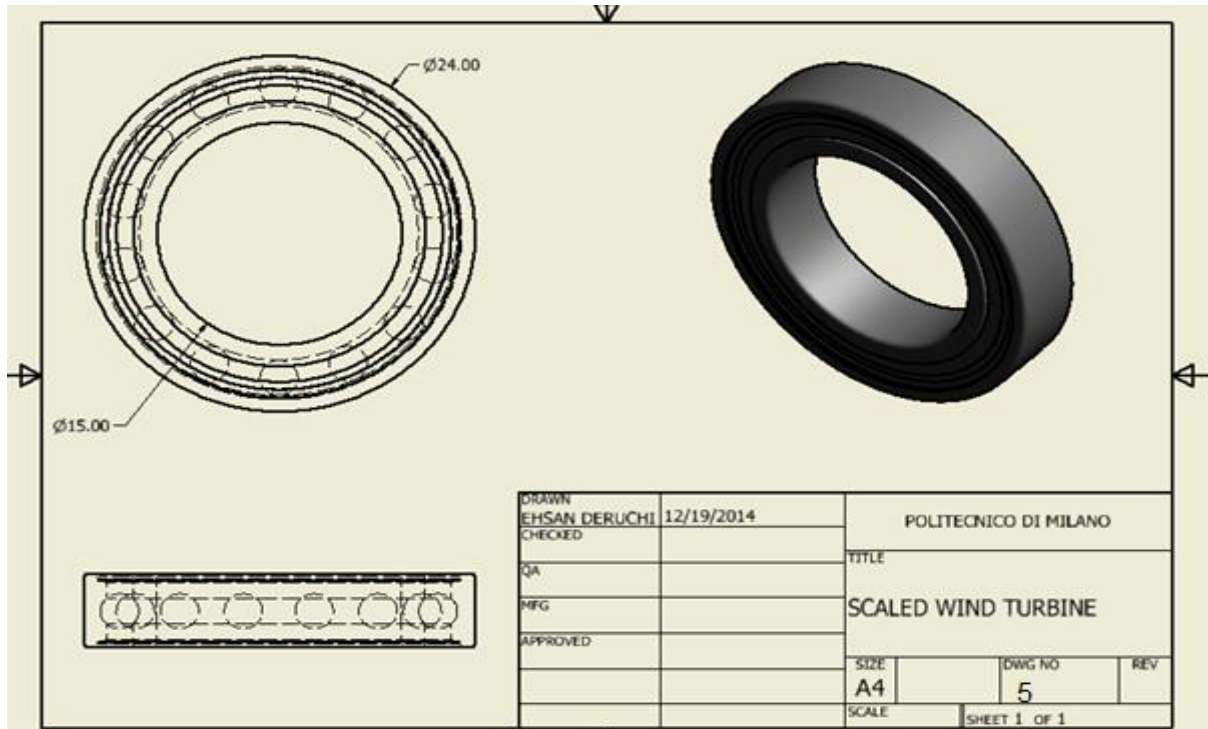
Please contact us to learn about other available windings

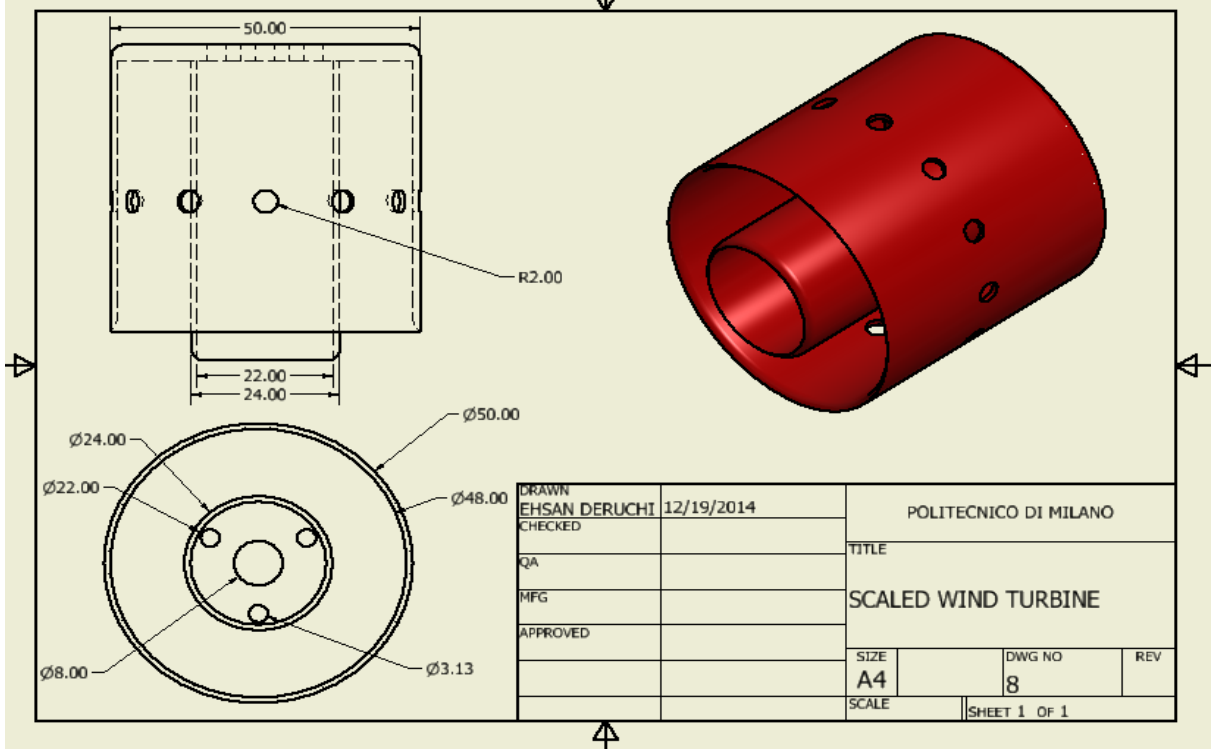
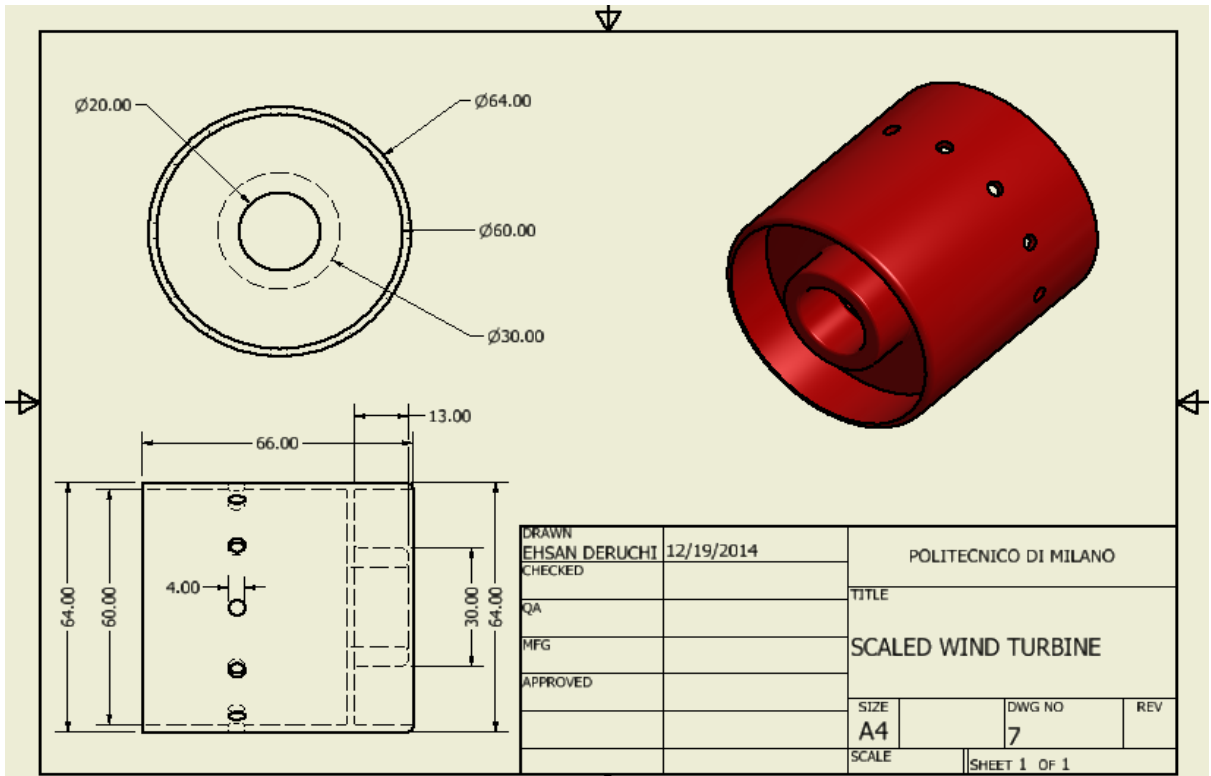
APPENDIX C

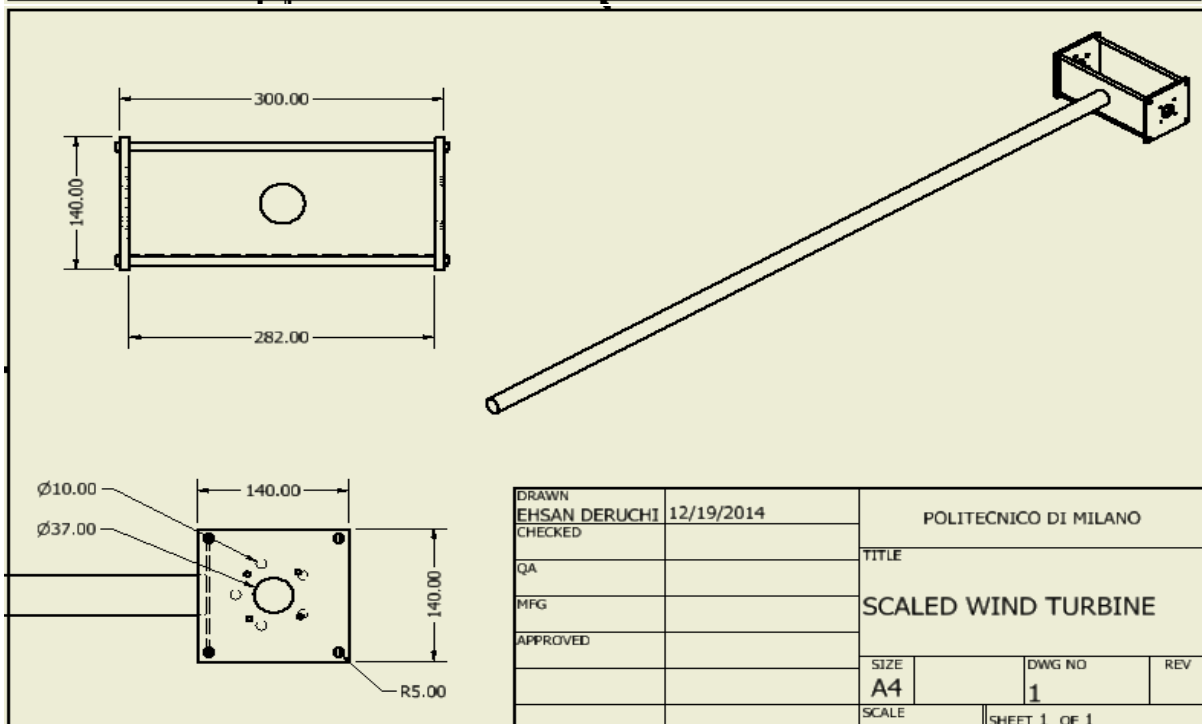
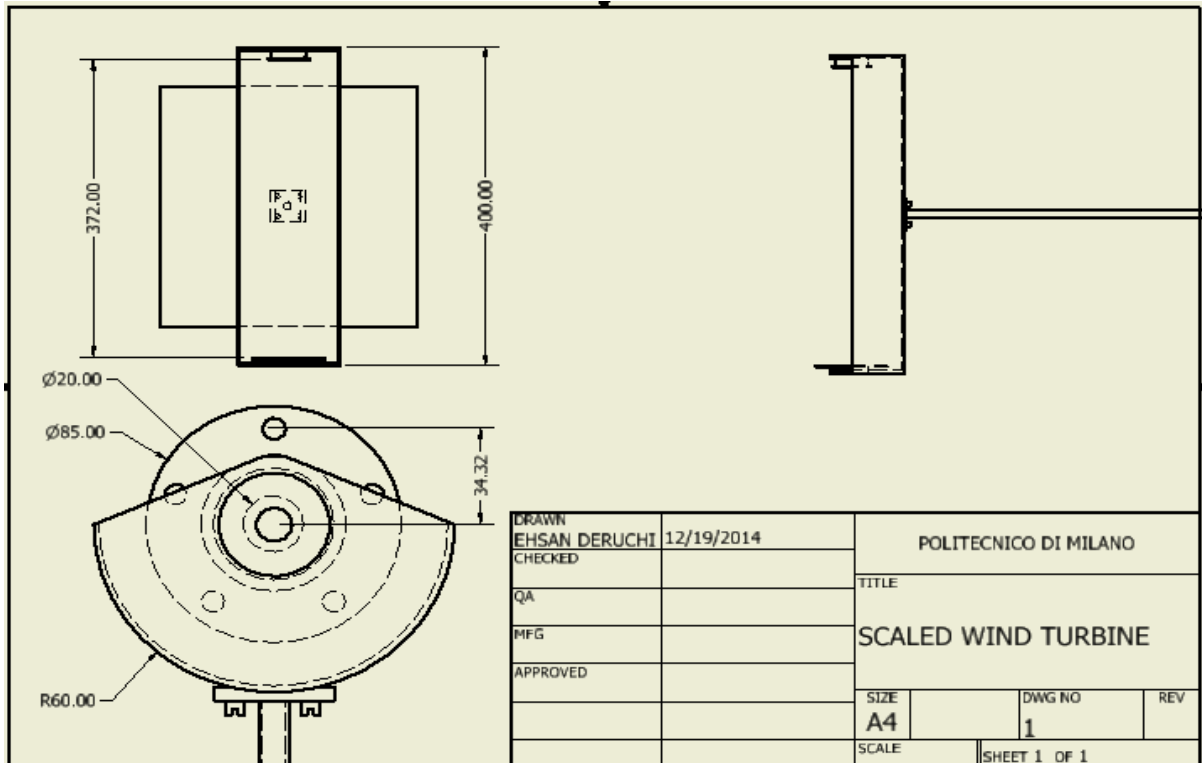












NOMECLATURE

λ_L	=	Geometrical scaling factor	y	=	Profile displacement
λ_V	=	Wind velocity scaling factor	\dot{y}	=	Profile velocity
λ_f	=	Frequency scaling factor	\ddot{y}	=	Profile acceleration
λ_{Re}	=	Reynolds scaling factor	c_a	=	Maximum acceleration coefficient
λ_m	=	Mass scaling factor	T	=	Torque, Time period
λ_a	=	Acceleration scaling factor	\ddot{y}_q	=	Mean quadratic acceleration
λ_t	=	Time scaling factor	ω	=	Rotational velocity (rad/s)
λ_F	=	Force scaling factor	$\dot{\omega}$	=	Rotational acceleration
λ_A	=	Area scaling factor	τ	=	Reduction ratio
λ_ω	=	Rotational speed scaling factor	J	=	Inertia
λ_T	=	Torque scaling factor	C	=	Torque
λ_W	=	Power scaling factor	α	=	Accelerator coefficient
λ_I	=	Inertia scaling factor	β	=	Resistance coefficient
λ_{Ma}	=	Mach scaling factor	b	=	Blade chord
K	=	Optimization parameter	C_M	=	Aerodynamic Pitch Coefficient
ρ	=	Density	n	=	Rotational speed (rpm)
M	=	Mass	i	=	Reduction ratio
V	=	Wind velocity	η	=	Efficiency
L	=	Length	F	=	Force
A	=	Section	Δ	=	Variation
R	=	Radius	Ω_0	=	Rated rotational velocity
t	=	Time			

θ	=	Pitch angle	$\dot{\varphi}$	=	Variation of rotor velocity
y	=	Displacement	P	=	Power
K_P	=	Proportional gain	P_0	=	Rated power
K_I	=	Integral Gain	$\omega_{\varphi n}$	=	Natural frequency
K_D	=	Derivative Gain	$\zeta_{\varphi n}$	=	Damping ratio
N	=	Reduction ratio	K_φ	=	Stiffness

Subscripts

rms	Root mean square
r	Resistance
m	Motor
q	Quadratic
n	Nominal

ABBREVIATIONS AND ACRONYMS

ADAMS	Multibody dynamics and motion analysis software
B.M.A	Bending moment absorber
COE	Cost of energy
CM	Center of mass
CML	Mean sea level
DOE	Department of Energy
DOF	Degree of Freedom
DOWEC	Dutch Offshore Wind Energy Converter
DTU	Technical University of Denmark
DU	Delft University
FAST	An aeroelastic design code for horizontal axis wind turbines
GVPM	Galleria dell Vento Politecnico di Milano
HAWT	Horizontal-axis Wind Turbine
IEA	international energy agency
IPC	Independent Pitch control
MATLAB	high-level technical computing language
NACA	National Advisory Committee for Aeronautics
NREL	National Renewable Energy Laboratory
PID	Proportional Integral Derivative
POLIMI	Politecnico di Milano
Q-BLADE	simulation software for wind turbine blade design
RMS	Root mean square
RPM	Rotations per minute
TSR	Tip speed ratio

REFERENCES

- [1] Fthenakis, V and Kim, H,C. *Land use and electricity generation*.s.l. :Renewable and Sustainable Energy Reviews, 2009.
- [2] Robert Gasch, Jochen Twele. *Windkraftanlagen Geundlagen, Entwurf,Planung und Bertieb*. wiesbaden : Springer, 2013.
- [3] Gipe , Paul. *The wind Industry's Experience with Aesthetic Criticism*. s.l. : Leonardo, 1993.
- [4] *Design and Operation of Power Systems with LargeAmounts of Wind Power*. Holttinen, Hannele et al. Adelaide, Australia : IEA Wind Summary Paper, Global Wind Power Conference, september 2006.
- [5] *Wind Power delivers too much to ignore* . Platt, Reg. s.l. : New Scientist, 21 January 2013.
- [6] *Meteorologically defend limits to reduction in the variability of outputs from a coupled wind farm system in the central US*. Junling Huang, Michael B. McElory : Renewable Energy, 2014, Vol. 62. 331-340.
- [7] Association, The World Wind Energy. *Half Year Report*. WWEA. 2014.
- [8] *Wind tunnel testing of scaled wind turbine models:Beyond aerodinamics*. Carlo L.Bottasso, Filippo Campagnolo, Vlaho Petrovic. Milan : ScienceDirect ELSEVIER Journal of Wind Engineering and Industrial Aerodynamics, 2014. 127 (2014) 11-28.
- [9] J. Jonkman, S. Butterfield, W. Musial,G.scott. *Definition of a 5-MW Reference Wind Turbine for Offshore System Development*. U.S : NREL, 2009.
- [10] Heather Rae Martin. *DEVELOPMENT OF A SCALE MODEL WIND TURBINE FOR TESTING OF OFFSHORE FLOATING WIND TURBINE*. s.l. : The University of Maine, 2009.
- [11] H.J.T Kooijman, C. Lindenburg, D.Winkelaar, E.L. van der Hooft. *Aero-elastic modeling of the DOWEC 6 MW pre-design in PHATAS*. 2003.
- [12] Wind Turbine Blades, Product Overview, Standard Products . *Max. Rated Power <=5000 kW*. [Online] LM Glasfiber Group,, January 4, 2006. <http://www.lmglasfiber.dk/UK/Products/Wings/ProductOverView/50000kw.htm>

- [13] GVPM. [Online] Politecnico Di Milano.
<http://www.windtunnel.polimi.it/impianto/impianto.htm>.
- [14] *Wind tunnel testing of scaled wind turbine models: Beyond aerodynamics*. Carlo L. Bottasso, Filippo Campagnolo, Vlaho Petrovic. 2014, Journal of Wind Engineering and Industrial Aerodynamics.
- [15] Buckingham, E. *illustrations of the use of dimentional equations*. 1914.
- [16] *Size effect on wind turbine Blades design drivers*. Taruj Ashuri, M.B.Zaaijer. Delft : Wind energy research group, Faculty of aerospace engineering.
- [17] *The Scientist and Engineer's Guide to Digital Signal Processing*. smith, S. San Diego : California Technical Publishing, 2006.
- [18] ADAMS. *MSC ADAMS*[Online] <http://www.mscsoftware.com/it/product/adams>.
- [19] Eckhardt, Homer D. *Kinematic Design of Machines and Mechanisms*. s.l. : McGraw-Hill ISBN-13: 978-0070189539, 1998.
- [20] *IMPLEMENTATAION OF PITCH ANGLE WIND TURBINE POSISION*. Ali Musyafa Ronny, Dwi Noriati. INDONESIA : Academic Research International, 2012, Vol. 3.
- [21] E. Bossanyi, A. Wright and P.Fleming. *Controllor Field Tests on the NREL CART2 Turbine*. Colorado : NREL, 2010.
- [22] *Motor-Reducer Sizing Through a MATLAB-Based Graphical Technique*. H. Giberti, S. Cinquemani. (ISSN: 0018-9359), s.l. : IEEE TRANSACTIONS ON EDUCATION , Vol. 55.
- [23] Wikieducator. [Online] <http://wikieducator.org/images/1/12/Mec0001.pdf>.
- [24] wind turbine design and simulation. *Q blade*. [Online] <http://www.q-blade.org/>.
- [25] *State of the art in wind turbine aerodynamics and aeroelasticity*. M.O.L. Hansen, J.N. Sørensen, S. Voutsinas, N. Sørensen, H.Aa. Madsen. Lyngby, Denmark : Science Direct, 2006.
- [26] G. LEGNANI, M. TIBONI, R. ADAMINI. *Meccanica degli azionamenti*. Bologna : Progetto Leonardo, 2002. Vol. 1.
- [27] Faulhaber Company. [Online] www.faulhaber.com.
- [28] Christian Bak, Fredrik Zahle, Robert Bitsche, Taeseong Kim, Anders Yde, Lars Christian Henriksen, Anand Natarajan, Morten Hatvin Hansen. *Description of the DTU Reference Wind Turbine*. Denmark : DTU wind energy, 2013.

- [29] Morten Hartvig Hasen, Lars Christian. *Basic DTU Wind Energy controller*. Denmark : Department of Wind Energy, 2013.
- [30] Katherine Dykes, Peter Graf, George Scott, Andrew Ning, Ryan King, Yi Guo, Taylor Parsons, Rick Damiani, and Paul Veers. *Integrated System Modeling for Wind Turbines and Plants*. s.l. : national laboratory of the U.S. Department of Energy, 2014.
- [31] Motion Control Systems, North America. *Parker Motion Company*. [Online] 2015. <http://www.parkermotion.com/>.
- [32] portescap company. [Online] www.portescap.com.
- [33] maxon motor company. [Online] www.maxonmotor.it.
- [34] *Control of Variable Speed Variable Pitch Wind Turbine at Above and Below Rated Wind Speed*. S.Ragendran, D.Jena. s.l. : Hindawi Publishing Corporation ournal pf Wind Energy, 2014.
- [35] SKF. [Online] SKF Group. <http://www.skf.com/group/splash/index.html>.
- [36] Inventor. [Online] Autodesk.<http://www.autodesk.it/products/inventor/overview>.
- [37] Comparison of Gear Efficiencies - Spur, Helical, Bevel, Worm, Hypoid, Cycloid. [Online] 10 23, 2012.
https://www.google.it/search?q=perpendicular+gears&biw=1366&bih=667&source=lnms&sa=X&ei=ByMRVaWtGIP0aqi7grgJ&ved=0CAYQ_AUoAA&dpr=1.
- [38] Senring company. [Online] www.senring.com.
- [39] *Simulation of Power Control of a Wind Turbine Permanent Synchronous Generator*. Huang, Nantao. s.l. : Marquette University, 2009.
- [40] Johnson, Kathryn E. *Adaptive Torque Control of Variable Speed Wind Turbines*. Colorado : NREL, 2004.
- [41] MortenH.Hasen, Anca Hansen, Torben J.Larsen, Stig ye, Poul Sorensen ,peter Fuglsang. *Control design for a pitch-regulated, variable speed wind turbine*. Roaklide Denmark : Riso national Library , 2005.
- [42] Bossanyi, Ervin. *Controller for 5MW reference turbine*. s.l. : European Commission (Project Upwind), 2009.
- [43] Jonkman, J.M. *Dynamics Modeling and Loads Analysis of an offshore Floating Wind Turbine*. s.l. : NREL, 2007.

- [44] *Wind Turbine Pitch Optimization*. Benjamin Biegel, Morten Juelsgaard, Matt Kraning, Stephen Boyd, Jakob Stoustrup. Multi Conference on Systems and Control, Denver,CO,USA : IEEE International Conference on Control Applications(CCA), 2011.
- [45] *Stability Augmentation of a Grid-connected Wind farm(Chapter 2)*. Muyeen , S.M, Tamura, J and Murata, T. ISBN: 978-1-84800-315-6, s.l. : Springer, 2009.
- [46] Selvam, Kausihan. *Individual Pitch Control for Large scale wind turbines*. Amsterdam : Energy research Center of the Netherlands.
- [47] B Savini, E A Bossanyi, GL Garrad Hassan & Partners Ltd. *Supervisory control logic design for Individual Pitch Control*. s.l. : GL.
- [48] Petersson, Torbjorn Thiringer and Andreas. *Control of a Variable Speed Pitch Regulated Wind Turbine*. Goteborg, Sweden : Department of Energy and Environment, 2005.
- [49] V. Ramakrishnan, S. K. srivatsa. *Pitch Control of Wind Turbine Generator by using New Mechanism*. India : Bharath University.
- [50] D.A.KIRBY. *Low Speed Wind Tunnel Measurements of the Lift, Drag and Pitching Moment of a Series of Cropped Delta Wings*. Loonden : HER MAJESTY's STATIONERY OFFICE, 1974.
- [51] *Pitch Controlled Variable Speed Wind Turbine Generation*. Butterfield, E. Muljadi and C. P. Phoenix, Arizona : IEEE industry Application Society Annual Meeting, 1999.
- [52] *Pitch Angle Control for Variable Speed Wind Turbines*. Jianzhong Zhang, Ming Cheng, Zhe Chen, Xiaofan Fu. Nanjing China : DRPT, 2008.
- [53] Campagnolo, Filippo. *Wind Tunell Testing of Scaled Wind Turbine Models:AERODINAMICS AND BEYOND*. Milan : Politecnico di Milano, 2013.